Super-terahertz heterodyne spectrometer using a quantum cascade laser

Yuan Ren

Super-terahertz heterodyne spectrometer using a quantum cascade laser

Proefschrift

ter verkrijging van de graad van doctor
aan de Technische Universiteit Delft,
op gezag van de Rector Magnificus prof. ir. K. C. A. M. Luyben,
voorzitter van het College voor Promoties,
in het openbaar te verdedigen op dinsdag 4 december 2012 om 10:00 uur

door

Yuan REN

Astronomy, Purple Mountain Observatory, Chinese Academy of Sciences,
Nanjing, China
geboren te Xi'an, China.

Dit proefschrift is goedgekeurd door de promotor:
Prof. dr. ir. T. M. Klapwijk.
Prof. dr. S. C. Shi
Copromotor:
Dr. J. R. Gao

Samenstelling promotiecommissie:

Rector Magnificus,	voorzitter
Prof. dr. ir. T. M. Klapwijk,	Technische Universiteit Delft, promotor
Prof. dr. S. C. Shi,	Purple Mountain Observatory, promotor
Dr. J. R. Gao,	SRON/TU Delft, copromotor
Prof. dr. L. B. F. M. Waters,	SRON/Universiteit van Amsterdam
Prof. dr. A. Neto,	Technische Universiteit Delft
Prof. dr. ir. H. S. J. van der Zant,	Technische Universiteit Delft
Dr. M. R. Hogerheijde,	Universiteit Leiden

Yuan Ren was supported by CAS-KNAW Joint PhD Training Programme by the Chinese Academy of Sciences (CAS) and the Royal Netherlands Academy of Arts and Sciences (KNAW). The work described in this thesis was performed at the Faculty of Applied Sciences, Group of Physics of Nanoelectronics, Technische Universiteit Delft, The Netherlands.

Printed by: Uitgeverij BOXPress
Casimir PhD series, Delft-Leiden 2012-20
ISBN/EAN: 978-90-8593-131-7

Contents

1 Introduction **1**
- 1.1 Terahertz astronomy . . . 1
- 1.2 Incoherent detection . . . 5
  - 1.2.1 Transition Edge Sensor (TES) . . . 5
  - 1.2.2 Kinetic Inductance Detector (KID) . . . 6
- 1.3 Coherent detection . . . 7
  - 1.3.1 Mixers . . . 8
  - 1.3.2 Local oscillators . . . 13
- 1.4 Thesis outline . . . 15
- Bibliography . . . 18

2 Terahertz quantum cascade laser as a local oscillator **21**
- 2.1 Terahertz quantum cascade laser . . . 21
  - 2.1.1 Active-region design . . . 22
  - 2.1.2 Waveguide design . . . 25
- 2.2 High temperature operation . . . 27
- 2.3 Beam quality . . . 29
  - 2.3.1 Surface emitting, second-order DFB THz QCLs . . . 30
  - 2.3.2 Third-order distributed feedback QCL . . . 33
  - 2.3.3 2-D Photonic crystal THz QCLs . . . 36
- 2.4 Frequency or phase locking of a THz QCL . . . 37
  - 2.4.1 Locking to an external source . . . 38
  - 2.4.2 Locking to a frequency comb . . . 39
  - 2.4.3 Locking to a molecular absorption line . . . 40

Bibliography 42

3 Laboratory heterodyne spectroscopy 45
3.1 Introduction 45
3.2 Line profile modelling 46
3.2.1 Natural broadening 46
3.2.2 Thermal Doppler broadening 47
3.2.3 Pressure broadening 47
3.2.4 Opacity broadening 48
3.2.5 Line profile generation 48
3.3 Application of laboratory heterodyne gas cell measurement . . 49
3.3.1 HIFI gas cell analysis 49
3.3.2 Heterodyne gas cell spectroscopy using a quantum cascade laser 51
Bibliography 54

4 3.5 THz surface emitting distributed feedback QCL operated at 70 K as local oscillator 55
4.1 Introduction 56
4.2 Terahertz surface emitting DFB QCL 57
4.3 Experiment setup 58
4.4 FTS, beam pattern, and pumping HEB experiment results . . . 58
4.5 Conclusions 61
Bibliography 63

5 Terahertz heterodyne spectrometer using a quantum cascade laser 65
5.1 Introduction 66
5.2 Experiment setup 66
5.3 Heterodyne spectroscopy experiment results 69
5.4 Conclusions 72
Bibliography 73

6 High-resolution heterodyne spectroscopy using a QCL around 3.5 THz 75
6.1 Introduction 76
6.2 Experiment setup 76
6.3 Tunable high-resolution heterodyne spectroscopy experiment . . 78
6.4 Temperature and frequency resolution 81
6.5 Conclusions 84

Bibliography 86

7 Frequency locking of single-mode 3.5-THz quantum cascade lasers using a gas cell 89
7.1 Introduction 90
7.2 Experiment setup 91
7.3 Frequency locking of a THz QCL to a molecular absorption line 92
7.4 Conclusions 96
Bibliography 97

8 Frequency and amplitude stabilized terahertz quantum cascade laser as local oscillator 99
8.1 Introduction 100
8.2 Experiment setup 101
8.3 Frequency with amplitude stabilisation measurement results . . 103
8.4 Conclusions 109
Bibliography 110

Summary 113

Samenvatting 117

Curriculum Vitæ 121

List of publications 123

Acknowledgements 127

Chapter 1

Introduction

1.1 Terahertz astronomy

From ancient history, human interest naturally turned into astronomy as long as they had been looking at the sky and wondering what it all means. All these early observations of sunrise, rain, season and tide, helped to our understanding of "the heavens". Furthermore, such observations of the Sun and Moon oriented the direction to broaden our horizon, and also led to the establishment of early calendars, which drives agricultural development. Human observations were limited to the naked eye until, in 1610, when Galileo pointed a small telescope towards the heavens, two years after the invention of the telescope by Dutch lensmaker Hans Lippershey. Using a 20x reflector telescope, he discovered the four largest moons of Jupiter in what is regarded as the beginning of modern astronomy. After 400 years, with more advanced telescopes, the study of star and planet formation became a central theme of modern astrophysics [1, 2]. Important questions include the detailed physical conditions for star-formation, the evolution of circumstellar disks, and the chemistry that leads to the pre-biotic conditions of early Earth-like planets. On a larger scale, the process of star formation and, in particular, starbursts in external galaxies, needs to be investigated to understand how radiation and dynamical feedback affect the overall interstellar medium of galaxies.

The phenomena connected to the formation of stars and planets are best (and often uniquely) studied in the far-infrared regime (0.5 THz to 6 THz). The low extinction at these long wavelengths allows unique observations of details of the star formation process, in particular, during its early phases, when these regions are completely obscured at optical wavelengths by the surrounding dust. The far-infrared wavelength range holds, in fact, the most important spectral signatures of the relevant gas constituents: ions, atoms,

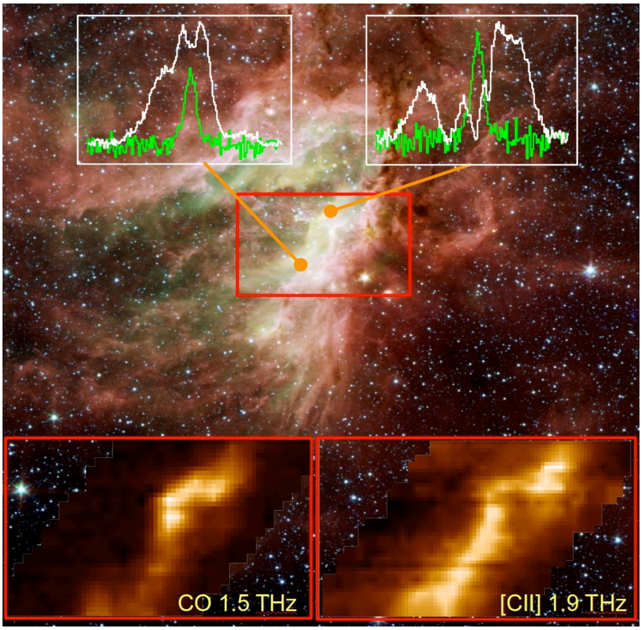

Figure 1.1. The Omega nebula is a nearby region of massive star formation where the winds and radiation of the newly formed stars set their environment aglow in emission lines of atomic and molecular species, while they erode and evaporate the clouds in which they were formed, inhibiting further star and planet formation. The top two insets show spectra in the 1.9 THz line of ionized carbon (white) and the 1.5 THz line of carbon monoxide (green) obtained by the GREAT instrument aboard SOFIA. The bottom two panels show the intensity distribution of these two transitions outlining the regions of intense interaction in the red box. (figure from [3])

and molecules. Fig 1.1 shows an example from the GREAT (the German Receiver for Astronomy at Terahertz Frequencies) instrument on board of SOFIA (Stratospheric Observatory For Infrared Astronomy). As the star and planet formation process proceeds, the newly formed stars alter their environment through strong shocks and radiation, leading to dissociation and ionization of atoms/molecules (collisions and photo processes), and an overall heating of the gas. The gas in these regions then cools predominantly through line radiation of warm molecules and ions. Thus, the measurement of these cooling line fluxes and detailed spectral line shapes directly reveals the energetics and kinematics in these astrophysical environments.

Species	Frequency (THz) (λ in μm)	Importance to the science theme
CII	1.90 (158)	the dominant cooling line of neutral atomic gas and probes directly the energy balance of the interstellar medium of galaxies.
OI	4.74(63)	the strongest line in the neutral regions heated by newly formed massive stars either through radiation in so-called photodissociation regions or in shocks driven by strong stellar winds or jets.
HD	2.67(112)	the main reservoir of deuterium in molecular gas which can be used as a proxy for molecular hydrogen in those environment.
OH	2.50(120)	the key intermediary in interstellar oxygen chemistry.
OH	5.61(53.5)	key pumping line for the 18 cm OH maser in regions of massive star formation and in he nuclei of starburst galaxies and ultra luminous Infrared galaxies (OH mega maser).
OIII	5.77(52); 3.41(88)	the key cooling lines of gas ionized by nearby massive stars.

Table 1.1. An overview of a few key species and the related science at super-terahertz frequency region, data from [4].

Especially at the super-terahertz frequency region (2-6 THz), it features a diversity and large number of fine structure and molecular lines associated with the formation of stars and planets in the Milky Way and nearby galaxies. These include singly ionized carbon CII, neutral oxygen OI, highly ionized atoms such as OIII and NII, as well as key molecules such as HD, H_2D^+, OH, CO, and H_2O. Table 1.1 provides an overview of a few key species together with their frequencies and importance to the different science themes. To detect these terahertz molecular lines, there are two general approaches: incoherent (direct) detection and coherent detection (heterodyne technique).

- incoherent (direct) detection : with low spectral resolution ($\upsilon/\Delta\upsilon<10^3$, where υ is the frequency), and advantages in the study of broadband emission from interstellar dust, unresolved ultra luminous infrared galaxies, and the cosmic background radiation.

- coherent (heterodyne) detection : with high spectral resolution ($\upsilon/\Delta\upsilon > 10^6$, where υ is the frequency), and especially useful in high resolution spectroscopy astrophysics, like studying the atomic and molecular line transitions, but limited by a relative small bandwidth and intrinsic sensitivity limit ($h\upsilon/2k_B$, quantum noise originating from both amplitude and phase are detected)

The choice of optimal detection approach is determined by the goals of the instrument. Among all these key species, the fine-structure line of OI at 4.74 (4.7448) THz is the second brightest line next to the CII line in most galaxies. The fine-structure OI is the dominant cooling line of warm, dense, and neutral atomic gas. In strongly ultraviolet irradiated photodissociation regions (PDRs) and shocks, the OI line flux is generally larger than that of the CII line, making it thus an ideal diagnostic for probing the physical conditions in regions of massive star formation and centers of galaxies. In those regions, it is a unique probe of PDRs, shock waves from stellar winds/jets, supernova explosions, and cloud-cloud collisions. All these radiative and mechanical interactions can excite OI emission over many parsecs and thus shape the interstellar medium of galaxies and drive the overall galactic evolution. Moreover, the emitting regions are often complex, with multiple energetic sources processing the environment. Spectrally resolved observations of the OI line with a heterodyne receiver are key in disentangling this convoluted interaction scheme and permit for the first time the study of the energy balance, physical conditions, morphology and dynamics on scales of entire star forming regions in our Milky Way and also across entire nearby galaxies. In this way, one will gain new and unique insights into the interaction of newly forming stars and gas for a wide range of galactic and extragalactic environments.

HIFI (Heterodyne Instrument for the Far-Infrared) on Herschel is a versatile instrument that can address many key issues in modern astrophysics [5]. However, the upper operating frequency is limited to 1.9 THz. Moreover, Herschel has a limited angular resolution. ALMA (the Atacama Large Millimeter/submillimeter Array), based on telescope arrays, is able to overcome this limit in angular resolution and will offer the observation capability not only at high spectral resolution, but also with unprecedented high angular resolution [6]. Unfortunately ALMA, being a ground-based observatory, is limited to about 1 THz, due to the opacity of the atmosphere. Therefore, a next generation of space- or ballon-borne telescopes will be either operating in an interferometer mode with a few telescopes, like Far-Infrared Interferometer (FIRI) [7], or a telescope with a larger diameter (10 meter), like Millimetron [8], and will be in the frequency range between 1.5-6 THz. And especially, the OI-line at

4.7 THz, as explained, is likely to be one of the key target lines.

Before moving to the detailed description of a super-terahertz heterodyne spectrometer, we will briefly introduce incoherent detection at first.

1.2 Incoherent detection

1.2.1 Transition Edge Sensor (TES)

Transition edge sensor (TES) is a simple bolometer, which contains three parts: an absorber with heat capacity C, a thermometer, and a weak thermal link to a cold bath temperature with thermal conductance G. When photons heat the absorber, the photon energy is converted into heat, which raises the temperature of the absorber. A very sensitive thermometer registers this increase in temperature. The device then cools through the weak thermal link and returns to its quiescent state, ready to detect new coming photons. The time constant of a TES is described as:

$$\tau = \frac{C}{G}, \tag{1.1}$$

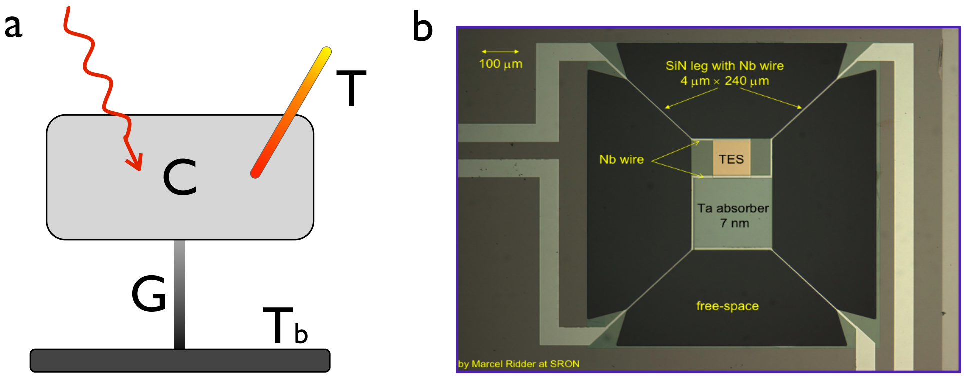

Figure 1.2. A transition-edge sensor detects and counts photons through the change in temperature of a superconducting metal. (a): Schematic of thermal model of a TES. (b): Optical micrograph of a TiAu TES detector integrated with a Ta absorber on Si_3N_4 membrane. The four narrow Si_3N_4 legs, with a thickness of 1 μm, a width of 6 μm and a length of 240 μm, act as low thermal-conductance links between TES and bath temperature. (Figure from J. R. Gao)

where τ is the time constant, C heat capacity and G the thermal conductance. The noise equivalent power (NEP) of a TES, a measure of the sensitivity, is fundamentally limited by the thermal fluctuation noise (or phonon noise) and is expressed as [9]:

$$NEP = \sqrt{\gamma 4 k_B T^2 G}, \tag{1.2}$$

where γ is a constant between 0.5 and 1 that accounts for temperature gradient along the supporting legs. k_B is the Boltzmann's constant, T is the superconducting critical temperature of a TES and G is the thermal conductance. By integrating the TES with SQUID (Superconducting Quantum Interference Device), large pixel arrays can be achieved. For example, more than 6,000 pixels arrays in three bands are planned for SAFARI (SpicA FAR-infrared Instrument) on SPICA (Space Infrared Telescope for Cosmology and Astrophysics) [11] space telescope, and 10,000 pixel arrays for SCUBA-2 (Submillimetre Common User Bolometer Array-2) have already been achieved [12].

1.2.2 Kinetic Inductance Detector (KID)

A new approach to the detection of terahertz photons is to use superconducting resonators [13]. When the terahertz radiation with photon energy larger than the gap energy 2Δ hits the superconducting film cooled below T_c, it breaks up Cooper pairs into unpaired quasiparticles. The increase in quasiparticle density changes the surface impedance $Z_s = R_s + i\omega L_s$, which is probed by applying a microwave signal.

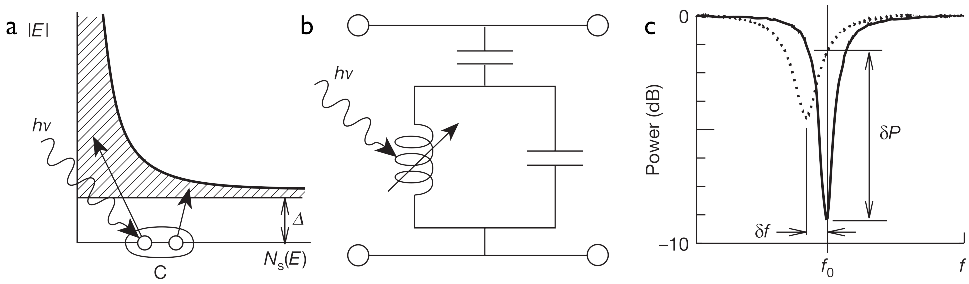

Figure 1.3. An illustration of the detection principle of a Kinetic Inductance Detector. a: A photon with energy larger than the gap energy 2Δ is absorbed and will break a Cooper pair and create quasiparticle on top of the thermal background. b: The variation in the Cooper Pair and quasiparticle densities leads to a change in the kinetic inductance. c: Subsequently the resonance frequency of the circuit shifts.

These devices are simple to fabricate and allow passive frequency-domain multiplexing of up to thousands of resonators through a single coaxial cable and a single HEMT (high electron mobility transistor) amplifier, and as a result it holds great advantages when used for future large pixel array applications. Furthermore, these devices are extremely sensitive and already demonstrated background noise limited sensitivity, which is very promising for next generation instrument, like the newly developed MKID camera for APEX [14] and on-chip spectrometer DESHIMA [15].

1.3 Coherent detection

Coherent detection (heterodyne detection) is a radiation detecting technique by mixing the signal radiation with a reference radiation source using a non-linear mixing element. The mixing process down converts the weak signal at a frequency of f_s together with a local oscillator (LO) at a frequency of f_{LO}, and generates an intermediate frequency (IF) $f_{IF} = |f_s - f_{LO}|$. As an illustration in Fig. 1.4, the intermediate frequency signal preserves both the intensity and phase information of the observing signal, and the frequency will be resolved by a back-end spectrum analyzer. The fundamental spectral resolution of the intermediate frequency signal is determined by a convolution of the local oscillator and the observing signal, but practically, the back-end spectrometer also limits it. The accessible spectral range of f_s around f_{LO} are in practice limited by the receiver detection bandwidth and depends on the frequency roll-off behaviour of the mixer, called the "IF bandwidth".

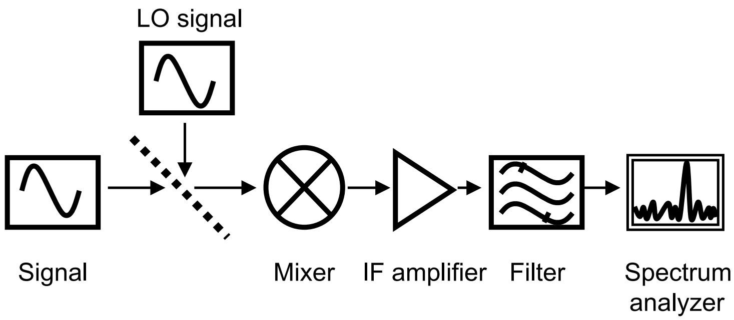

Figure 1.4. Schematic layout of a heterodyne receiver. The local oscillator signal and observing signal are combined and coupled to a mixer. The intermediate frequency signal is generated, amplified and then processed by a spectrum analyzer.

To understand the mixing process, a simple nonlinear device is considered as the mixer with a current (I) and voltage (V) characteristic, *i.e.* $I = \alpha V^2$. By applying the observing signal $V_s(t) = V_s sin(2\pi f_s t)$ and the local oscillator signal $V_{LO}(t) = V_{LO} sin(2\pi f_{LO} t)$ to the mixer, the total voltage V across the device will be $V_s + V_{LO}$. And the resulting current response through the device is:

$$I = \alpha[V_{LO} sin(2\pi f_{LO} t) + V_s sin(2\pi f_s t)]^2, \tag{1.3}$$

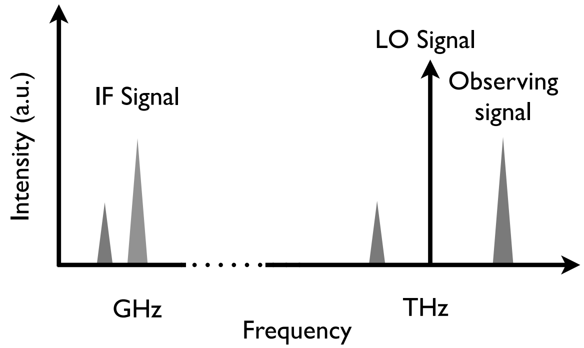

Figure 1.5. Schematic representation of heterodyne detection. The observing signal is combined with a strong local oscillator signal and down-converted to an intermediate frequency f_{IF}.

By solving the simple equation, the resulting current response contains frequencies at $|mf_{LO} + nf_s|$. Limited by the response time of the mixer and back-end circuit, by filtering out all higher frequency terms, the intermediate frequency signal of $f_{IF} = |f_s - f_{LO}|$ is preserved. As shown in Fig. 1.5, signals at $f_{LO} + f_{IF}$ (upper sideband) and $f_{LO} - f_{IF}$ (lower sideband) are down-converted to the same intermediate frequency f_{IF}, which is called the double sideband (DSB) receiver. In contrast, a single sideband (SSB) receiver only down-converts the signal either in the upper or the lower sideband to f_{IF}.

1.3.1 Mixers

Basically, any device with non-linear characteristics could be used as a mixer. However, for astronomical observation, where the signals are in general very weak and deeply embedded within the noise, there are three kinds of mixers available.

Schottky-diodes

Schottky-diodes take advantage of the non-linear current voltage characteristic of a metal-semiconductor junction. Schottky-diodes fabricated with GaAs work over a wide frequency range (up to a few THz), and do not require cryogenic temperature operation. The advantage of such a mixer is a wide IF bandwidth, exceeding 50 GHz [16]. Schottky mixers have been used at terahertz frequencies by a number of groups over the past several decades for astronomical observations at 700 GHz up to 5 THz. However, the main drawback of such mixers is relative poor sensitivity, where the best T_{rec} is about 70,000 K at 4.75 THz [17]. Also the high local oscillator power requirement, about 3-8 mW [18, 19], limits its application.

Superconductor-Insulator-Superconductor mixers

The Superconductor-Insulator-Superconductor (SIS) device is usually made up of SIS tunnel junctions and associated superconducting thin film circuits such as impedance transformer, resonance tuning circuit and RF choke-filter, which are lithographically fabricated as a whole junction device. There are two different tunneling mechanisms in SIS junctions, namely Cooper-pair tunneling originated from zero-dc-bias voltage and quasi-particle tunneling from the junction gap voltage, with the latter used for SIS mixers. Since the Cooper-pair tunneling interferes with the quasi-particle tunneling, it is usually suppressed by a magnetic field in SIS mixers. When a photon is absorbed in an SIS junction biased at a dc voltage lower than the junction gap voltage, Cooper pairs in one superconducting electrode with higher voltage potential can be broken into quasi-particles so long as the total applied energy exceeds the threshold gap energy and subsequently the quasi-particles tunnel into the other superconducting electrode. It is this photon-assisted quasi-particle tunneling that leads to the quantum mixing of SIS junctions, whose details can be found in a comprehensive review paper by Tucker and Feldman [20].

As is well known, SIS tunnel junctions have two unique features, namely a gap voltage (V_{gap}, typically a few millivolts) with extremely narrow transition (ΔV_{gap}) and nearly zero leakage current below the gap voltage, which are essential for SIS mixers to achieve quantum-limited performance. Furthermore, SIS junctions require extremely low LO power in comparison to Schottky diodes. Since the junction's upper frequency is limited by the gap voltage following $\nu_{max} = 2eV_{gap}/h$, which is about 1.4 THz for conventional $Nb/AlO_x/Nb$ tunnel junctions, developing SIS tunnel junctions of higher gap

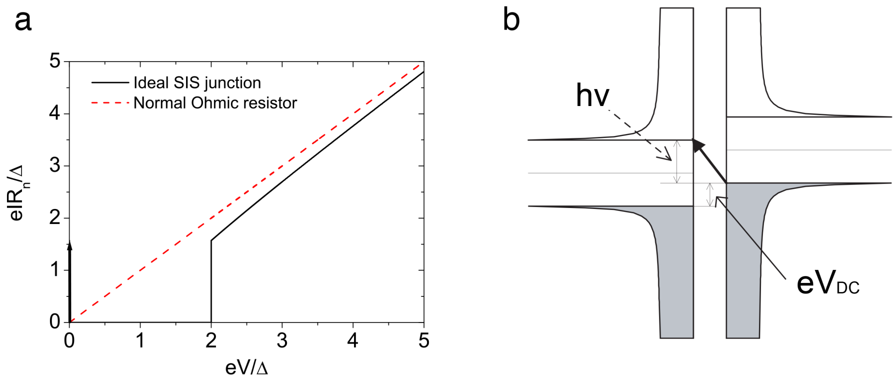

Figure 1.6. (a): Current-voltage (IV) characteristic of an ideal SIS junction at 0 K, and the arrow at V = 0 shows the maximum of the critical current I_c. (b): Quasiparticle tunnelling through an SIS junction, explained by the semi-conductor model, where a photon with energy $h\nu + eV_{DC} > 2\Delta = 2eV_{gap}$, an increasing number of states becomes available for tunneling.

voltages is of particular interest [21]. The required local oscillator power can be relative low, in the μW range. A key advantage of SIS mixers is their near quantum limited sensitivity, especially at frequencies that are low compared to the superconductor's gap frequency. Also the intrinsic IF bandwidth is very large, more than 10 GHz in practice. However, the noise performance dramatically becomes worse as the frequency goes beyond $\nu_{max} = 2eV_{gap}/h$. Until now, the SIS mixers have been only demonstrated up to 1.2 THz [22].

Hot electron bolometer mixers

Superconducting hot electron bolometer (HEB) mixer is based on a microbridge made of an ultra-thin superconducting film such as Nb, NbN and NbTiN, with a typical thickness a few nanometers. The microbridge joins two metallic contact pads that are also part of the antenna for radiation coupling. Since the superconducting films have a sharp transition of resistance at a critical temperature (T_c). The resistance of the device around T_c can be strongly influenced by the absorption of radiation, which makes such devices sensitive incoherent and coherent detectors. For a superconducting hot electron bolometer mixer, with photons absorbed in the superconducting microbridge, electrons in the thin film are heated above the phonon temperature and become "hot electrons", as shown in Fig. 1.7. Then, by either strong electron-phonon interaction and fast phonon escaping (into the substrate) or by a fast electron out-diffusion (into the contact pads), the "hot electrons" relax to the bath temperature. They are thus named as phonon cooled HEB mixers [23] and diffusion cooled HEB mixers [24], respectively. And superconducting hot electron bolometer mixers rely on a bolometric effect and use the power-law as the mixing principle, *i.e.* $V^2/R \propto T(t)$, where $V = V_s cos(\omega_s t) + V_{LO} cos(\omega_{LO} t)$. Since the thermal response of the device is too slow to follow terahertz radiation, only the intermediate frequency term ($|f_s - f_{LO}|$) is left.

The main advantage of superconducting HEB mixer is that they do not suffer from an upper frequency limit set by the superconductor's energy gap frequency. In addition, since the RF impedance of superconducting HEB mixer is essentially resistive [26], the optical coupling of the RF and LO signal to the device can be achieved using a waveguide or quasi-optical structure, without further tuning circuit like a SIS mixer. The sensitivity of superconducting HEB mixers at frequencies above 1 THz is superior to the other mixer concepts. Fig. 1.8 summarizes the current status of the measured noise performance of superconducting HEB mixers from different groups in the world. As shown, the best T_{rec} at 5.3 THz is 1150 K. Also the LO power requirement for superconducting HEB mixers is very low, around a hundred nW on the mixer itself,

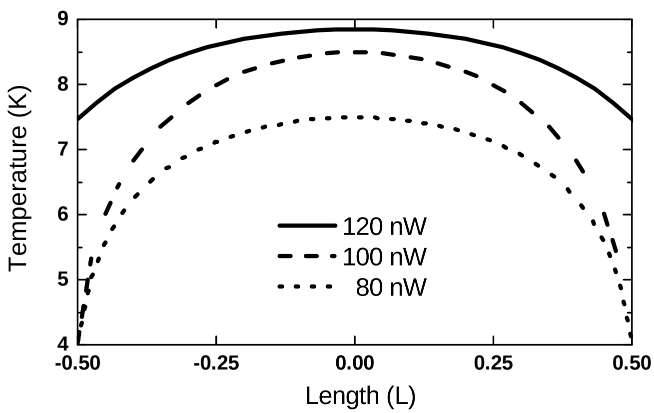

Figure 1.7. Theoretical calculated temperature profiles of the microbridge under constant DC bias current of 25 μA but for different local oscillator power, which indicates the "hot electron" effect of a superconducting HEB mixer, where the bath temperature is 4.2 K. (Figure from [25])

with a device even as low as 30 nW having been demonstrated [27].

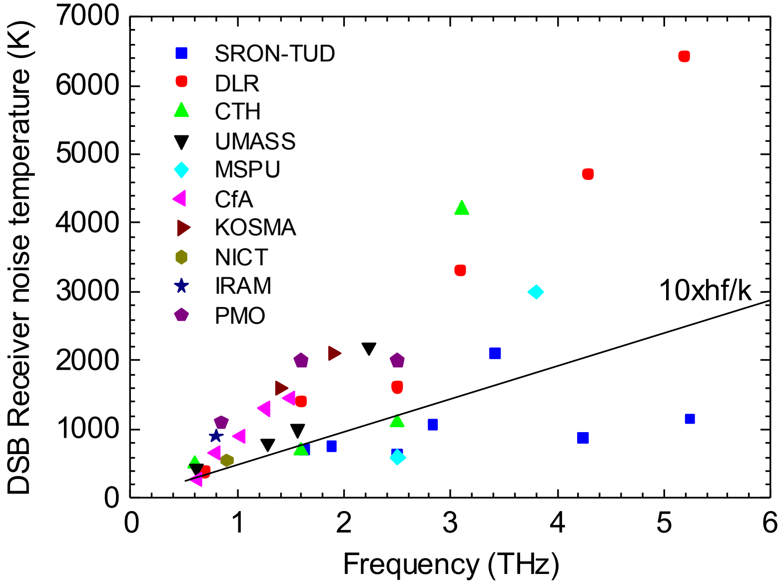

Figure 1.8. State-of-the-art double side band noise temperatures of superconducting HEB mixers from 0.6 to 5.3 THz, reported by different research groups in the world. The sensitivity data at 4.3 and 5.3 THz by SRON-TUD in this plot are obtained in a close collaboration with PMO in China. (Figure from J. R. Gao)

The IF bandwidth is also an important characteristic to the performance of a mixer. For a superconducting HEB mixer, the IF bandwidth is mainly limited by the total thermal relaxation time of the HEB device [27]. By improving the HEB film quality and the interface between the film and the substrate, so far an IF bandwidth of around 5 GHz is measured, which is still smaller than a SIS or a Schottky mixer. Recently, further improvement has been demonstrated for HEB devices combing phonon cooling and diffusion cooling [28], where even larger IF bandwidth is in principle accessible in the future. Over all, superconducting HEB mixers are the best mixer for heterodyne receivers at the frequency range between 1.5 to 6 THz, because of their sensitivities and low local oscillator power requirement.

1.3.2 Local oscillators

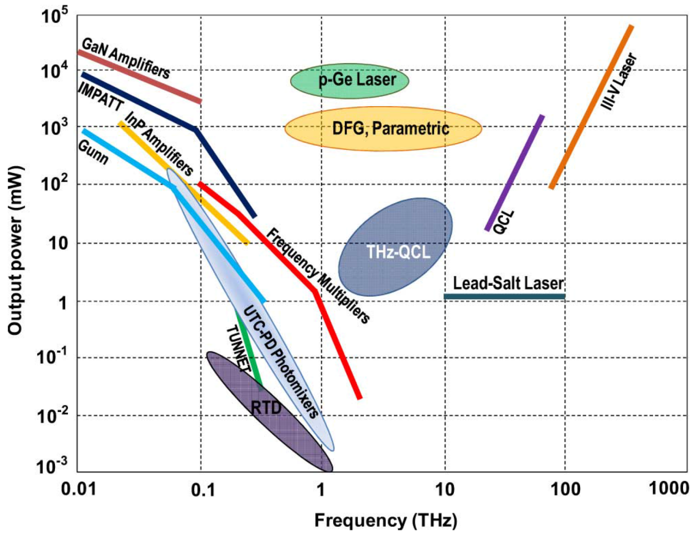

Figure 1.9. Output power as a function of frequencies for terahertz sources. For majority of the sources, the power shown is CW power at room temperature. Power for QCL and III-V lasers are peak power. THz-QCL power is at cryogenic temperatures. IMPATT diode stands for impact ionization avalanche transit-time diode, MMIC stands for microwave monolithic integrated circuit, and TUNNET stands for tunnel injection transit time. (Figure from [29])

As the superconducting detectors have shown superior performance at terahertz frequencies, the local oscillator technology becomes the primary hindrance for future progress of receiver systems. During the last decade, driven by space based missions, solid-state sources based on frequency multiplier chains have dominated at frequencies below 2 THz, and recently are progressing towards 3 THz. With ten years development, terahertz quantum cascade lasers (QCLs) have made tremendous developments and show increasing potential in the future applications. We will go to details of THz QCLs in the next Chapter.

Solid-state Gunn oscillator

Gunn oscillator, consists of two heavily N-doped terminals with a thin layer of lightly doped material in between. As a compact, reliable and long-life duration solid-state system, it is widely used as a local oscillator at low frequencies. For terahertz signal generation, the first stage Gunn oscillator generates a powerful, tunable signal at frequency around 100 GHz, combined with further amplification by solid-state InP microwave monolithic integrated circuit (MMIC) amplifier, the frequencies reach up to 2 THz with 5-20 μW output power [30]. Recently this upper frequency limitation has been pushed up to 2.7 THz by the JPL group [31]. Due to the parasitic inductance and also the response time limitation, output power from a Gunn oscillator drops dramatically as the frequency goes higher. Therefore, an alternative solid-state local oscillator source is desired.

Backward wave oscillator

Backward wave oscillator (BWO) is based on a vacuum tube to generate microwaves up to terahertz frequencies. It provides relative high output power ($\sim$ mW) with a wide frequency tuning range (180-1500 GHz). However, it is high power consumption (2-6 kV operation voltage), and requires high magnetic field ($\sim$1 T) with water cooling. As a result, this bulky construction makes it is impractical for any space- or balloon-borne instrument application. Moreover, the life time of the vacuum tube is relative short ($\sim$hundred hours). A 1.9 THz frequency source, based on a frequency tripled BWO with 1.5 μW output power, is developed as the local oscillator for the GREAT heterodyne receiver on the SOFIA telescope [32], where the output power is enough to operate a superconducting HEB mixer.

Far-infrared gas laser

The optically pumped gas laser is widely used as a signal source at terahertz frequencies in the laboratory, since it provides high output power ($\geqslant$ mW), wide frequency operation range and Gaussian output beam. Moreover, it is commercially available from several companies, like: Edinburgh Instrument and Coherent Inc. Typically, for a far-infrared (FIR) gas laser, a 9 μm or 10 μm signal is generated using a CO_2 laser with relatively high output power (20-100 W) which is then coupled to a resonance cavity filled with certain gas containing molecular transition features at terahertz frequencies (like: CH_3OH), and terahertz signals are generated. For different gases with different transition lines, the output frequencies of a FIR gas laser can be selected. However, high power consumption, finite discrete line frequency and bulky size limit its application.

Photomixer

Photomixer is based on a low temperature growth GaAs semiconductor material as a photoconductor combined with a radiating antenna. Using two continuous infrared lasers with identical polarization but slightly different frequency, a terahertz beat frequency component can be generated. The advantage of the photomixer signal source at terahertz frequencies is a wide continuous tuning bandwidth. However, the conversion gain from infrared to terahertz frequency is pretty low for such a photomixer, which largely limits the output power (1 μW at 1THz and 0.1 μW at 3 THz [33]). Recently, photomixers have been demonstrated as local oscillators at 450 GHz with a SIS mixer and 750 GHz with a superconducting HEB mixer, where an equivalent noise temperature was measured compared with a multiplier based solid-state LO signal source [34].

1.4 Thesis outline

This thesis focuses on a series of experiments to demonstrate a high resolution heterodyne spectrometer using novel terahertz quantum cascade lasers as local oscillators, as well as to identify fundamental limitations for a THz QCL for high resolution spectroscopy applications.

Chapter 2 : Here we briefly introduce terahertz quantum cascade lasers, and the progress made on it for local oscillator applications, including the high temperature performance, far field beam quality and phase locking capability.

Chapter 3 : The principle of a heterodyne spectroscopy and a line profile model are discussed.

Chapter 4 : In this chapter we report a set of measurements to demonstrate a new type of surface emitting distributed feedback quantum cascade laser operated at 3.5 THz as a local oscillator. The emission frequency and tuning capability is characterized using a Fourier Transform Spectrometer, and the far field beam pattern is measured with a less divergent beam along the laser's ridge direction. Also a pumping experiment is made at different operating temperature for the QCL with a superconducting hot electron bolometer mixer, which suggests that such a laser is in principle able to be used as a LO at 70

K.

Chapter 5 : By employing a metal-metal waveguide quantum cascade laser, we demonstrate for the first time a high resolution heterodyne spectrometer at 2.9 THz. High resolution molecular spectral lines are measured and the pressure broadening effect of the gas is also demonstrated.

Chapter 6 : A more advanced high resolution heterodyne spectrometer at 3.5 THz is demonstrated based on a frequency tunable third-order distributed feedback quantum cascade laser. By varying the bias voltage of the laser, we achieved a tuning range of ∼1 GHz of the lasing frequency, within which the molecular spectral lines were recorded. The measured spectra show excellent agreement with modelled ones. Also the frequency and temperature resolution of such a spectrometer are addressed.

Chapter 7 : We report frequency locking of two 3.5-THz third-order distributed feedback (DFB) quantum cascade lasers by using methanol molecular absorption lines, a proportional-integral-derivative controller, and a NbN superconducting bolometer. We show that the free-running linewidths of the QCLs are dependent on the electrical and temperature tuning coefficients. For both lasers, the frequency locking induces a similar linewidth reduction factor whereby the narrowest locked linewidth is below 18 kHz with a Gaussian-like shape, which is sufficient for local oscillator application.

Chapter 8 : In this chapter, we perform an experimental scheme to simultaneously stabilize the frequency and amplitude of a 3.5 THz third-order distributed feedback quantum cascade laser as a local oscillator. The frequency stabilization has been realized using the same principle as in chapter 7. The amplitude stabilization of the incident power has been achieved using a swing-arm voice coil actuator as a fast optical attenuator, using the direct detection output of a superconducting mixer in combination with a 2nd PID loop. Improved Allan Variance times of the entire receiver, as well as the heterodyne molecular spectra, have been demonstrated.

As a result of this work, terahertz quantum cascade lasers become technologically much more mature and convincing such that a new NASA mission: Galactic/Xgalactic Ultra long duration balloon Spectroscopic Stratospheric THz Observatory (GUSSTO) has proposed terahertz quantum cascade lasers as local oscillators together with superconducting hot electron bolometer mixers for a heterodyne cameras at 4.7 THz for detecting neutral oxygen (OI) line. GUSSTO is a long duration balloon based heterodyne spectrometer which contains three frequency bands: 1.4, 1.9 and 4.7 THz. GUSSTO was recently selected as an Explorer Mission of Opportunity proposal for a Phase A-Concept Study, and with the hope to achieve for the first time, the realization of terahertz quantum cascade laser for astronomical observation. Also the local oscillator technology demonstrated in this thesis offers the technique for other instruments, like Oxygen Heterodyne Camera (OCAM), proposed for the 2nd generation instrument on SOFIA.

Bibliography

[1] E. F. van Dishoeck, and A. G. G. M. Tielens, *Space-borne observations of the lifecycle of interstellar gas and dust*, The Century of Space Science, eds. J.A.M. Bleeker et al. 607 (2001).

[2] The Science Vision for the Stratospheric Observatory for Infrared Astronomy (SOFIA), http://arxiv.org/abs/0905.4271v2.

[3] GREAT instrument on SOFIA collected its first THz photons from the M17 SW star forming cloud, http://www.nasa.gov/mission-pages/SOFIA/11-104.html

[4] C. Walker, C. Kulesa, J. Kloosterman, D. Lesser, T. Cottam, C. Groppi, J. Zmuidzinas, M. Edgar, S. Radford, P. Goldsmith, W. Langer, H. Yorke, J. Kawamura, I. Mehdi, D. Hollenbach, J. Stutzki, H. Huebers, J. R. Gao, and C. Martin, *Large format heterodyne arrays for observing far-infrared lines with SOFIA*, Proceedings of SPIE, 77410Z (2010).

[5] Th. de Graauw, et. al, *The herschel-Heterodyne Instrument for the Far-Infrared (HIFI)*, Astronomy and Astrophysics, **518**, L6 (2010).

[6] ALMA-the Atacama Large Millimeter/submillimeter Array, http://www.almaobservatory.org

[7] F. Helmich, and R. Ivison, *FIRI - a Far-Infrared Interferometer*, arXiv:0707.1822

[8] W. Wild, et. al, *Millimetron-a large Russian-European submillimeter space observatory*, Experimental Astronomy, **23**, 221 (2009).

[9] M. Galeazzi, *Fundamental Noise Processes in TES Devices* IEEE Transactions on Applied Superconductivity, **21**, 3 (2011).

[10] D. T. Leisawitz et. al., *Scientific motivation and technology requirements for the SPIRIT and SPECS far-infrared/submillimeter space interferometers*, Proceeding of SPIE, **4013**, edited by J. B. Breckinridge and P. Jakobsen (2000).

[11] SPICA, http://www.ir.isas.jaxa.jp/SPICA/SPICA-HP/index-English.html

[12] SCUBA-2, http://www.roe.ac.uk/ukatc/projects/scubatwo/

[13] P. K. Day, H. G. LeDuc, B. A. Mazin, A. Vayonakis, and J. Zmuidzinas, *A broadband superconducting detector suitable for use in large arrays*, Nature, **425**, 817 (2003).

[14] S. Heyminck, B. Klein, R. Gusten, C. Kasemann, A. Baryshev, J. Baselmans, S. Yates, and T. M. Klapwijk, *Development of a MKID camera for APEX*, Proceeding of 21th International Symposium on Space Terahertz Technology, UK. (2010).

[15] A. Endo, J. J. A. Baselmans, P. P. van der Werf, B. Knoors, S. M. H. Javadzadeh, S. J. C. Yates, D. J. Thoen, L. Ferrari, A. M. Baryshev, Y. J. Y. Lankwarden, P. J. de Visser, R. M. J. Janssen, and T. M. Klapwijk, *Development of DESHIMA: A Redshift Machine Based on a Superconducting On-Chip Filterbank*, Proceeding of SPIE Astronomical Telescopes + Instrumentation, Amsterdam (2012).

[16] M. Morgan and S. Weinreb, *A monolithic HEMT diode balanced mixer for 100-140 GHz*, IEEE MTT-S International Microwave Symposium Digest, 99 (2001).

[17] A. L. Betz and R. T. Boreiko, *A Practical Schottky Mixer for 5 THz*, Proceeding of 6th International Symposium on Space Terahertz Technology, California (1995).

[18] B. N. Ellison, B. J. Maddison, C. M. Mann, D. N. Matheson, M. L. Oldfieldt, S. Marazita, T. W. Crowe, P. Maaskant, W. M. Kelly, *First Results for a 2.5 THz Schottky Diode Waveguide Mixer*, Proceeding of 7th International Symposium on Space Terahertz Technology, Charlottesville (1996).

[19] M. C. Gaidis, H. M. Pickett, C. D. Smith, S. C. Martin, R. P. Smith, and P. H. Siegel, *A 2.5 THz Receiver Front End for Space Borne Applications*, IEEE Transactions on Microwave Theory and Techniques, **48**, 733 (2000).

[20] J. R. Tucker, M. J. Feldman, *Quantum detection at millimeter wavelengths*, Reviews of Modern Physics, **57**, 1055 (1985).

[21] S. C. Shi, *Development of superconducting mixers for THz astronomy*, Science China Information Sciences, **55**, 120 (2012).

[22] A. Karpov, D. Miller, F. Rice, J. A. Stern, B. Bumble, H. G. LeDuc, and J. Zmuidzinas, *Low Noise 1 THz1.4 THz Mixers Using Nb/Al-AlN/NbTiN SIS Junctions*, IEEE Transactions on Applied Superconductivity, **17**, 2 (2007).

[23] E. Gershenzon, G. Gol'tsman, Y. Gousev, et. al. *Electromagnetic-radiation mixer based on electron heating in resistive state of superconductive Nb and YBaCuO films*, IEEE Transactions on Magnetics, **27**, 1317 (1991).

[24] D. Prober, *Superconducting terahertz mixer using a transition-edge microbolometer*, Applied Physics Letters, **62**, 2119 (1993).

[25] W. Miao, Y. Delorme, A. Feret, R. Lefevre, B. lecomte, F. Dauplay, J. M. Krieg, G. Beaudin, W. Zhang, Y. Ren, and S.C. Shi, *Comparison between hot spot modeling and measurement of a superconducting*

hot electron bolometer mixer at submillimeter wavelengths, Journal of Applied Physics, **106**, 103909 (2009).

[26] E. L. Kollberg, K. S. Yngvesson, Y. Ren, W. Zhang, P. Khosropanah, and J. R. Gao, *Impedance of Hot-Electron Bolometer Mixers at Terahertz Frequencies*, IEEE Transactions on Terahertz Science and Technology, **1**, 2 (2011).

[27] M. Hajenius, J. J. A. Baselmans, A. Baryshev, J. R. Gao, T. M. Klapwijk, J. W. Kooi, W. Jellema, and Z. Q. Yang, *Full characterization and analysis of a terahertz heterodyne receiver based on a NbN hot electron bolometer*, Journal of Applied Physics. **100**, 074507 (2006).

[28] I. Tretyakov, S. Ryabchun, M. Finkel, A. Maslennikova, N. Kaurova, A. Lobastova, B. Voronov, and G. Gol'tsman, *Low noise and wide bandwidth of NbN hot-electron bolometer mixers*, Applied Physics Letters, **98**, 033507 (2011).

[29] G. Chattopadhyay, *Technology, capabilities, and performance of low power terahertz sources*, IEEE Transactions on Terahertz science and technology, **1**, 33 (2011).

[30] J. Ward, F. Maiwald, G. Chattopadhyay, E. Schlecht, A. Maestrini, J. Gill, and I. Mehdi, *1400-1900 GHz Local Oscillators for the Herschel Space Observatory*, Proceeding of 14th International Symposium on Space Terahertz Technology ISSTT, Arizona (2003).

[31] A. Maestrini, I. Mehdi, R. Lin, J. V. Siles, C. Lee, J. Gill, G. Chattopadhyay, E. Schlecht, B. Thomas, and J. Ward, *A 2.5-2.7 THz Room Temperature Electronic Source*, Proceeding of 22nd International Symposium on Space Terahertz Technology, Arizona (2011).

[32] M. Philipp, U. U. Graf, A. Wagner-Gentner, D. Rabanus, and F. Lewen, *Compact 1.9THz BWO local-oscillator for the GREAT heterodyne receiver*, Infrared Physics and Technology, **51**, 54 (2007).

[33] S. Marsuura, G. A. Blake, R. A. Wyss, J. C. Pearson, C. Kadow, A. W. Jackson and C. Gossard, *A traveling-wave THz photomixer based on angle-tuned phase matching*, Applied Physics Letters, **74**, 2872 (1999).

[34] I. C. Mayorga, P. Munoz, E. A. Michael, M. Mikulics, A. Schmitz, P. van der Wal, C. Kaseman, R. Gusten, K. Jacobs, M. Maeso, H. Luth and P. Kordos, *Terahertz photonic mixers as local oscillators for hot electron bolometer and superconductor-insulator-superconductor astronomical receivers*, Journal of Applied Physics, **100**, 043116 (2006).

Chapter 2

Terahertz quantum cascade laser as a local oscillator

2.1 Terahertz quantum cascade laser

Quantum cascade lasers (QCLs), based on the idea of using artificially engineered materials to achieve desired transition energies, were demonstrated at 4 μm (75 THz) at Bell Labs in 1994 [1]. Its radiative transition takes place entirely within the conduction band between quantized states in the heterostructure quantum wells, which is fundamentally different from conventional semiconductor lasers. The advantage of this approach is that the photon energy results from an inter-subband transition and can be artificially modified by adjusting for the thickness of the coupled wells and barriers. Additionally, the cascading process increases the quantum efficiency of the device, since each electron will generate N photons while cascading through the N identical quantum modules. Furthermore, the inter-subband transition inherently provides high optical gain and narrow optical gain width, which will be further discussed in this chapter. Since their introduction, QCLs have become the dominant signal source at mid-infrared frequencies, with wide frequency coverage (λ= 3-24 μm), room temperature operation and high output power (> 100 mW).

At terahertz frequencies, because of the lack of appropriate inter-band materials, this inter-subband transition approach seems to be a natural route to generate terahertz radiation. However, it took about 8 years after the first mid-infrared QCL to realize the first terahertz QCL [2]. It is more challenging to realize a THz QCL, partially because photon energies at terahertz frequencies are small ($h\nu$ = 4-24 meV). With the small photon energies, to achieve population inversion for such closely spaced subbands, selective injection and removal of electrons become difficult. Moreover, THz radiation is more lossy

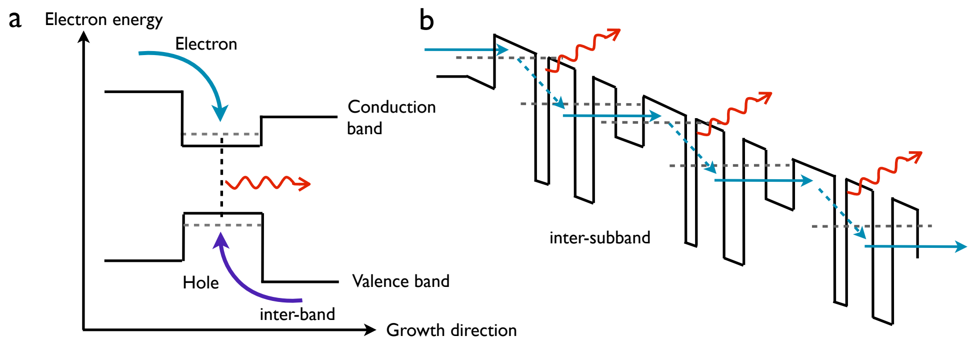

Figure 2.1. Schematics of (a), inter-band transition, where a conventional semiconductor laser emits light as a result of electron-hole inter-band transition. (b), inter-subband emission, where a quantum cascade laser emits light as a result of inter-subband transition within the conduction band. Electron energy is on the vertical axis, growth direction (that is, depth within laser material) on the horizontal axis. The valence band for the inter-subband structure is not shown. (Figure from [3])

within the laser cavity due to the increase of absorption by free carriers with wavelength [4].

2.1.1 Active-region design

To understand the principle of a terahertz quantum cascade laser, in Fig. 2.2 we plot a schematic drawing of basic transport. Basically, the performance of a certain laser is evaluated by the gain, which defines the ability of a laser medium to transfer the part of its energy to the emitted electromagnetic radiation. For a quantum cascade laser, the gain is given by:

$$g \propto \frac{\Delta N f_{32}}{\Delta \nu}, \tag{2.1}$$

where ΔN is the population inversion between the radiative levels 3 and 2 as shown in Fig. 2.2, f_{32} the oscillator strength of the radiative transition and $\Delta\nu$ the spontaneous emission linewith of the radiation. With a certain current density J, electrons are injected into level 3. These electrons could either relax to level 2 with a time τ_{32}, parasitically scatter out to level 1 with a time τ_{31}, or escape to the continuum with a time τ_{esc}. The depopulation rate of the lower state is τ_2, and the population inversion factor ΔN is expressed as:

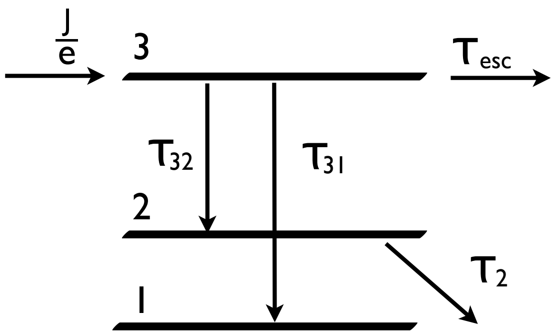

Figure 2.2. Basic transport schematic for generic terahertz quantum cascade laser

$$\Delta N \propto \frac{J}{e}\tau_3(1-\frac{\tau_2}{\tau_{32}}), \tag{2.2}$$

From this equation, it can be seen that to obtain a large population inversion, one requires $\tau_{32} \gg \tau_2$ and τ_3 as much as possible.

For a mid-infrared QCL, to achieve the population inversion, longitudinal-optical phonon scattering is the dominant carrier scattering mechanism. However, at terahertz frequencies, the photon energy (4-24 meV) is smaller than the longitudinal-optical phonon energy in GaAs ($E_{LO} = 36\ meV$), which makes such scattering mechanism difficult in the THz range. In fact, at terahertz frequencies, to achieve the population inversion for such closely spaced subbands requires more selective injection and relaxation of electrons. Here we briefly introduce various quantum well active region designs.

Chirped superlattice

Despite all the difficulties mentioned, several groups have developed certain approaches leading to successful THz QCL realization. For the first THz QCL [2], it was based on the chirped superlattice active region design, which has been previously used for mid-infrared QCLs. Such active region design is based on several quantum well states coupled together to form the so called minibands separated by minigap, where the well width determines the minigap and the barrier thickness determines the miniband. The radiation transition is designed to take place between the bottom state of the upper miniband and the top state of the lower miniband. A population inversion is established on the principle that the scattering of electrons within the miniband (intra-miniband scattering) occurs much faster than inter-miniband scattering. As a result, the carriers tend to relax to the bottom of each miniband, and leave the lower radiative state relative empty. Thus, an electron scatters from the upper miniband to the lower miniband, and generates a terahertz photon emission. Then due to a fast intra-miniband relaxation process, the electron moves to the bottom of the lower miniband, and injected into the upper miniband of the next unit. For a superlattice QCL, due to the large overlap of minibands, the oscillator strength of the transition f_{32} is very large.

Bound-to-continuum

The original chirped superlattice has led to a new bound-to-continuum structure [5], which still relies on the mini bands for depopulation of the lower radiative state. The difference is that, the upper radiative state is essentially made to be an isolated state instead of a miniband, for the bound-to-continuum structure. By doing this, a more diagonal radiative transition is achieved with a slightly reduced oscillator strength. However the injection process is more effective, since the injection states couple more strongly with the upper state compared with miniband configuration. As a result, the temperature and power performance is improved for the bound-to-continuum quantum cascade lasers.

Resonant phonon

The other major active region type is the resonant phonon design, which is fundamentally different from the previous two approaches. It does not rely on a superlattice for depopulation, but uses a combination of resonant tunneling and direct electron longitudinal-optical phonon scattering. For conventional mid-infrared wavelength QCLs, the energy separation between injection states and lower radiative states is designed to be approximately $E_{LO} = 36\ meV$, which makes electrons in the lower radiative state scatter very quickly into the injection states by emitting a longitudinal-optical phonon. However, for the early THz QCLs, it was difficult to use longitudinal-optical phonon scattering mechanism to depopulate the lower radiative states rather than also depopulating the upper radiative states, because of the close subband energy spacing. So the main advantage of the resonant phonon scheme is bringing the lower radiative state into a broad tunneling resonance with the excited state in the adjacent quantum wells. The lower radiative states remain in a strong spatial overlap with the injection states. Thus a fast and selective depopulation via longitudinal-optical phonon scattering is achieved. Inherently, the upper radiative states have little overlap with the injection states, which suppresses non-radiative scattering. Furthermore, the large energy separation between the injector states and the lower radiative states ($> E_{LO} = 36\ meV$) inherently provides intrinsic protection against thermal backfilling of the lower radiative states. So the resonant phonon design is in potential simply the quantum well design, where with only two wells per module has been demonstrated [6]. And all these properties for the resonant phonon design allow higher temperature operation of lasers at longer wavelengths.

2.1.2 Waveguide design

In general, a laser contains two critical components: a gain medium to amplify the radiation, and a waveguide to confine the radiation and provide optical feedback. A major challenge to realize a terahertz quantum cascade laser is the strong absorption of radiation by free carriers at longer wavelengths for the doped semiconductor cladding layers. Thus, a low loss waveguide is crucial in order to achieve THz radiation from a quantum well structure. In fact, the threshold condition for a waveguide is usually expressed as:

$$\Gamma g_{th} = \alpha_w + \alpha_m, \tag{2.3}$$

where g_{th} is the threshold bulk gain of the active region and Γ is the confinement factor of the mode in the active region. α_w is the waveguide absorption loss and α_m is the mirror loss due to the finite mirror reflectivities, which is:

$$\alpha_m = -\frac{ln(R_1 R_2)}{2L}, \tag{2.4}$$

where R_1 and R_2 are the waveguide facet reflectivities, and L is the cavity length. Until now, the dominant waveguide designs are the semi-insulating surface plasmon (SI-SP) and the metal-metal (MM) waveguide, and also some new types of waveguide are introduced, like the waveguide with distributed feedback (DFB) structures, which will be discussed later in this chapter.

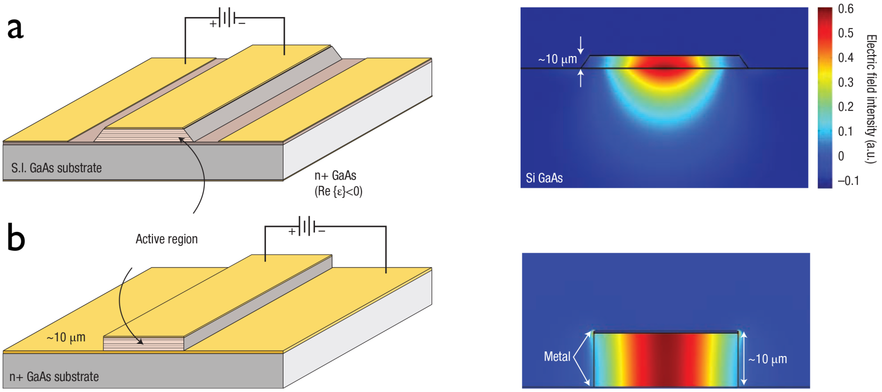

Figure 2.3. Schematic diagram of terahertz quantum cascade lasers (a) a semi-insulating surface plasmon waveguide and (b) a metal-metal waveguide. The right panel shows two-dimensional mode intensity patterns. (Figure from [4])

Semi-insulating surface plasmon

The first THz QCL was based on the surface plasmon waveguide [2]. It contains a growth of a thin (0.1-1 μm thick) heavily doped layer underneath the 10 μm thick active region. As shown in Fig. 2.3, the entire structure lays on top of a semi-insulating GaAs substrate. The mode field penetrates into the substrate (GaAs), since the highly doped layer is thinner than its own skin depth. The confinement factor Γ is about 0.1-0.5, where the mode is loosely confined and enables wider ridges without multi-mode emission. As a result, the emission far-field beam pattern from a semi-insulating surface plasmon QCL is in general a more directional beam (small divergence) due to a relatively large emitting area. Furthermore, it also generates relatively high output power because of the wide ridge. However, the drawback of such a waveguide is that, the modes tend to be squeezed into the substrate if the ridge is too small, which to some extent limit the device size and high temperature performance.

Metal-metal

Metal-metal waveguide employs two metal layers for mode confinement, where the active region is placed in between the metallic waveguides. This scheme is essentially a microstrip waveguide which is commonly used at microwave frequencies. Thus, a mode confinement factor with a value of approximately 1 is achieved. As show in Fig. 2.3, the mode does not propagate beyond the metal plates. Because of impedance mismatch of the sub wavelength mode at the waveguide facet with free-space propagating modes, metal-metal waveguides have a higher facet reflectivity of R = 0.5-0.9. As the threshold current density J_{th} is expressed:

$$J_{th} \propto \frac{\alpha L_P}{f_{osc}}, \tag{2.5}$$

where $\alpha = \alpha_w + \alpha_m$ is the total loss, L_P the length of the period and f_{osc} the oscillation strength. As a result, the metal-metal waveguides, with relative small mirror losses, exhibit smaller threshold current density J_{th} and increased operating temperatures.

Because the mirror losses (α_m = 1-2 cm^{-1}) are only 5-20 % compared with the waveguide losses (α_w = 10-20 cm^{-1}), only a small portion of the generated photons are radiated instead of being absorbed. In contrast, for a semi-insulating surface plasmon waveguide, a more favorable ratio of mirror losses to waveguide losses makes higher power out-coupling efficiency. On the other hand, the subwavelength dimension of metal-metal waveguide ($\sim$ 10 μm high), causes highly divergent far-field beam since the free space wavelength ($\sim$ 100-200 μm) is typically much larger than the waveguide dimension. However, many efforts have been made to improve the radiation out-coupling efficiency and the far-field beam pattern. As in [7], a metal-metal waveguide quantum cascade laser together with a silicon lens has demonstrated a peak pulsed power of 145 mW at 5 K with a wall-plug power efficiency of 0.7 %.

2.2 High temperature operation

The improvement of temperature performance of a terahertz quantum cascade laser appears to be the most important research goal in the field, as the first terahertz QCL demonstrated in 2002 only operated up to a maximum temperature of $\sim$40 K in the pulsed mode [2]. Until now, remarkable improvements in the active region and waveguide design have been made that, for instance: the maximum reported operating temperature is $\sim$200 K for a 3.2 THz laser in pulsed mode [8], in the continuous wave mode with over milliwatts of power at the liquid nitrogen temperature and lasing up to 117 K [9].

For a terahertz QCL, the major challenge for high temperature operation is the degradation of population inversion. As clearly explained in [4], there

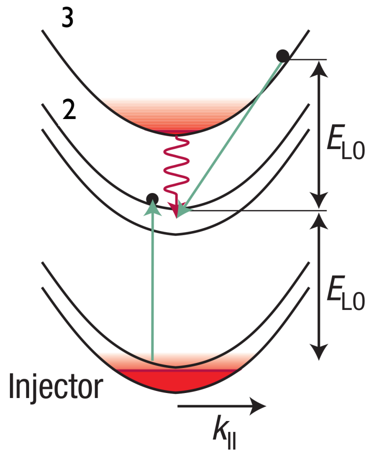

Figure 2.4. Schematic of the subband in-plane dispersion diagram for an resonant phonon device, with the two major temperature degradation processes illustrated as green arrows. (Figure from [4])

are primarily two processes causing the deterioration of the high temperature performance: thermal backfilling and thermally activated phonon scattering. Fig. 2.4 schematically depicts these two process. Backfilling (arrow in Fig. 2.4) of the lower radiative state with electrons from the heavily populated injector takes place by either thermal excitation, or by re-absorption of non-equilibrium longitudinal-optical phonons. The other mechanism is the onset of thermally activated longitudinal-optical phonon scattering, as electrons in the upper subband acquire sufficient in-plane kinetic energy to emit a phonon and relax to the lower subband. This causes the upper state lifetime to decrease exponentially according to

$$\tau_{32}^{-1} \propto exp[-(E_{LO} - h\nu)/k_B T_e], \tag{2.6}$$

also, the threshold current density increases exponentially as shown in Fig. 2.4:

$$J_{th} = J_0 + J_1 exp(T/T_0), \tag{2.7}$$

Until now, numerous terahertz QCL designs have been reported in literature. As shown in [4,10], in the plot of maximum operating temperature versus frequency survey for terahertz QCLs, all the designs with resonant-tunnelling injection technique show the highest operation temperature, which is empirically not higher than hν/k_B across the entire frequency range. And this linear dependence for the maximum temperature with operation frequency is partly because the dynamic range in lasing for bias current diminishes as the operation frequency goes lower. The low frequency $h\nu$ exhibits a weaker increase in J_{th} versus temperature but also smaller dynamic range for lasing, which is due to the reduced injection and depopulation selectivity from the very closely spaced energy levels [4, 10]. This $h\nu/k_B$ limitation suggests a trend that a room temperature terahertz QCL with the present material is difficult.

However, recently, a new high temperature record is reached by optimizing the lasing transition oscillator strength of the resonant phonon based on a three well design [8]. With operation at 8 K, the device showed a peak output power of $\sim$ 38 mW, and the emission frequency blue-shifting from 2.6 to 2.85 THz with increasing bias. At maximum operating temperature of 199.5 K, the emission frequency shifted to 3.22 THz. Also as demonstrated by the MIT group [10], based on a new scattering-assisted injection mechanism, a 1.8 THz QCL operates up to a heat-sink temperature of $\sim$163 K, which is 1.9 $h\nu/k_B$. The peak output power at 155 K is in excess of 2 mW. This development breaks the $h\nu/k_B$ limitation and initiates new design strategies for realizing a room temperature terahertz QCL.

For the purpose of a local oscillator, high temperature operation of a terahertz quantum cascade laser is also critical. Because of the strong opacity of the Earth atmosphere, ground based astronomical observation is limited up to roughly 1.5 THz on the best sites such as Chile and Antarctica. As a result, the application of terahertz QCL as a local oscillator for any space- or ballon-borne project is not favourable, due to the requirement of cryogenic operation. A surface-emitting distributed feedback QCL at 3.5 THz has been demonstrated to be operated at 60 K as a local oscillator, and suggested enough power even at 70 K by estimation, which is discussed in Chapter 4. Combined with a Stirling cooler, a 3.1 THz QCL has been demonstrated as a compact and low power consumption terahertz radiation source [11]. For such a cryocooler, it only requires 240 W of electrical input power, and generates 7 W cooling power at 65 K. This approach is an attractive option for terahertz QCLs as local oscillator and may result in future scientific instruments.

2.3 Beam quality

As it is shown in a terahertz QCL with metal-metal waveguide Fabry-Perot cavity, due to sub-wavelength dimensions of the cavity, the far-field emission beam is strongly divergent [12]. Because of coherent radiation and interference of the radiation emitting from the entire laser bar, the far-field beam also shows ringlike interference patterns [12]. All these facts make a relative low power coupling efficiency, when guiding THz QCL radiation to a Gaussian beam and phase sensitive detector, like a superconducting HEB mixer. As shown in [13], for the first demonstration of a heterodyne receiver based on a terahertz quantum cascade laser, only 1.4% of the total output power from a 2.8 THz QCL was coupled to a superconducting HEB mixer. Since a terahertz QCL in general provides high output power ($\sim$ mW), it is more than enough to drive a superconducting HEB mixer which requires typically only hundreds of nW of LO power. However, this poor beam coupling efficiency becomes a serious problem for practical instrument application, where a single terahertz QCL operated at a relative high operation temperature needs to drive a multi-pixels mixer array. As a result, a terahertz QCL with low divergent and symmetric, ideally Gaussian-like, beam pattern is highly desired.

2.3.1 Surface emitting, second-order DFB THz QCLs

Distributed feedback (DFB) lasers do not rely on conventional cavity mirrors (Fabry-Perot cavity), but provide a feedback mechanism based on backward Bragg scattering from periodic perturbations of the refractive index or the laser gain medium itself. The main advantage of a DFB waveguide is to provide strong spectral selection, which leads to a single-mode operation, as required by local oscillators.

As for the Bragg condition:

$$2\Lambda n_{eff} = N\lambda_0, \tag{2.8}$$

where Λ is the grating periodicity, n_{eff} the average refractive index, λ_0 the wavelength in the air. By considering the propagation constant β:

$$\beta = n_{eff}k_0 = \frac{2\pi n_{eff}}{\lambda_0}, \tag{2.9}$$

and the reciprocal vector G:

$$G = \frac{2\pi}{\Lambda_0}, \tag{2.10}$$

For an N_{th} order distributed feedback laser, according to the Bragg condition, the grating structures provide N diffraction wave vectors as shown in Fig. 2.5. Also the N_{th} diffraction wave vector β_n has to reach -β propagation constant in order to generate feedback. The wave vectors which locate within the light cone will be coupled out for emission, where the dimension of the

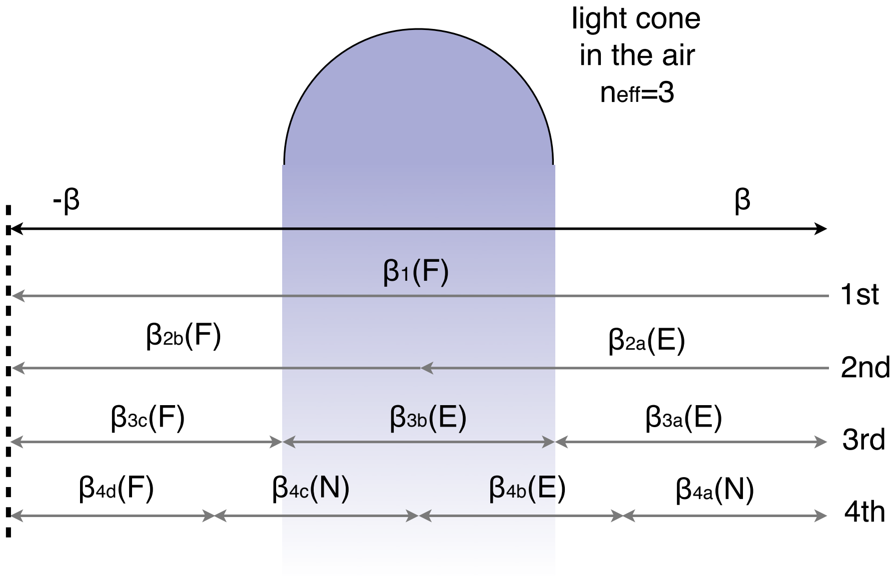

Figure 2.5. Schematic of the Bragg reflection conditions for gratings of various order N. Arrows labelled β represents mode propagating inside the semiconductor and $\beta_{Na,b,c}$ represent the grating diffraction vectors, with the label of emission mode (E), feedback mode (F), and non-coupling mode (N). The upper half circle represents the light cone, which has a radius equal to the wave vector of the mode propagating constant in the air k_0 (n_{eff}=3 in this case). (Figure from [14])

light cone and the emission angle are determined by the refractive index of the medium.

To preserve the advantage of a metal-metal waveguide structure, a new concept of laser structure, surface emitting second-order distributed feedback THz QCL has been developed [15,16]. By implementing second-order gratings in metal-metal waveguides, the radiation is coupled out from the top surface. As a result, due to a larger emitting area (40 μm $\times$ 1070 μm [15]), a narrow far-field beam pattern is achieved. Alternatively, having periodic discontinuity in the laser's top metallic lay will also increase the cavity mirror loss α_m. As the laser's output power is proportional to the factor $\alpha_m/(\alpha_w + \alpha_m)$, where α_w is the waveguide loss, the output power has the potential to be improved due to the increased α_m. Furthermore, a combination of techniques including precise control with the phase of reflection at the facets, and use of metal on the sidewalls to eliminate higher-order lateral modes, allow robust single-mode

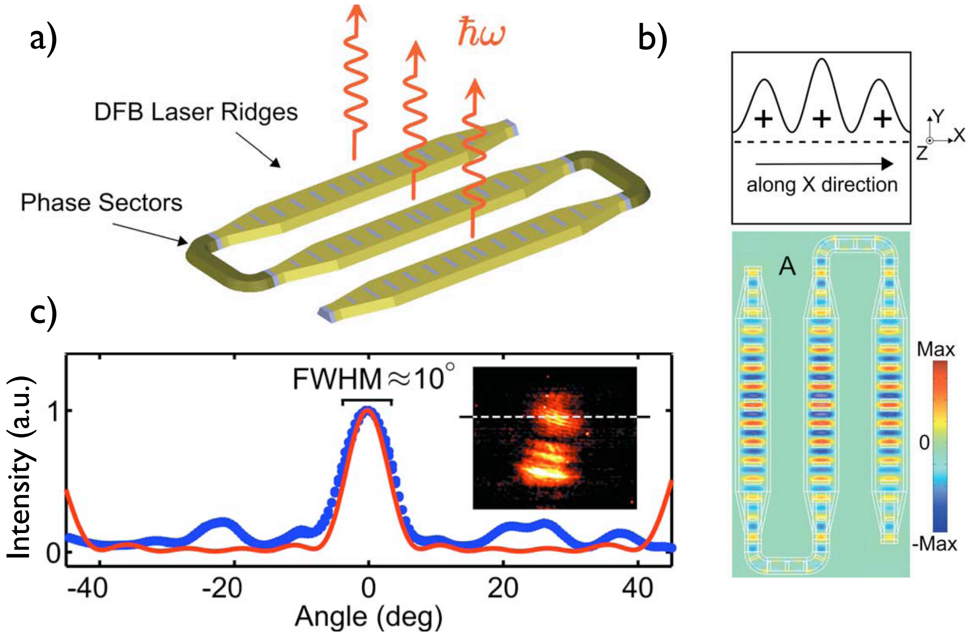

Figure 2.6. (a) Schematic of a three-ridge THz QCL array for single-mode DFB operation to obtain narrow beam pattern in both the transverse and the longitudinal directions. (b) Magnetic field inside the laser ridges for the desired "in-phase" mode from a 3-D full-wave finite-element method simulation. (c) Measured (blue) and calculated (red) far-field "in-phase" beam pattern along the transverse direction from the six-ridge array. (Figure from [17])

operation over a range of approximately 0.35 THz. A single-lobed far-field radiation pattern is obtained using a π phase-shift in the center of the second-order Bragg grating [15]. Such a device has been studied and characterized as a local oscillator using a superconducting HEB mixer, which is in detail described in Chapter 4.

However, the far-field beam pattern of such surface emitting terahertz QCL shows an asymmetric pattern, where the beam is narrow along the laser ridge direction but broad in the slit direction. Recently, a new approach based on phase-locked array of such surface emitting terahertz QCLs has been demonstrated [17]. As shown in Fig. 2.6, the beam along the transverse direction from the laser array is much improved, where a measured full width at half maximum (FWHM) is around 10 deg. As a result, a two dimensional phase-locked laser array with more symmetric and less divergent beam pattern has been achieved. In addition, the phase sector between each laser can be individually biased to provide another fine frequency tuning mechanism which could be used for frequency or phase locking applications.

2.3.2 Third-order distributed feedback QCL

As can be seen, for the first- and second-order grating structure, the feedback does not depend on the initial propagation constant β. And especially for the second-order, both backscattering and vertical emission are always possible. For the third-order DFB structure, with a GaAs gain medium ($n = 3.6$), essentially the emission is only possible inside the medium because of the large refractive index difference, where total internal reflection happens. It can be noticed that if the condition $n = 3$ is fulfilled, then the diffraction vectors β_1 and β_2 can reach the light cone and be emitted. This originates the birth of the first third-order DFB QCL at terahertz frequencies. Furthermore, for a realistic case, the laser structure has a finite length L. As a result, the coupling strength between the different modes of the waveguide is no longer a delta function but has certain width, which is related to the numbers of the periodicity.

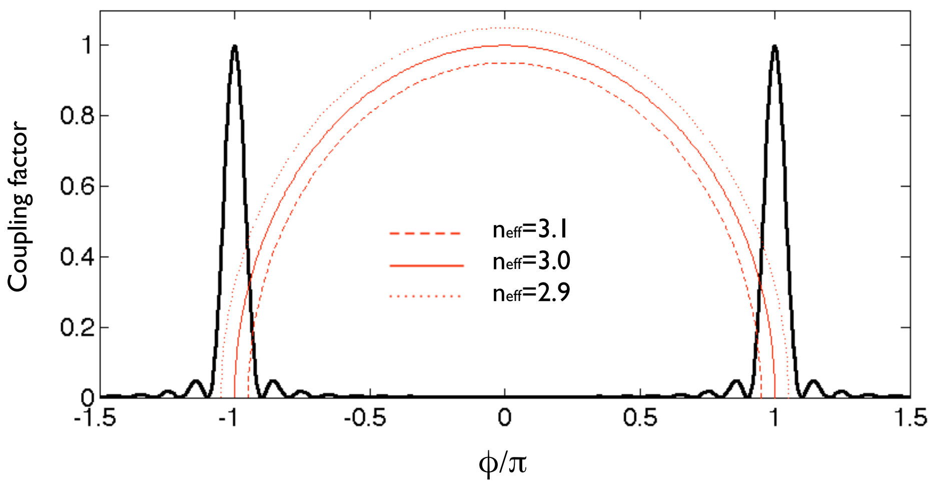

Figure 2.7. Calculated antenna array coupling factor based on 20 element array with a periodicity $2\Lambda = \lambda_0$, which is plotted as the black curve in the figure. Also shown are the half circles indicate the coupling conditions for structures with different refractive index ($n_{eff} = 3.1$, 3, and 2.9 respectively).

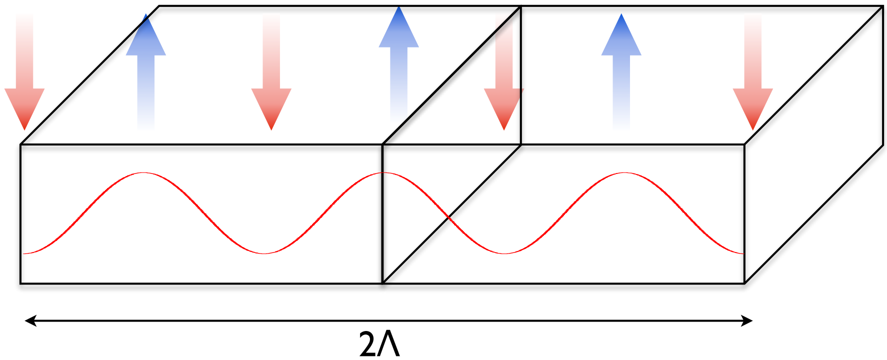

Figure 2.8. Electrical field inside a third-order DFB waveguide where the periodicity $\Lambda = 3/2\lambda_0$.

As shown previously, due to a relatively large refractive index contrast between GaAs and the air medium, the first and second-order diffraction vectors cannot be coupled out. The main challenge in achieving a third-order DFB laser based on the GaAs is to lower the refractive index of the gain medium. It was in 2009, that M. I. Amanti in ETH first realised a terahertz third-order DFB QCL. As shown in [18], it was achieved by deep dry etching of the semiconductor along the waveguide, alternating the active region and air with a duty cycle of $\sim$ 10% ((3.6x9+1x1)/10 = 3.34). And due to the finite length of the laser cavity, a relatively high coupling strength can still be achieved with a refractive index slightly higher than 3. Also, according to an antenna model theory [19], it contributes to the small tilting of the far-field beam pattern.

As from the Bragg condition for a third-order DFB, it is shown, by making the $n_{eff} = 3$, the grating periodicity becomes: $2\Lambda = 3\lambda_0$. As plotted in Fig. 2.8, the electrical field is anti-phased for the adjacent two grating sections and provides a phase shift of π. From the antenna theory, all the periodic structures contribute as an antenna array, which holds an array factor:

$$(AF)_N = \frac{sin(\frac{N}{2}\phi)}{Nsin(\frac{1}{2}\phi)}, \tag{2.11}$$

and,

$$\phi = k\Lambda cos\theta + \beta, \tag{2.12}$$

where k is the wave vector, Λ is the grating periodicity, θ is the tilting angle and β is the phase shift which equals to π here. With $\Lambda = 0.5 \times \lambda_0$, the maximum of the array factor happens at $\phi = \pm 2\pi$:

$$k\Lambda cos\theta + \beta = \pm 2\pi, \tag{2.13}$$

then we have the $\theta = 0°$ or $180°$, where the array antenna becomes an end-fire antenna radiating towards only one direction.

Based on the antenna theory, the far-field beam pattern of a third-order DFB QCL can be calculated by considering the end-fire antenna condition. As shown in Fig. 2.9, when the refractive index $n_{eff} = 3$, the far-field beam pattern shows a low divergent beam with very high main beam coefficient ($>$ 90%). As the n_{eff} deviates from 3, the pattern becomes more divergent with relative strong high order diffraction rings.

The significant advantages of such a third-order DFB grating structure are as follows [20]: a.) the gratings provide feedback for the single optical mode and also enhance the emission power coupling efficiency b.) all the grating structures behave like an end-fire antenna, which makes a low divergent far-

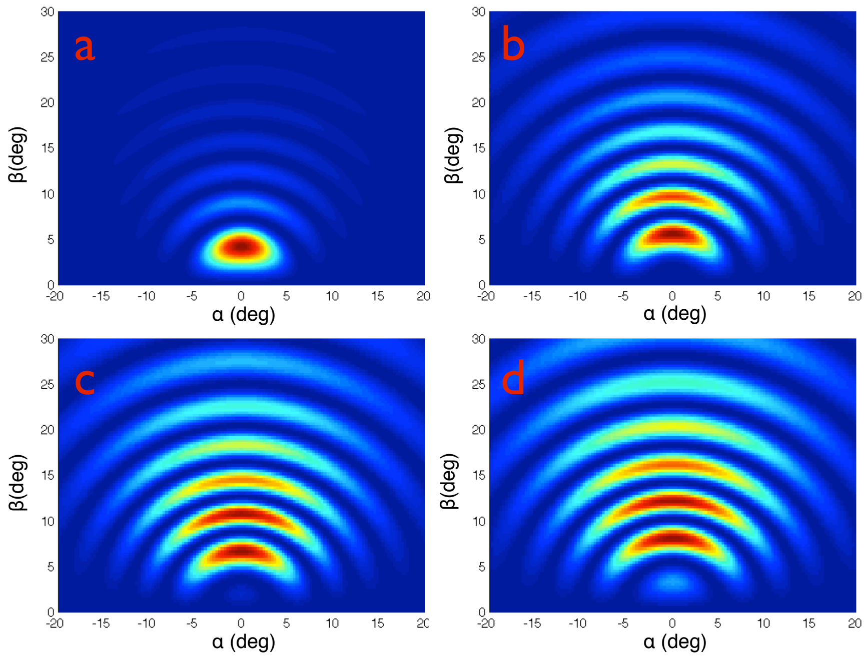

Figure 2.9. Calculated two dimensional far-field beam pattern for a third-order DFB QCL with 30 elements and different refractive index a: 3.0, b: 3.2, c: 3.4, d: 3.6, respectively. The pattern is calculated at a distance of 100×λ from the QCL as a function of angle in degree.

field beam pattern. In fact, these advantages make such lasers favourable for local oscillator application since the enhanced power efficiency facilitates the low power consumption requirement and the low divergent beam improves the beam coupling efficiency to a mixer. Furthermore, a third-order DFB terahertz quantum cascade laser has been demonstrated as a local oscillator with both frequency and amplitude stabilised for a heterodyne spectroscopy experiment, which will be further discussed in Chapter 6, 7, and 8.

2.3.3 2-D Photonic crystal THz QCLs

A different approach to achieve less divergent far-field beam pattern has been realized with two-dimensional photonic crystal lasers. As shown in [21], with photonics crystal structure by sole patterning of the device top metallization, and carefully designed boundary conditions, a frequency tunable, symmetric far-field beam pattern and single mode laser emission for a two dimensional photonics crystal THz QCL have been realized.

However, the continuous wave operation of such 2D photonics crystal terahertz QCL is deteriorated since a large operating current is required to pump

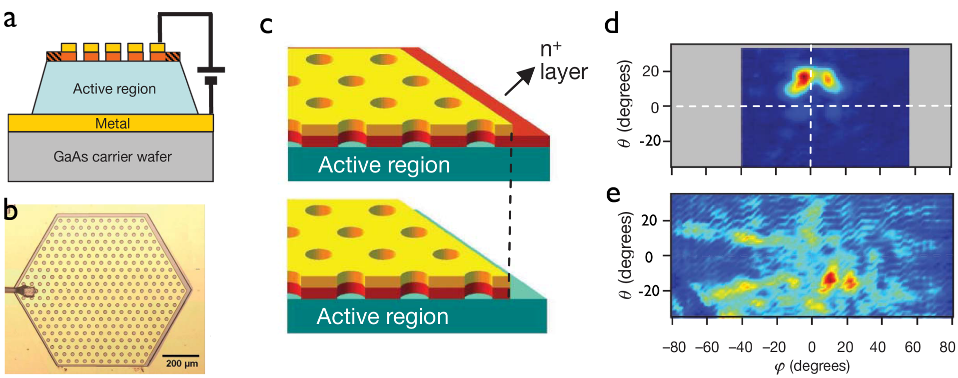

Figure 2.10. (a) Schematic cross-section of the device. The laser active region (blue) is sandwiched between two metal Ti/Au contact layers. The top metal is patterned with the desired photonic-crystal design. (b) Optical microscope image of the surface of a typical device. (c) Detailed scheme of the boundary conditions implementation technique. Top panel is the device with absorption boundary and bottom panel is the mirror boundary condition. (d) Far-field beam pattern of a device with absorbing boundary condition. (e) Far-field beam pattern of a device with mirror boundary condition. (Figure from [21])

the bulky contiguous gain medium. Therefore, although the far-field beam quality is considerably improved, much greater improvement on the robust continuous wave operation, high output power and high operation temperature still needs to be satisfied.

2.4 Frequency or phase locking of a THz QCL

As described, a quantum cascade laser emits light based on the inter-subband transition, while conventional semiconductor lasers using the inter-band transition. The main advantage rising from such inter-subband transitions is the high optical gain and narrow optical gain bandwidth. As shown in Fig. 2.11, for a conventional semiconductor laser, the radiative transition takes place as an electron-hole recombination with an energy gap between conduction and valence band energies. The radiation frequency is essentially determined by the band gap energy. Since the curvatures of the dispersion curves hold opposite signs for the conduction and valence bands, the transition energy depends on k in this manner. As result, the gain spectrum is typically broad in this case. In contrast, the inter-subband transition takes place within either the conduction or the valence band, which presents the same curvature. As a result, the gain spectrum is described by a delta-function, where the joint density of states at the optical transition energy is $\rho(E) = \delta(E - h\nu)$, δ is the Dirac delta function. All of these suggest that all the injected carriers contribute to gain at the same transition energy of $h\nu$ in the emission process, and consequently provides large optical gain (where $g(E) \propto \delta(E)$) [22]. Therefore, the linewidth enhancement factor for an inter-subband laser is in principle much smaller than that of an inter-band laser, which has been experimentally proved in mid-infrared and terahertz QCLs [23, 24].

At terahertz frequencies, a frequency- or phase-stabilized, solid state signal source is crucial for astronomical observation, atmospheric sensing and also laboratory high precision molecular gas spectroscopy applications. Based on the measurement of the frequency noise power spectral density (FNPSD), the laser emission spectral linewidth can be resolved by the amount of noise contribution for each frequency component. Recently, it was from this approach that a quantum-limited linewidth was demonstrated for a THz QCL, where a intrinsic linewidth of about 110 Hz was measured [24]. However, for the free running case, the practical linewidth of a THz QCL is broadened by several external factors, such as: bias current noise, operation temperature fluctuation and so on. As a result, in order to be used as a local oscillator, the emission frequency of a THz QCL has to be locked to an external stable reference signal.

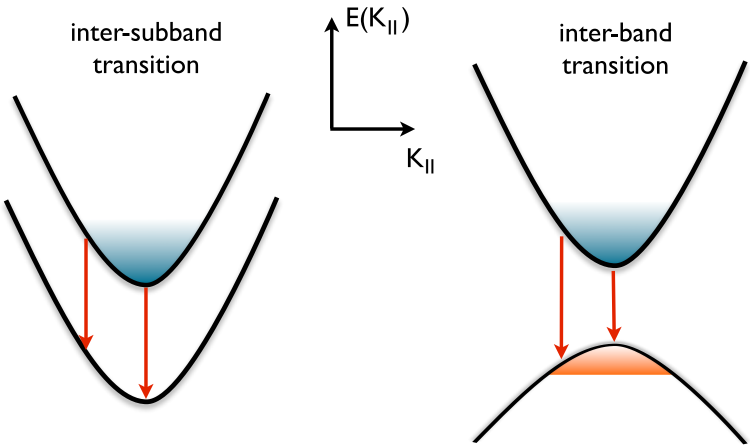

Figure 2.11. Schematic drawing of energy dispersion curves parallel to the layers of the quantum wells for (a) inter-band, and (b) inter-subband optical transitions in two-dimensional quantum wells.

Until now, a considerable amount of progress has been made to achieve either frequency- or phase-locking of a THz QCL.

2.4.1 Locking to an external source

As demonstrated by several groups, a THz QCL, like other solid-state oscillators, is a voltage-controlled oscillator (VCO), whose frequency is determined by a control DC voltage. By using the heterodyne technique and implementing a feedback control loop to the bias circuit of the laser, the emission frequency of a THz QCL can be stabilized to an external reference signal. For frequency locking case, the QCL's average frequency is stabilized, but its linewidth remains intrinsic. For the phase locking case [27], not only the THz QCL emission frequency is stabilized, but also the phase of the QCL radiation is fully synchronised to the reference signal. As demonstrated, this reference signal could be a far-infrared gas laser [25], or a solid-state multiplier source [26, 27]. The gas laser is not practical for a telescope application, while the solid-state multiplier is preferred. However, there are a few issues regarding to the latter in the application at super-terahertz frequencies. Firstly, a solid-state multiplier generates radiation only up to over 2 THz [28]. Moreover, the upper conversion efficiency of a semiconductor superlattice nonlinear harmonic generator decreases dramatically as frequency goes above 3 THz. As a result, it is still

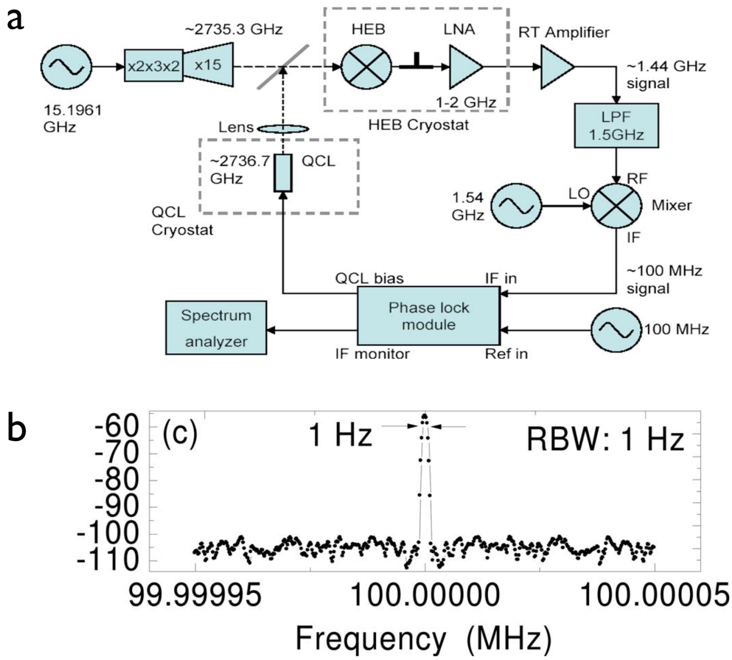

Figure 2.12. (a) Schematic of the experiment setup to phase lock a terahertz QCL at 2.7 THz to a microwave reference. Not shown is that all the spectrum analyzers and the signal generators are phase locked to a common 10 MHz reference. (b) Power spectra of the beat signal of the phase- locked terahertz QCL recorded by the spectrum analyzer with different RBWs and spans, but with a fixed video bandwidth of 300 Hz. (Figure from [27]).

not available to have such a technique at higher terahertz frequencies, like 4.7 THz for GUSSTO and SOFIA.

2.4.2 Locking to a frequency comb

Recently, it has been demonstrated that a 2.7 THz quantum cascade laser is successfully stabilized to a commercial, mode-locked erbium-doped fiber laser [29]. This method takes advantage of the electro-optic effect in ZnTe, a THz QCL is mixed with the N_{th} harmonic of the 90 MHz repetition rate of the mode locked fiber laser. Then with phase locking electronics generating a feedback bias signal, the QCL emission signal is phase locked with over 80 dB signal to noise ratio and more than 90% power locking efficiency. This technique is inherently broadband, up to more than 5 THz due to the bandwidth of the femtosecond laser. Furthermore, the implementation of a silicon photodiode is more convenient than using a superconducting mixer. However, the bulky femtosecond laser and high incident power requirement for the photodiode (~2 mW) limit its space- or ballon-borne application.

2.4.3 Locking to a molecular absorption line

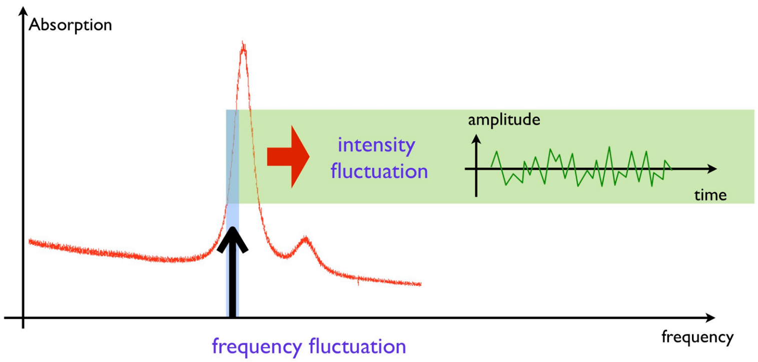

Figure 2.13. Schematic of the principle of frequency stabilization using a molecular absorption line. The red curve represents a molecular absorption line, where the THz QCL emission signal locates within the absorption frequency range. Thus, by guiding the THz QCL radiation though the molecular absorption line, the frequency fluctuation is transformed into amplitude fluctuation.

Phase locking is crucial for many applications, such as a interferometer, like the Atacama Large Millimeter/submillimeter Array (ALMA), where over sixty telescopes require local oscillator sources with synchronized frequency and phase. However, for single dish observation, only a frequency stabilized local oscillator is sufficient. Using a molecular absorption line serving as reference frequency, a mid-infrared QCL has been stabilized to a side of rovibrational resonance of nitrous oxide (N_2O) at 1176.61 cm^{-1} [30]. Recently, this frequency stabilization scheme has also been realized for a THz QCL, to a methanol absorption line at 2.5 THz [31]. The linewidth is reduced from a free running state of 15 MHz down to around 300 kHz. And this linewidth is in principle at least several orders of magnitude greater than the intrinsic linewith of a

THz QCL [24], which suggests that the full potential of this technique was not achieved yet.

The working principle of this stabilization scheme is straightforward. Based on the molecular lines absorption feature, when the QCL frequency locates exactly within the absorption line, this absorption curve is capable to transform the frequency fluctuation into amplitude fluctuation, as shown in fig. 2.13. Then the amplitude noise is detected by a fast and sensitive power detector, which is used for a control loop to generate a feedback signal to the QCL bias supply in order to maintain a constant power value. In reality, the locking scheme is more complicated and will be further described in Chapter 7. In fact, this molecular spectral line is extremely stable and favourable to be used for local oscillator stabilisation application. And it is simple and robust, since it requires in essence only a gas cell unit and a direct power detector, which can easily be applied to a space- or ballon-borne instrument. Also it is easily applicable at higher THz frequencies, due to rich absorption spectra of molecular, like CH_3OH and H_2O [31,32]. However, a drawback for such approach is the lack of continuous frequency tuning range.

Bibliography

[1] J. Faist, F. Capasso, D. L. Sivco, C. Sirtori, A. L. Hutchinson, and A. Y. Cho. *Quantum cascade laser*, Science, **264** 553 (1994).

[2] R. Köhler, A. Tredicucci, F. Beltram, H. E. Beere, E. H. Linfield, A. G. Davies, D. A. Ritchie, R. C. Iotti, and F. Rossi, *Terahertz semiconductor-heterostructure laser*, Nature, **417**, 156 (2002).

[3] Y. Bonetti, and J. Faist, *Quantum cascade lasers entering the mid-infrared*, Nature Photonics, **3**, 32 (2009).

[4] B. S. Willams, *Terahertz quantum-cascade lasers*, Nature Photonics, **1**, 517 (2007).

[5] G. Scalari, L. Ajili, J. Faist, H. Beere, E. Linfield, D. Ritchie, and G. Davies, *Far-infrared ($\lambda \sim 87\ \mu m$) bound-to-continuum quantum-cascade lasers operating up to 90 K*, Applied Physics Letters, **82**, 3165 (2003).

[6] S. Kumar, C. W. I. Chan, Q. Hu, and J. L. Reno, *Two-well terahertz quantum-cascade laser with direct intrawell-phonon depopulation*, Applied Physics Letters, **95**, 141110 (2009).

[7] A. W. M. Lee, Q. Qin, S. Kumar, B. S. Williams, Q. Hu, and J. L. Reno, *High-power and high-temperature THz quantum-cascade lasers based on lens-coupled metal-metal waveguides*, Optics Letters, **32**, 2840 (2007).

[8] S. Fathololoumi, E. Dupont, C. W. I. Chan, Z. R. Wasilewski, S. R. Laframboise, D. Ban, A. Mátyás, C. Jirauschek, Q. Hu, and H. C. Liu, *Terahertz quantum cascade lasers operating up to 200 K with optimized oscillator strength and improved injection tunneling*, Optics Express, **20**, 3866 (2012).

[9] B. S. Williams, S. Kumar, Q. Hu, and J. L. Reno, *Operation of terahertz quantum-cascade lasers at 164 K in pulsed mode and at 117 K in continuous-wave mode*, Optics Express, **13**, 3331 (2005).

[10] S. Kumar, C. W. I. Chan, Q. Hu, and J. L. Reno, *A 1.8-THz quantum cascade laser operating significantly above the temperature of $h\omega/k_B$*, Nature Physics, **7**, 166 (2011).

[11] H. Richter, M. Greiner-Bär, S. G. Pavlov, A. D. Semenov, M. Wienold, L. Schrottke, M. Giehler, R. Hey, H. T. Grahn, and H.-W. Hübers, *A compact, continuous-wave terahertz source based on a quantum-cascade laser and a miniature cryocooler*, Optics Express, **18**, 10177 (2010).

[12] A. J. L. Adam, I. Kašalynas, J. N. Hovenier, T. O. Klaassen, J. R. Gao, E. E. Orlova, B. S. Williams, S. Kumar, Q. Hu, and J. L. Reno, *Beam pattern of Terahertz quantum cascade lasers with sub-wavelength cavity dimensions*, Applied Physics Letters, **88**, 151105 (2006).

[13] J. R. Gao, J. N. Hovenier, Z. Q. Yang, J. J. A. Baselmans, A. Baryshev, M. Hajenius, T. M. Klapwijk, A. J. L. Adam, T. O. Klaassen, B. S. Williams, S. Kumar, Q.Hu, and J. L. Reno, *Terahertz heterodyne receiver based on a quantum cascade laser and a superconducting bolometer*, Applied Physics Letters, **86**, 244104 (2005).

[14] M. I. Amanti, *Photonics for THz Quantum Cascade Lasers*, PhD Thesis, ETH (2010).

[15] S. Kumar, B. S. Williams, Q. Qin, A. W. M. Lee, Q. Hu and J. L. Reno, *Surface-emitting distributed feedback terahertz quantum-cascade lasers in metal-metal waveguides*, Optics Express, **15**, 113 (2007).

[16] J. A. Fan, M. A. Belkin, F. Capasso, S. Khanna, M. Lachab, A. G. Davies, and E. H. Linfield, *Surface emitting terahertz quantum cascade laser with a double-metal waveguide*, Optics Express, **14**, 11672 (2006).

[17] T.-Y. Kao, Q. Hu, and J. L. Reno, *Phase-locked arrays of surface-emitting terahertz quantum-cascade lasers*, Applied Physics Letters, **96**, 101106 (2010).

[18] M. I. Amanti, M. Fischer, G. Scalari, M. Beck, and J. Faist, *Low-divergence single-mode terahertz quantum cascade laser*, Nature Photonics, **3**, 586 (2009).

[19] C. A. Balanis, *Antenna Theory: Analysis and Design*, John Wiley & Sons, New York (2007).

[20] M. I. Amanti, G. Scalari, F. Castellano, M. Beck, and J. Faist, *Low divergence Terahertz photonic-wire laser*, Optics Express, **18**, 6390 (2010).

[21] Y. Chassagneux, R. Colombelli, W. Maineult, S. Barbieri, H. E. Beere, D. A. Ritchie, S. P. Khanna, E. H. Linfield, and A. G. Davies, *Electrically pumped photonics-crystal terahertz lasers controlled by boundary conditions*, Nature, **457**, 174 (2009).

[22] S. Kumar, *Development of terahertz quantum-cascade lasers*, PhD Thesis, MIT (2007).

[23] S. Bartalini, S. Borri, P. Cancio, A. Castrillo, I. Galli, G. Giusfredi, D. Mazzotti, L. Gianfrani, and P. De Natale, *Observing the Intrinsic Linewidth of a Quantum-Cascade Laser: Beyond the Schawlow-Townes Limit*, Physics Review Letters, **104**, 083904 (2010).

[24] M. S. Vitiello, L. Consolino, S. Bartalini, A. Taschin, A. Tredicucci, M. Inguscio, P. De Natale, *Quantum-limited frequency fluctuations in a Terahertz laser*, Nature Photonics, **6**, 525 (2012).

[25] A. L. Betz, R. T. Boreiko, B. S. Williams, S. Kumar, Q. Hu and J. L. Reno, *Frequency and phase-lock control of a 3 THz quantum cascade laser*, Optics Letters, **30**, 1837 (2005).

[26] D. Rabanus, U. U. Graf, M. Philipp, O. Ricken, J. Stutzki, B. Vowinkel, M. C. Wiedner, C. Walther, M. Fischer, and J. Faist, *Phase locking of a 1.5 Terahertz quantum cascade laser and use as a local oscillator in a heterodyne HEB receiver*, Optics Express, **17**, 1159 (2009).

[27] P. Khosropanah, A. Baryshev, W. Zhang, W. Jellema, J. N. Hovenier, J. R. Gao, T. M. Klapwijk, D. G. Paveliev, B. S. Williams, S. Kumar, Q. Hu, J. L. Reno, B. Klein, and J. L. Hesler, *Phase locking of a 2.7 THz quantum cascade laser to a microwave reference*, Optics Letters, **34**, 2958 (2009).

[28] A. Maestrini, I. Mehdi, R. Lin, J. V. Siles, C. Lee, J. Gill, G. Chattopadhyay, E. Schlecht, B. Thomas, and J. Ward, *A 2.5-2.7 THz Room Temperature Electronic Source*, Proceeding of 22nd International Symposium on Space Terahertz Technology, Tucson (2011).

[29] S. Barbieri, P. Gellie, G. Santarelli, L. Ding, W. Maineult, C. Sirtori, R. Colombelli, H. Beere and D. Ritchie, *Phase-locking of a 2.7-THz quantum cascade laser to a mode-locked erbium-doped fibre laser*, Nature Photonics,**4**, 636 (2010).

[30] R. M. Williams, J. F. Kelly, J. S. Hartman, S. W. Sharpe, M. S. Taubman, J. L. Hall, F. Capasso, C. Gmachl, D. L. Sivco, J. N. Baillargeon, and A. Y. Cho, *Kilo-hertz linewidth from frequency stabilized midinfrared quantum cascade lasers*, Optics Letters, **24**, 1844 (1999).

[31] H. Richter, S. G. Pavlov, A. D. Semenov, L. Mahler, A. Tredicucci, H. E. Beere, D. A. Ritchie, and H.-W. Hübers, *Submegahertz frequency stabilization of a terahertz quantum cascade laser to a molecular absorption line*, Applied Physics Letters, **96**, 071112 (2010).

[32] Y. Ren, J. N. Hovenier, M. Cui, D. J. Hayton, J. R. Gao, T. M. Klapwijk, S. C. Shi, T-Y. Kao, Q. Hu, and J. L. Reno, *Frequency locking of signle-mode 3.5-THz quantum cascade lasers using a gas cell*, Applied physics letters, **100**, 041111 (2012).

Chapter 3

Laboratory heterodyne spectroscopy

3.1 Introduction

Laboratory heterodyne spectroscopy, based on the absorption, emission or scattering of electromagnetic radiation by molecules or atoms, is a crucial tool for the analytical studies of molecules and atoms themselves, or related physical processes. In the gas phase at low pressures, molecules exhibit absorption or emission features with narrow spectral lines, whereby the frequency and intensities are determined by the quantized rotational motion of the molecule. Furthermore, the spectral lines are also characterized by the ambient temperature and the pressure of its environment. For the heterodyne spectroscopy, with a superior spectral resolution ($v/\Delta v > 10^6$, where v is frequency), it provides a unique advantage in molecular spectroscopy which is capable of, not only detecting molecules, but also studying and predicting molecular structures [1].

On the other hand, based on the knowledge of the molecule that we have, heterodyne spectroscopy also provides a unique way to characterize the entire receiver system, including: standing waves, local oscillator spurs and diplexer calibration. Furthermore, it is also used to characterize properties of the mixer itself, like the side band ratio, which is the ratio of the gain between the lower sideband and upper sideband. As a result, heterodyne spectroscopy is widely used as an important tool for a variety of space missions in order to do a ground lab test campaign, like SWAS (Submillimeter Wave Astronomy Satellite) [2], TELIS Ballon mission [3] and also HIFI instrument on Herschel Space Telescope [4].

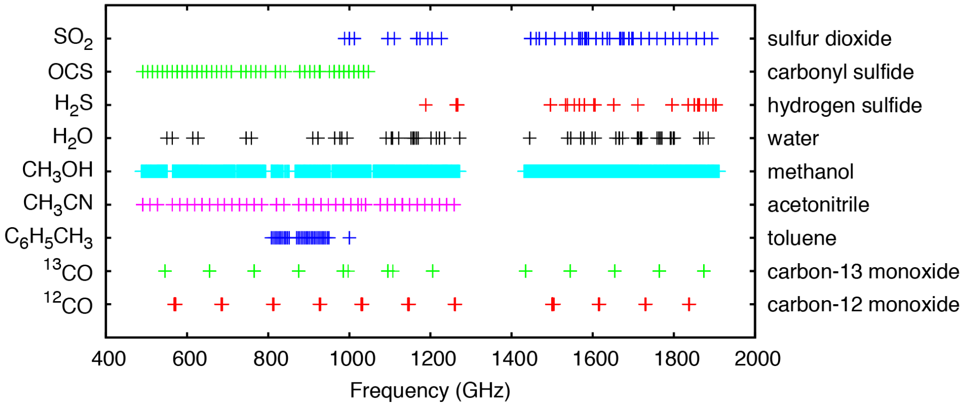

Figure 3.1. Summary of local oscillator frequency coverage for all gases used during the HIFI gas cell testing. (Figure from [5])

3.2 Line profile modelling

Please notice that for side band ratio extraction, in general it is limited to the analysis of saturated lines at certain frequencies, where the line intensity at particular frequency is equal to that of a blackbody emission of the gas temperature. However, this saturation is largely limited by the gas sample and also calibration frequency. Unfortunately, at higher frequencies (approaching 2 THz for HIFI), there are no molecules with saturated lines. It is therefore important to understand and predict a precise line profile for certain molecules which includes: line frequency, peak intensity and also linewidth. Thus, it becomes crucial to generate a model to estimate the line profile including the gas molecule properties (line frequencies and intensities), and also the gas cell properties (optical length, gas pressure, and gas temperature). For this, I will briefly introduce several broadening mechanisms for a natural spectral line profile.

3.2.1 Natural broadening

For spectral lines, it is inherently a natural feature that is due to the uncertainty principle related to the lifetime of an excited state with the uncertainty of the energy, where $\Delta E \Delta t \sim \hbar/2$. The spectral line shape results in a Lorentzian profile. For terahertz frequencies, the natural broadening linewidth is of the order of kHz, which is 0.1% smaller than the other dominant broadening mechanism, as discussed below.

3.2.2 Thermal Doppler broadening

Thermal Doppler broadening is a result of a molecule as it emits radiation. The molecules that are emitting radiation have a distribution of velocities, and the frequency of the transition is shifted depending on the direction of the molecule relative to the observer. The photon emitted will have a red shifted line if the molecule moving away from the observer, and it blue shifted if it is moving towards the observer. As explained in [5], such thermal Doppler broadening results in a Gaussian line shape:

$$\phi_\nu = \frac{1}{\sqrt{\pi}\delta\nu_D} e^{-\ln(2)(\nu-\nu_0)^2/\delta\nu_D^2}, \tag{3.1}$$

where $\delta\nu_D$ is defined as:

$$\delta\nu_D = \frac{\nu_0}{c}\sqrt{\frac{2\ln(2)kT}{m}}, \tag{3.2}$$

where ν_0 is the spectral frequency of the gas, c the speed of light, k the Boltzmann constant, T the gas temperature, m the molecular mass. As shown, a higher molecular temperature provides a broader distribution of velocities of the emitted photons.

3.2.3 Pressure broadening

Pressure broadening is a result of collision or other interaction among nearby particles, which affects the radiation emission. This effect is highly related to the density (pressure) and the temperature of the molecules. Similar to the natural line profile, pressure broadening is also described by a Lorentzian profile:

$$\phi_\nu = \frac{\delta\nu_L}{\pi((\nu-\nu_0)^2 + \delta\nu_L^2)}, \tag{3.3}$$

where,

$$\delta\nu_L = \gamma_{self} P_{gas}, \tag{3.4}$$

and P_{gas} is the gas pressure and γ_{self} is the gas pressure broadening parameter.

3.2.4 Opacity broadening

Opacity broadening is a non-local effect (not from gas properties), which is a result of transmission of the photons through the optical length. It could be described as:

$$\delta\nu = e^{-\alpha L}, \tag{3.5}$$

where α is the opacity parameter for a certain gas molecule and L is the gas cell optical length.

3.2.5 Line profile generation

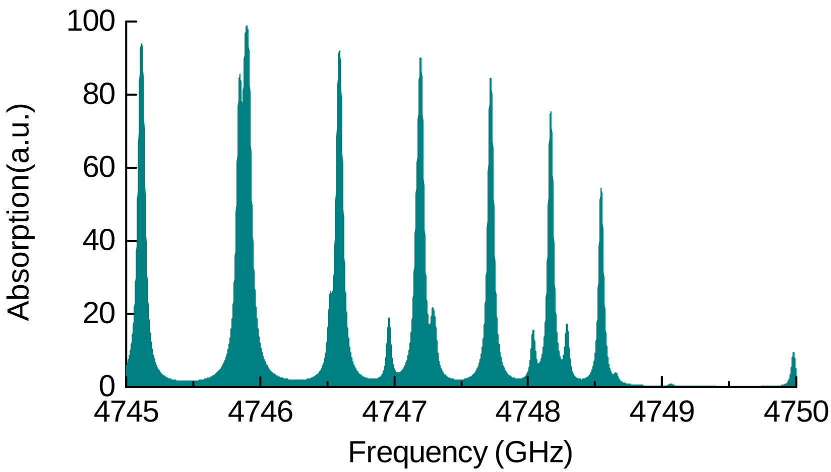

Figure 3.2. Theoretical calculation of methanol (CH_3OH) spectra with a optical path length of 41 cm, gas temperature of 300 K and gas pressure at 1 mbar from 4745 to 4750 GHz, where several strong methanol absorption lines located within the superconducting HEB mixer IF bandwidth (4∼5 GHz) that could be used as the QCL frequency locking reference signal for OI line detection.

By considering all the local effects due to motion or interactions of individual molecules, the convolution of a Gaussian and Lorentzian profile is known as a Voigt profile:

$$\phi_{\nu V} = \frac{c_l(1/\pi)\delta\nu_V}{(\nu-\nu_0)^2+\delta\nu_V^2} + c_d\frac{\sqrt{ln(2)}}{\sqrt{\pi}\delta\nu_V} \times exp(\frac{-ln(2)(\nu-\nu_0)^2}{\delta\nu_V^2}), \tag{3.6}$$

where

$$d = \frac{\delta\nu_L - \delta\nu_D}{\delta\nu_L + \delta\nu_D}, \tag{3.7}$$

$$c_l = 0.68188 + 0.61293 \times d - 0.18382 \times d^2 - 0.11568 \times d^3, \tag{3.8}$$

$$c_d = 0.32460 - 0.61825 \times d + 0.17681 \times d^2 + 0.12109 \times d^3, \tag{3.9}$$

$$\delta\nu_V = 0.53456 \times \delta\nu_L + \sqrt{0.2166 \times \delta\nu_L^2 + \delta\nu_D^2}, \tag{3.10}$$

The next step is to scale this profile using the integrated line intensity, I_{ba}, taken from the JPL catalog [6] and the density of gas. As a result, the final line profile is:

$$I(\nu - \nu_o) = exp(-\alpha(\nu - \nu_o) \times L) \tag{3.11}$$

where,

$$\alpha(\nu - \nu_o) = \alpha_{max} \times \frac{\phi_{\nu V}}{c_l/(\pi\delta\nu_V) + c_d\sqrt{(ln(2)/\pi)}/(\delta\nu_V)} \tag{3.12}$$

and,

$$\alpha_{max} = \frac{I_{ba}}{\pi\delta\nu_L + \sqrt{\pi/ln(2)}\delta\nu_D} \times \frac{P}{kT} \tag{3.13}$$

Using this theoretically calculated line profile, combined with the JPL line intensity data base [6], which is calculated based on quantum mechanical models, we can generate the final molecule spectrum. As shown in Fig. 3.3, a calculated methanol (CH_3OH) spectrum around 4.744 THz (OI line). Several strong absorption lines can be used as a reference frequency for the frequency locking.

3.3 Application of laboratory heterodyne gas cell measurement

3.3.1 HIFI gas cell analysis

Since a mixer, like a superconducting hot electron bolometer on HIFI, is operated in the double sideband mode, the knowledge of the side band ratio is necessary in order to resolve the double sideband spectrum observed by HIFI.

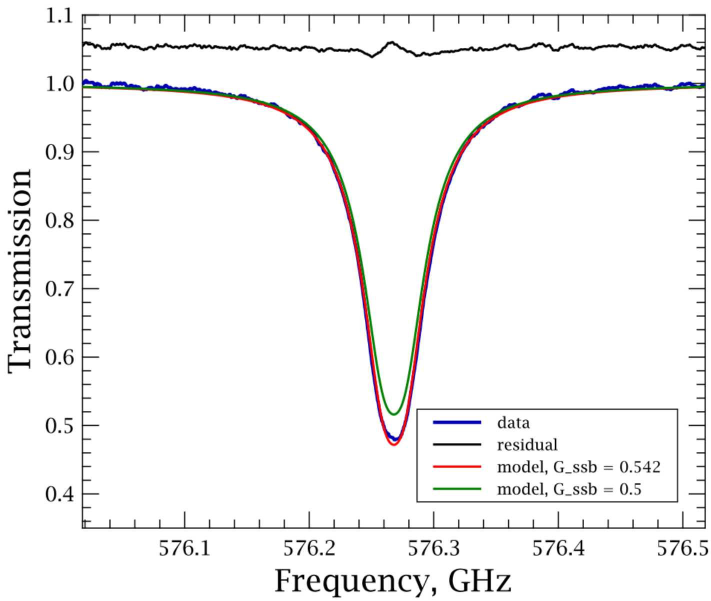

Figure 3.3. ^{12}CO gas cell data at 570.4 GHz (highlighted in blue on the left). Green line shows spectral line fit for a balanced mixer ($G_{ssb} = 0.5$), red line shows the fitted profile where $G_{ssb} = 0.542$.(Figure from [4])

The basic concept of a gas cell calibration of a heterodyne receiver is to observe well understood molecules (known line frequencies, intensities and pressure broadening parameters) and then, using a radiative transfer model, to generate a model line profile. By comparing the model line profile with the observed line profile it is possible to extract the instrumental effects [4]. For the side band ratio test, it requires two observations, one with a filled gas cell (S_{gas}) and one with an evacuated gas cell (S_{empty}). By taking the ratio of these two spectra, one could extract the side band ratio of the mixer, if the spectral line locates in one single side band:

$$R = \frac{G_l}{G_u} = \frac{1 - S_{gas}/S_{empty}}{S_{gas}/S_{empty} - e^{-\tau}}, \tag{3.14}$$

where G_u and G_l are the mixer upper sideband gain and lower sideband gain, $e^{-\tau}$ is the line opacity of the center frequency. Fig. 3.1 shows an example during HIFI ground gas cell test, a ^{12}CO spectrum at 570.4 GHz was measured from a double side band mixer. By fitting the spectrum with different G_{sub}, one could extract the side band ratio of the mixer at this frequency.

3.3.2 Heterodyne gas cell spectroscopy using a quantum cascade laser

So far, laboratory heterodyne spectroscopy has been mostly focused at relatively low frequencies. The first heterodyne gas cell experiment at a frequency beyond 2 THz was done by the DLR group based on a gas laser at 2.5 THz as a local oscillator and a superconducting hot electron bolometer for the mixer [7]. As shown in Fig. 3.4, with a poor receiver sensitivity (14,000 K measured noise temperature) and a non-stabilized local oscillator (10% power variation during 10 min period for a 2.5 THz gas laser), to obtain a heterodyne spectrum, it took 300 sec integration time.

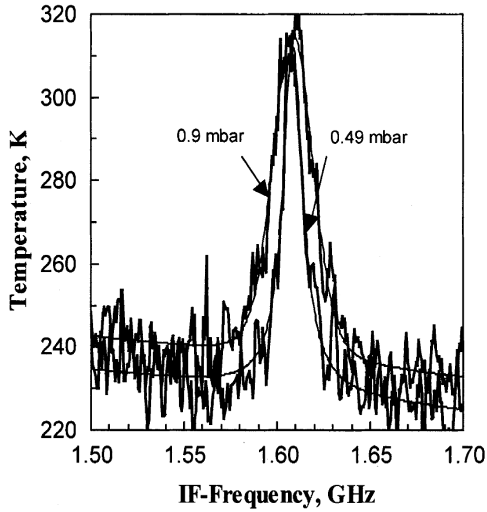

Figure 3.4. Methanol emission line measured at a local oscillator frequency of 2.52278 THz and the gas pressure 0.9 and 0.49 mbar. The temperature scale shows single side band values. The measurement was done in 300 s (150 s on source and 60 s on hot and cold calibration load each). Smooth lines show analytical fit using the Voigt profile. (Figure from [7])

After the first heterodyne sensitivity measurement using a terahertz quantum cascade laser as local oscillator, a heterodyne gas cell spectroscopy experiment becomes the next important demonstration. However, it requires several crucial preconditions like: a.) high sensitivity mixer at super-terahertz frequencies; b.) good receiver stability; c.) narrow local oscillator linewidth; and d.) advanced back-end spectrometer.

We start our spectroscopic experiment by recording three intermediate frequency power spectra:1) the spectrum $P_{emp,cold}(f)$ when the cold load is behind the evacuated gas cell; 2) the spectrum $P_{gas,cold}(f)$ when the cold load is behind the filled gas cell; 3) the spectrum $P_{gas,hot}(f)$ when the hot load is behind the filled gas cell. As shown in Fig. 3.5, the methanol (CH_3OH) spectra were down-converted to the intermediate frequency and each spectrum trace is recorded using the FFTS at the frequency 0-1.5 GHz with an integration time of 3 seconds.

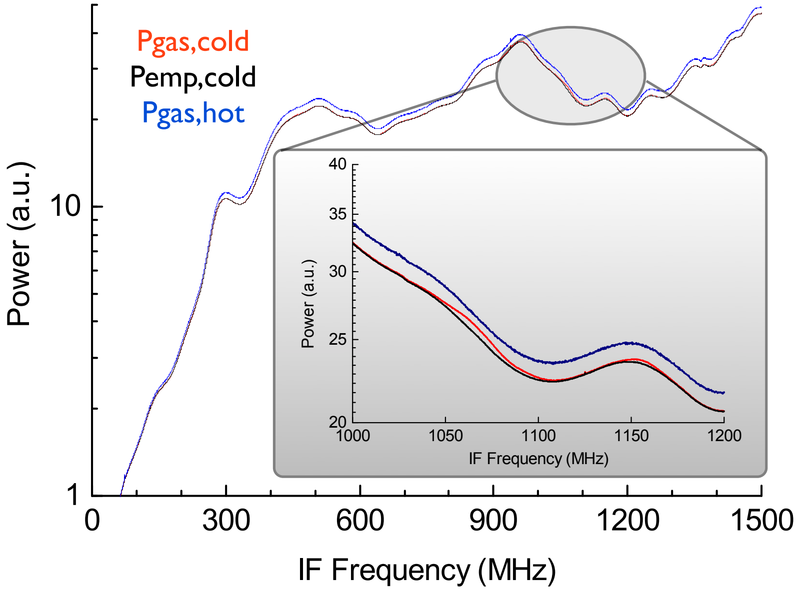

Figure 3.5. Measured methanol (CH_3OH) emission spectrum at 3.5 THz which is down-converted to the intermediate frequency, three power spectra: $P_{emp,cold}$, $P_{gas,cold}$, and $P_{gas,hot}$ were recorded. The inset picture indicates where the emission feature gives a relative higher radiative power at around 1050 MHz at IF frequency for $P_{gas,cold}$.

With the three traces, the brightness of the emission lines in terms of temperature is calculated using the following expression [8]

$$T_{gas}(f) = T_{cold} + 2(T_{hot} - T_{cold}) \frac{P_{gas,cold}(f) - P_{emp,cold}(f)}{P_{gas,hot}(f) - P_{emp,cold}(f)}, \tag{3.15}$$

where T_{hot} and T_{cold} are the effective hot and cold load temperatures defined by the Callen-Welton formula [9], and the factor of 2 in Eqs. (6.1) is derived from the DSB mode operation of the HEB mixer, where the term $(P_{gas,cold}(f) - P_{emp,cold}(f))/(P_{gas,hot}(f) - P_{emp,cold}(f))$, reflects the relative emission of the gas with respect to the 300 K blackbody radiation.

With all the efforts we made, finally a heterodyne spectroscopy experiment was demonstrated using a THz QCL, which will be further discussed in Chapter 5 and 6.

Bibliography

[1] J. C. Pearson, B. J. Drouin, S. S. Yu, and H. Gupta, *Microwave spectroscopy of methanol between 2.48 and 2.77 THz*, Journal of the Optical Society of America B, **28**, 2549 (2011).

[2] V. Tolls, G. J. Melnick, M. L. N. Ashby, E. A. Bergin, M. A. Gurwell, S. C. Kleiner, B. M. Patten, R. Plume, J. R. Stauffer, Z. Wang, Y. F. Zhang, G. Chin, N. R. Erickson, R. L. Snell, P. F. Goldsmith, D. A. Neufeld, R. Schieder, and G. Winnewisser *Submillimeter Wave Astronomy Satellite Performance on the ground and in orbit*, The Astrophysical Journal Supplement Series, **152**, 137 (2004).

[3] P. A. Yagoubov et al., *550-650 GHz spectrometer development for TELIS*, Proceeding of the 16th International Symposium on Space Terahertz Technology, Sweden (2005).

[4] R. D. Higgins, D. Teyssier, J. C. Pearson, C. Risacher, and N. A. Trappe, *Calibration of the Herschel HIFI Instrument using Gas Cell Measurements*, Proceedings of the 21st International Symposium on Space Terahertz Technology ISSTT, Oxford (2010).

[5] R. D. Higgins, *Advanced optical calibration of the Herschel HIFI heterodyne spectrometer*, PhD thesis, University of Maynooth (2011).

[6] Jet Propulsion Laboratory Molecular Spectroscopy Catalog *http://spec.jpl.nasa.gov/ftp/pub/catalog/catform.html.*

[7] A. D Semenov, H.-W. Hübers, H. Richter, M. Birk, M. Krocka, U. Mair, K. Smirnov, G. N Gol′tsman, and B. M Voronov, *2.5 THz heterodyne receiver with NbN hot-electron-bolometer mixer*, Physica C : Superconductivity, **372**, 448 (2002).

[8] S. Ryabchun, C.-Y. Tong, S. Paine, Y. lobanov, R. Blundell, and G. Goltsman, *Temperature Resolution of an HEB Receiver at 810 GHz*, IEEE Transactions on Applied Superconductivity, **19**, 293 (2009).

[9] H. B. Callen and T. A. Welton, *Irreversibility and Generalized Noise*, Physical Review, **83**, 34 (1951).

Chapter 4

3.5 THz surface emitting distributed feedback QCL operated at 70 K as local oscillator

We report a set of measurements to demonstrate a new type of surface emitting distributed feedback (DFB) quantum cascade laser (QCL) operated at 3.5 THz as local oscillator by pumping a superconducting hot electron bolometer (HEB) mixer. The second-order DFB surface emitting THz QCL, based on the Bragg gratings incorporated into the waveguide, shows single mode emission at 3.555 THz, which is only 4 GHz off from the hydroxyl (OH) line. This frequency can be slightly tuned with operating current or temperature. Because of the radiation being emitted from the surface, the far-field beam is much improved, with a divergent far field beam pattern only in one direction. We also notice that in the far field beam pattern, unlike conventional metal-metal waveguide QCLs, there are no interference patterns. All these make it possible to fully pump a superconducting NbN HEB mixer with a surface emitting DFB QCL at 60 K, and even at 70 K based on the estimated power.

The Chapter was published as Y. Ren, P. J. de Visser, J.N. Hovenier, W. Zhang, P. Khosropanah, J.R. Gao, T.M. Klapwijk, S.C. Shi, T-Y. Kao, Q. Hu, and J. L. Reno, Proceeding of 22nd International Symposium of Space Terahertz Technology, Tucson (2012).

4.1 Introduction

The hydroxyl (OH) radical has been identified to be a crucial probe for problems related to the atmosphere such as global warming and ozone destruction. The OH radical has spectral lines at terahertz frequencies such as 1.8, 2.5 and 3.5 THz [1]. Among them, the emission line at 3.551 THz has been identified as the best candidate for OH profile retrieval because of its brightness and isolation. With a nearly quantum noise limited sensitivity and a ultra high spectral resolution (($\upsilon/\Delta\upsilon$>10^6, where υ is the frequency), a heterodyne receiver based on a superconducting NbN HEB mixer will be ideal for detecting the OH line. Since such a mixer has shown a superior sensitivity up to 5.3 THz [2], suitable local oscillators at this particular frequency become the only obstacle for future development. Solid state LOs based on multipliers have only been demonstrated up to 2 THz, but the output power drops severely with frequency due to reduced multiplication efficiency at high frequencies. Also bulky and power consumptive FIR gas lasers have no strong molecular lines close to this specific frequency.

Based on the quantum well structure, photon energy of a quantum cascade laser is determined by the thickness of the coupled wells and barriers, which makes such structure ideal for generation of THz radiation [3]. Recently several progresses have been made for a THz QCL to be used as the LO in a heterodyne receiver, including a noise temperature measurement [4, 5], excellent power stability [4], phase-locking capability [6, 7] and also heterodyne spectroscopy experiment [8, 9].

Until now, most of the THz QCLs used for LO are based on a Fabry-Perot cavity. This cavity makes use of two facets as reflecting surfaces and a gain region in between. Although with specific cavity design, single mode emission could be achieved by edge-emission Fabry-Perot laser, it is still hard to control the emission frequency precisely. Furthermore, to achieve single mode lasing, the laser has to be narrow and often the width is much smaller than the wavelength. The latter causes a highly divergent beam with even strong interference fringes [10, 11], which makes it difficult to couple the radiation to any phase sensitive detector like a HEB mixer. As shown in Ref. [12], for a surface emitting DFB THz QCL, by incorporating the second-order Bragg gratings into the waveguide, a single mode emission is coupled out from the surface. These characteristics make surface emitting DFB QCL having the advantage in both the frequency selection and less divergent far-field beam in comparison with a typical metal-metal waveguide Fabry-Perot QCL. The single mode emission source at the exact targeting frequency is essential for high resolution spectroscopy application. And also the improved beam pattern will also lead to a better beam coupling to a HEB mixer, which is crucial for high temperature operation of QCL as LO since the emission power is limited in this case. Here we demonstrate this new type of surface emitting DFB QCL, operated at 3.5 THz, as local oscillator by pumping a superconducting HEB mixer.

4.2 Terahertz surface emitting DFB QCL

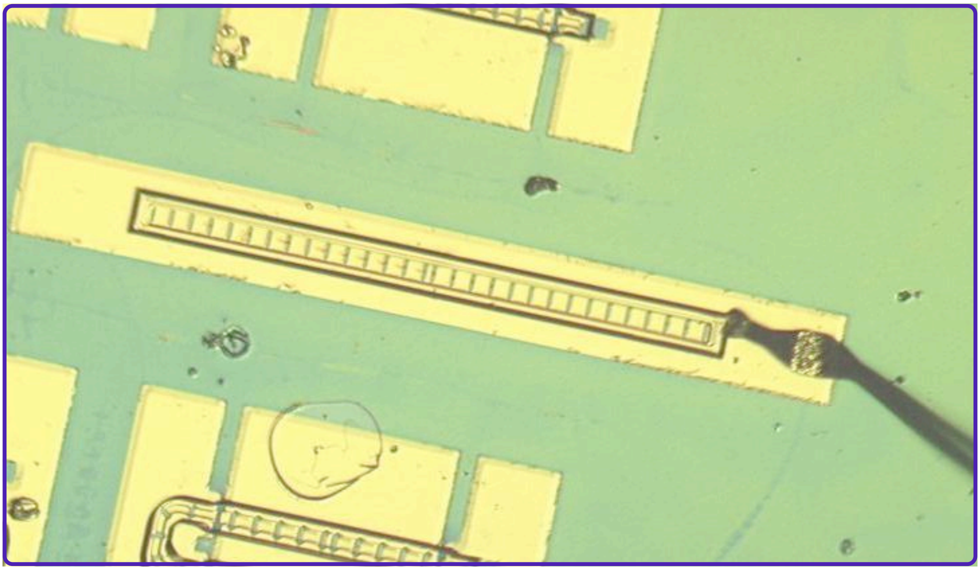

Figure 4.1. Picture of the surface emitting DFB QCL with a length of 754 μm and a width of 40 μm. Also shown is the Al wire bonding for biasing the laser

.

The surface emitting DFB QCL used in this experiment is described in Ref. [12]. The active region is based on a resonant-phonon depopulation scheme and a metal-metal waveguide is used for modal confinement. As shown in Fig. 4.1, by introducing a second-order Bragg grating on the top surface of the waveguide, the radiation is coupled out from the top surface. The DFB grating enables robust single-mode operation over a large operating range. By using a Pi phase-shift in the center of the grating, a single-lobed far beam pattern is obtained.

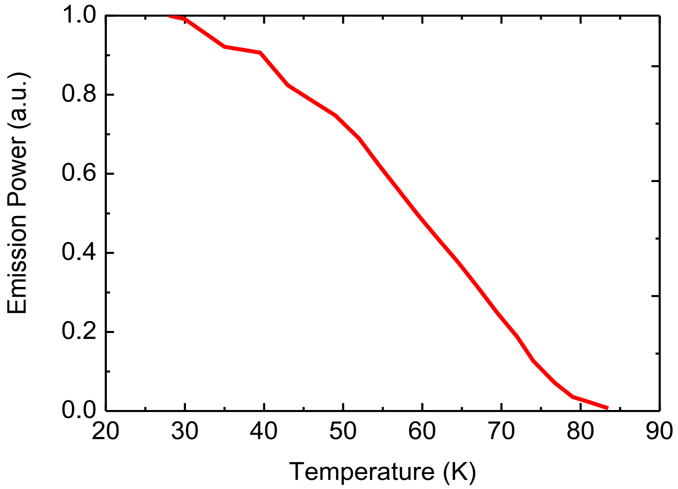

Figure 4.2. Emission power of the surface emitting DFB QCL as a function of the bath temperature. The power is measured in the pulsed mode with a pyrodetector after focusing the beam by a HDPE lens (f=26.5 mm).

4.3 Experiment setup

The QCL is indium soldered on a copper mount and is mounted on the cold stage of a helium-flow cryostat. The QCL consumes 4 W DC power in continuous wave mode and provides a maximum output power of 1 mW. This laser can also be operated at a relatively high temperature. As to be explained, the QCL working at 70 K can still provide about 25% of its maximum power (Fig. 4.2) and is estimated to have enough power to pump a HEB mixer at its optimal operating point.

4.4 FTS, beam pattern, and pumping HEB experiment results

The beam pattern measurement setup was described in [13] using a room temperature pyrodetector and two PC controlled stepper motors, the radiation beam was measured in both horizontal and vertical directions spherically.

As shown in Fig. 4.3, the radiation beam was measured with the pyrode-

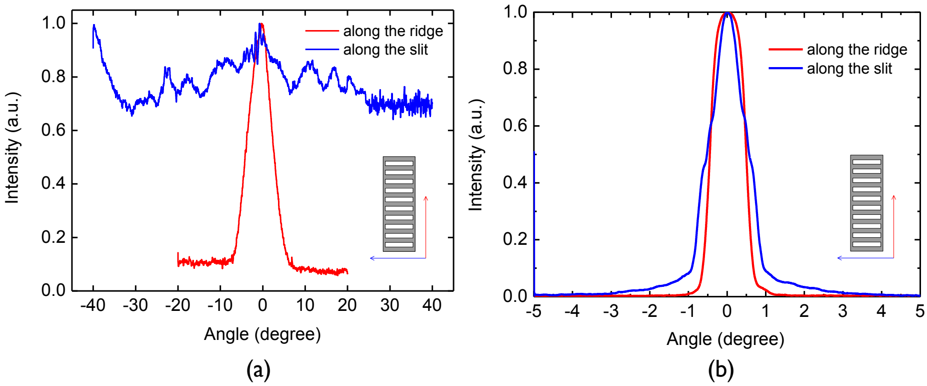

Figure 4.3. Far-field beam pattern measured for a second-order distributed feedback laser without (a) and with (b) focused by a HDPE lens (f=26.5 mm).

tector placed at a radial distance of 112 mm. Along the laser's ridge direction, a single-lobed beam was observed, where the full width at half maximum (FWHM) is 7 deg. However, along the laser's slit direction, the beam is highly divergent, which is mainly due to the subwavelength dimension of the waveguide in this direction. Compared with the beam patterns measured from metametal waveguide Fabry-Perot type QCLs [10, 11], surface emitting DFB QCL emits a directional beam in one direction. Another advantage is that there are no interference fringes in both directions. These features caused a higher power coupling efficiency from the laser to a HEB mixer, which typically holds a Gaussian beam [14]. Fig. 4.3 shows the beam pattern measured after focusing by a high-density polyethylene (HDPE) lens (f=26.5 mm). A single-lobed beam is found in both directions, where the divergence is less than 1 deg.

Emission spectra were measured using a Fourier-transform spectrometer (FTS) with a resolution of 0.7 GHz, which is much larger than the intrinsic linewidth of a THz QCL. As shown in Fig. 4.4, by changing the bias current, the surface emitting DFB QCL shows robust single mode emission over a wide operating range, which indicates a frequency tuning range of 5 GHz. With increasing the bath temperature from 30 K to 70 K, a frequency tuning range of around 10 GHz was measured in this case. It is interesting to note that the observed frequency range can cover the particular OH line at 3.551 THz. This single mode lasing together with a relative large tuning range makes surface emitting DFB laser ideal for high resolution molecular line detection.

We use a spiral antenna coupled NbN HEB mixer, which consists of a 2

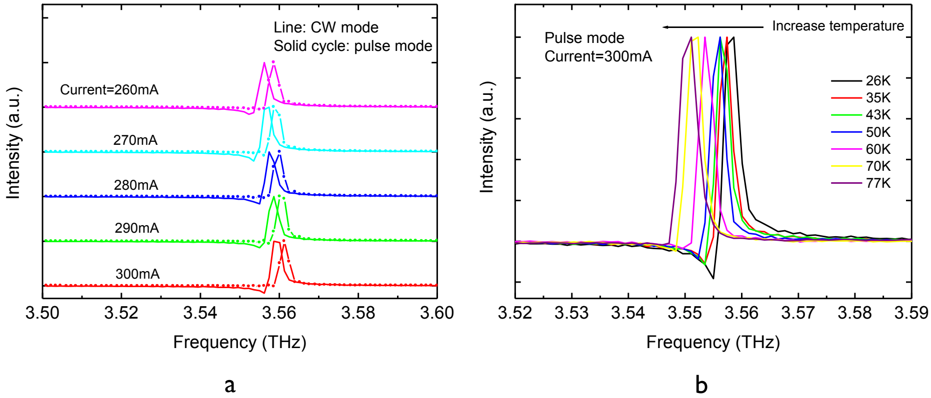

Figure 4.4. Measured emission spectra of the surface emitting DFB QCL. (a) Emission spectra measured at different bias current in pulsed and CW mode;(b) Emission spectra measured at different bath temperature in pulsed mode.

μm wide, 0.2 μm long, and 5.5 nm thick NbN bridge [2]. The HEB has a low-temperature normal-state resistance (R_N) of 83 Ω, a critical temperature of 9.3 K, and a critical current of 210 μA at 4.2 K. This device has already been performed with superior sensitivities from 1.6 to 5.3 THz, which also indicates the excellent beam efficiency from the detector.

As shown in Fig. 4.5, by placing the QCL and the HEB directly face to face, and using a HDPE lens (f=50 mm) to focus the laser's radiation, the current-voltage characteristics of the HEB at different pumping levels are obtained. It is clearly shown that the emission power from the surface emitting DFB QCL working at 60 K is enough to fully pump the HEB (bringing the HEB fully in the normal state). This enables the QCL to be operated as LO in a heterodyne receiver where a thin Mylar beam splitter is used to reflect the power to a HEB mixer [4]. Based on the pumping curve at 60 K with additional 10 dB attenuator, and using the iso-thermal method [15], the LO power absorbed at the HEB itself is estimated to be 530 nW. Taking all known losses (the HDPE window, air, heat filter, Si lens) into account, we found that 4% of total emission power from the QCL is absorbed by the HEB. Although this is still a low value, the coupling efficiency is improved by a factor of 3 compared with that obtained with a metal-metal waveguide Fabry-Perot cavity QCL as described in [4], which is mainly due to the improved far-field beam pattern.

We did not perform the pumping measurement directly at 70 K. However,

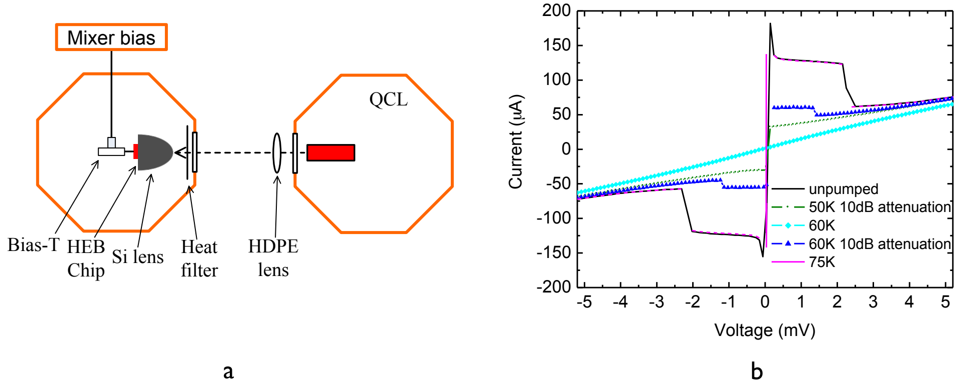

Figure 4.5. (a) Schematic view of the QCL-HEB coupling experimental setup. (b) Current-voltage characteristics of the HEB for different pumping levels caused by different operating temperature of the QCL. In some cases, an attenuation of the LO power is introduced in order to get a proper pumping curve.

we can predict that this laser would be powerful enough to pump the HEB at 70 K. Fig. 4.2 indicates that the output power of the QCL at 70 K is about half the power generated at 60 K. Based on the value of 530 nW at 60 K, we expect a power of 270 nW at the HEB itself with the QCL at 70 K. This value is more than the optimal LO power (140 nW). Since the beam is still highly divergent in one direction, further improvement can be made by placing the QCL closer to the cryostat window and using a short focal distance lens. The possibility of operating a QCL at 70 K or above is crucial for the application in a space instrument because it is technically much easier to have such a cooler in comparison with a cooler for, e.g. 10 K.

4.5 Conclusions

In conclusion we have made a set of measurements, like the beam pattern measurement, the spectra characteristics, and pumping a HEB mixer, to demonstrate that the surface emitting DFB QCL working at 3.5 THz can be used as LO in a heterodyne receiver for the OH line detection. We found that the new laser gives a better beam pattern. The QCL can fully pump a HEB mixer at 60 K, suggesting that there is enough power even at 70 K. We emphasize that operating a QCL at a temperature of 70 K or above is practically important for a real instrument.

Bibliography

[1] R. G. Prinn, J. Huang, R. F. Weiss, D. M. Cunnold, P. J. Fraser, P. G. Simmonds, A. McCulloch, C. Harth, P. Salameh, S. O'Doherty, R. H. J. Wang, L. Porter, and B. R. Miller, *Evidence for substantial variations of atmospheric hydroxyl radicals in the past two decades*, Science, **292**, 1882 (2001).

[2] W. Zhang, P. Khosropanah, J. R. Gao, E. L. Kollberg, K. S. Yngvesson, T. Bansal, R. Barends, and T. M. Klapwijk, *Quantum noise in a terahertz hot electron bolometer mixer*, Applied Physics Letters, **96**, 111113 (2010).

[3] R. Köhler, A. Tredicucci, F. Beltram, H. E. Beere, E. H. Linfield, A. G. Davies, D. A. Ritchie, R. C. Iotti, and F. Rossi, *Terahertz semiconductor-heterostructure laser*, Nature, **417**, 156 (2002).

[4] J. R. Gao, J. N. Hovenier, Z. Q. Yang, J. J. A. Baselmans, A. Baryshev, M. Hajenius, T. M. Klapwijk, A. J. L. Adam, T. O. Klaassen, B. S. Williams, S. Kumar, Q. Hu, and J. L. Reno, *Terahertz heterodyne receiver based on a quantum cascade laser and a superconducting bolometer*, Applied Physics Letters, **86**, 244104 (2005).

[5] H.-W. Hübers, S. G. Pavlov, A. D. Semenov, R. Kohler, L. Mahler, A. Tredicucci, H. E. Beere, D. A. Ritchie and E. H. Linfield, *Terahertz quantum cascade laser as local oscillator in a heterodyne receiver*, Optics Express, **13**, 5890 (2005).

[6] P. Khosropanah, A. Baryshev, W. Zhang, W. Jellema, J. N. Hovenier, J. R. Gao, T. M. Klapwijk, D. G. Paveliev, B. S. Williams, S. Kumar, Q. Hu, J. L. Reno, B. Klein, and J. L. Hesler, *Phase locking of a 2.7 THz quantum cascade laser to a microwave reference*, Optics Letters, **34**, 2958 (2009).

[7] H. Richter, S. G. Pavlov, A. D. Semenov, L. Mahler, A. Tredicucci, H. E. Beere, D. A. Ritchie, and H.-W. Hübers, *Submegahertz frequency stabilization of a terahertz quantum cascade laser to a molecular absorption line*, Applied Physics Letters, **96**, 071112 (2010).

[8] Y. Ren, J. N. Hovenier, R. Higgins, J. R. Gao, T. M. Klapwijk, S. C. Shi, A. Bell, B. Klein, B. S. Williams, S. Kumar, Q. Hu, and J. L. Reno, *Terahertz heterodyne spectrometer using a quantum cascade laser*, Applied physics letters, **97**, 161105 (2010).

[9] Y. Ren, J. N. Hovenier, R. Higgins, J. R. Gao, T. M. Klapwijk, S. C. Shi, B. Klein, T.-Y. Kao, Q. Hu, and J. L. Reno, *High-resolution heterodyne spectroscopy using a tunable quantum cascade laser around 3.5 THz*, Applied Physics Letters, **98**, 231109 (2011).

[10] A. J. L. Adam, I. Kašalynas, J. N. Hovenier, T. O. Klaassen, J. R. Gao, E. E. Orlova, B. S. Williams, S. Kumar, Q. Hu, and J. L. Reno, *Beam pattern of Terahertz quantum cascade lasers with sub-wavelength cavity dimensions*, Applied Physics Letters, **88**, 151105 (2006).

[11] E. E. Orlova, J. N. Hovenier, T. O. Klaassen, I. Kašalynas, A. J. L. Adam, J. R. Gao, T. M. Klapwijk, B. S. Williams, S. Kumar, Q. Hu, and J. L. Reno, *Antenna model for wire lasers*, Physics Review Letters, **96**, 173904 (2006).

[12] S. Kumar, B. S. Williams, Q. Qin, A. W. M. Lee, Q. Hu and J. L. Reno, *Surface-emitting distributed feedback terahertz quantum-cascade lasers in metal-metal waveguides*, Optics Express, **15**, 113 (2007).

[13] X. Gu, S. Paprotskiy, J. N. Hovenier, J. R. Gao, E. E. Orlova, T. M. Klapwijk, P. Khosropanah, S. Barbieri, S. Dhillon, P. Filloux, and C. Sirtori, *High angular resolution far-field beam pattern of a surface-plasmon THz quantum cascade laser*, 19th International Symposium on Space Terahertz Technology ISSTT, Groningen (2008).

[14] A. D. Semenov, H. Richter, H.-W. Hübers, B. Günther, A. Smirnov, K. S. Il'in, M. Siegel, and J. P. Karamarkovic, *Terahertz performance of integrated lens antennas with a hot-electron bolometer*, IEEE Transactions on Microwave Theory and Techniques, **55**, 239 (2007).

[15] H. Ekstrom, B. S. Karasik, E. L. Kollberg, and K. S. Yngvesson, *Conversion Gain and Noise of Niobium Superconducting Hot-Electron-Mixers*, IEEE Transactions on Microwave Theory and Techniques, **43**, 938 (1995).

Chapter 5

Terahertz heterodyne spectrometer using a quantum cascade laser

A terahertz (THz) heterodyne spectrometer is demonstrated based on a quantum cascade laser (QCL) as a local oscillator (LO) and an NbN hot electron bolometer (HEB) as a mixer, and it is used to measure high-resolution molecular spectral lines of methanol (CH_3OH) between 2.913-2.918 THz. The spectral lines are taken from a gas cell containing methanol gas and using a single-mode QCL at 2.9156 THz as an LO, which is operated in the free running mode. By increasing the pressure of the gas, line broadening and saturation is observed. The measured spectra showed good agreement with a theoretical model.

The Chapter was published as Y. Ren, J. N. Hovenier, R. Higgins, J. R. Gao, T. M. Klapwijk, S. C. Shi, A. Bell, B. Klein, B. S. Williams, S. Kumar, Q. Hu, and J. L. Reno, Appl. Phys. Lett. **97**, 161105 (2010).

5.1 Introduction

A high-resolution heterodyne spectrometer is of crucial importance for astronomical observation and atmospheric remote sensing in the terahertz (THz) frequency range. It consists of essentially a mixing detector, a local oscillator (LO), a low noise amplifier, and a GHz-band back-end spectrometer, providing both uniquely high spectral resolution ($\upsilon/\Delta\upsilon>10^6$, limited by the LO and back-end spectrometer, where υ is the frequency, and $\Delta\upsilon$ is the frequency resolution) and excellent sensitivity (e.g., receiver noise temperature of 1000 K at 3 THz). Heterodyne receivers based on superconducting mixers and electronically tunable solid-state multiplier-chain LO sources have been realized up to 2 THz for ground based, balloon-borne, and space telescope instruments, but the development of receivers at higher frequencies will be determined by the availability of suitable solid-state LO sources.

Recently developed THz quantum cascade lasers (QCLs) [1] are the candidates for the LO at frequencies above 2 THz. Heterodyne receivers using a THz QCL as an LO and an NbN hot electron bolometer (HEB) as a mixer have demonstrated high sensitivity using broadband blackbody radiation (hot/cold loads) as the calibration source [2, 3]. A number of milestones for use a THz QCL as an LO have been demonstrated, such as phase-locking capability [4], narrow intrinsic linewidth [5], and excellent power stability [2]. A remaining key step is a direct measurement of spectral lines by a heterodyne spectrometer using a THz QCL as an LO. A spectroscopic measurement using a THz QCL as an active tuning source has been reported for gas phase spectroscopy [6]. However, the detection itself was not based on the heterodyne principle.

In this chapter we report high-resolution spectroscopic measurements using a heterodyne spectrometer with a 2.9 THz QCL as an LO and an NbN HEB as a mixer. We observed simultaneously several molecular emission lines of methanol gas around 2.9 THz. By varying the pressure of the gas, we are able to follow the line broadening and also make a comparison between measured and theoretical spectra.

5.2 Experiment setup

The LO used in our experiment is a metal-metal Fabry-Perot ridge waveguide THz QCL, based on the resonant phonon depopulation design [7], with cavity dimensions of 1.45 mm x 25 μm. The QCL is mounted on the cold stage of a helium-flow cryostat, and emits a single-mode emission line at 2.9156 THz in continuous wave (CW) mode as measured by a Fourier-transform Spectrome-

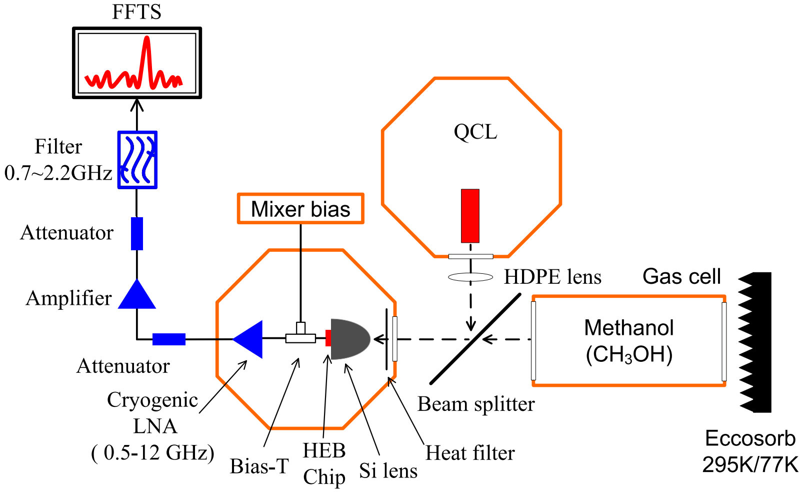

Figure 5.1. Schematic view of the heterodyne gas cell measurement.

ter. While the intrinsic linewidth of a QCL is expected to be in the range of 6∼30 kHz [5], in the current measurement, the QCL is operated in free-running mode without any stabilization on the phase and the amplitude. Based on the previous experience [4], we expect a free-running QCL linewidth of less than 1 MHz, which is sufficiently narrow for this laboratory spectroscopic measurement.

The mixer is a spiral antenna coupled NbN HEB, which is glued to the backside of an elliptical Si lens and is operated at 4.2 K. As shown in a separate experiment [8], the same mixer can have superior sensitivities across the frequency range of 1.6∼5.3 THz, from which the double sideband (DSB) receiver noise temperature [8] is expected to be 1000 K at 2.9 THz.

The spectroscopic measurement setup is sketched in Fig. 5.1. The THz radiation beam from the QCL first passes through the high-density polyethylene (HDPE) cryostat window and is then focused with a HDPE (f=26.5 mm) lens. The signal source is a combination of a gas cell and hot/cold (295 K/ 77 K) blackbody loads. The gas cell is a 41 cm long cylinder with an inner diameter of 10 cm at room temperature and has two 2 mm thick HDPE windows.

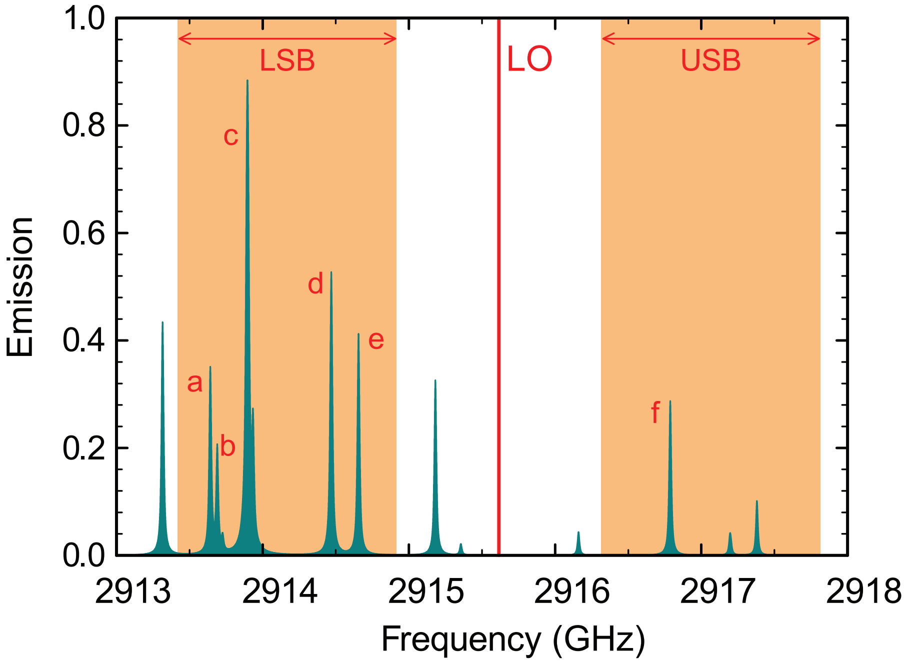

Figure 5.2. Calculated emission spectra of methanol (CH3OH) at a pressure of 1 mbar and at 300 K, for a 0.5 m optical path length. The red line indicates the LO at 2915.6 GHz. The shadow regions of the lower side band (LSB) and the upper side band (USB) correspond to the detection band of the FFTS for the IF signal by using a 0.7~2.2 GHz band pass filter. Several methanol lines within the shadow regions, labelled with a to f, are expected to be seen.

The gas pressure inside the cell is measured using a gas-independent gauge, where the pressure can be controlled with an accuracy of at least 0.1 mbar. In Fig. 5.2 shows a calculated methanol emission spectrum in the vicinity of the LO frequency (f_{LO}) [9], where the intensity is relative to the 300 K blackbody radiation. In the experiment, the signal source and the QCLs radiation are combined by a 3 μm thick Mylar beam splitter and fed further into the HEB mixer. The mixer down-converts a spectral line at f_s to an intermediate frequency f_{IF}, where f_{IF}=| f_{LO} - f_s |. Since the HEB mixer is operated in DSB mode, both the signal at above f_s=f_{LO}+f_{IF} (upper side band, USB) and below f_s=f_{LO}-f_{IF} (lower side band, LSB) will be converted to the same IF frequency range. The IF signal is amplified first using a wide band (0.5∼12 GHz) low noise amplifier at 4.2 K, and then followed by two stages of room-temperature amplifiers.

The back-end spectrometer is a Fast Fourier Transform Spectrometer (FFTS) [10], which samples the IF signals in the baseband (0∼1.5 GHz) or in the second Nyquist band (1.5∼3.0 GHz) with a spectral resolution of 183 kHz. In our experiment, a 0.7∼2.2 GHz band pass filter is applied at the input of the FFTS, which defines the actual band at the IF frequency. Consequently, we expect at least six emission lines, labelled with a to f in Fig. 5.2, distributed in the two corresponding bands (LSB and USB) at the THz frequencies. Because of a combination of the bandpass filter with the FFTS, there will be a so-called aliasing effect [11] which means that the methanol lines at $f_{LO} \pm f_{IF}$ (f_{IF}>1.5 GHz) in the second Nyquist band will overlap with the methanol lines at $f_{LO} \pm f_{IF}$ (f_{IF}<1.5 GHz) in the baseband at the same IF frequency.

5.3 Heterodyne spectroscopy experiment results

We start our spectroscopic experiment by characterizing the sensitivity of the whole receiver system. The measured $T_{DSB,Rec}$ was 2500 K for the case where the hot/cold loads are positioned just behind the beam splitter. This value is higher than the expected one [8] (1000 K) which can be attributed to the extra losses due to air and the HEB cryostat window, the non-optimised IF chain, and the direct detection effect. To measure the spectral lines of the gas, three IF power spectra were measured [12]: 1) the spectrum Pemp,cold(f) when the cold load is behind the evacuated gas cell; 2) the spectrum Pgas,cold(f) when the cold load is behind the filled gas cell; 3) the spectrum Pgas,hot(f) when the hot load is behind the filled gas cell. Each trace is recorded using the FFTS with an integration time of 5 seconds. With the three spectra, the brightness of the emission lines in terms of temperature is calculated using the following expression [12]

$$T_{gas}(f) = T_{cold} + 2(T_{hot} - T_{cold}) \frac{P_{gas,cold}(f) - P_{emp,cold}(f)}{P_{gas,hot}(f) - P_{emp,cold}(f)}, \qquad (5.1)$$

where T_{hot} and T_{cold} are the effective hot and cold load temperatures defined by the Callen-Welton formula [13], and the factor of 2 in Eqs. (5.1) is derived from the DSB mode operation of the HEB mixer. The term $[P_{gas,cold}(f) - P_{emp,cold}(f)]/[P_{gas,hot}(f) - P_{emp,cold}(f)]$, reflects the relative emission of the gas with respect to the 300 K blackbody radiation. Due to the aliasing effect an additional factor of two was introduced into the relative emission term in Eqs.

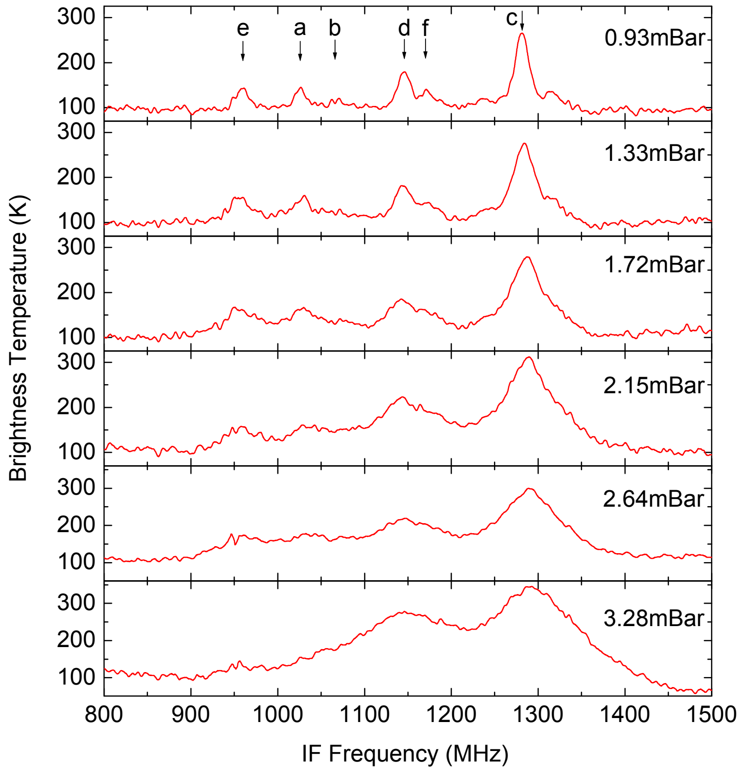

Figure 5.3. Measured methanol (CH_3OH) emission spectra within the IF range between 0.8 and 1.5 GHz at different gas cell pressure which varies from 0.93 to 3.28 mbar. The QCLs frequency is 2915.6 GHz.

(5.1), which accounts for the additional folding of the data for our particular experiment.

By varying the gas pressure we are able to map out the methanol spectral lines at different pressures. Fig. 5.3 shows such spectra within the IF frequency range between 0.8 and 1.5 GHz and with increased pressures from 0.93 to 3.28 mbar, where several lines with different intensity were simultaneously observed within the IF band. A relatively strong emission line at 1281 MHz is observed, which is assumed to be the c line at 2913.896 GHz in the LSB of Fig. 5.2 (corresponding to R-branch transition from the upper state (J =23, K=10, and v=0) to the lower state (J=22, K=9, and v=0), E symmetry) [14]. Additionally, several relatively weak lines from both LSB and USB are observed. With increasing gas pressure, the spectral linewidths become broader and the line intensities increase, until at a high pressure of 3.28 mbar the spectral lines are observed to saturate.

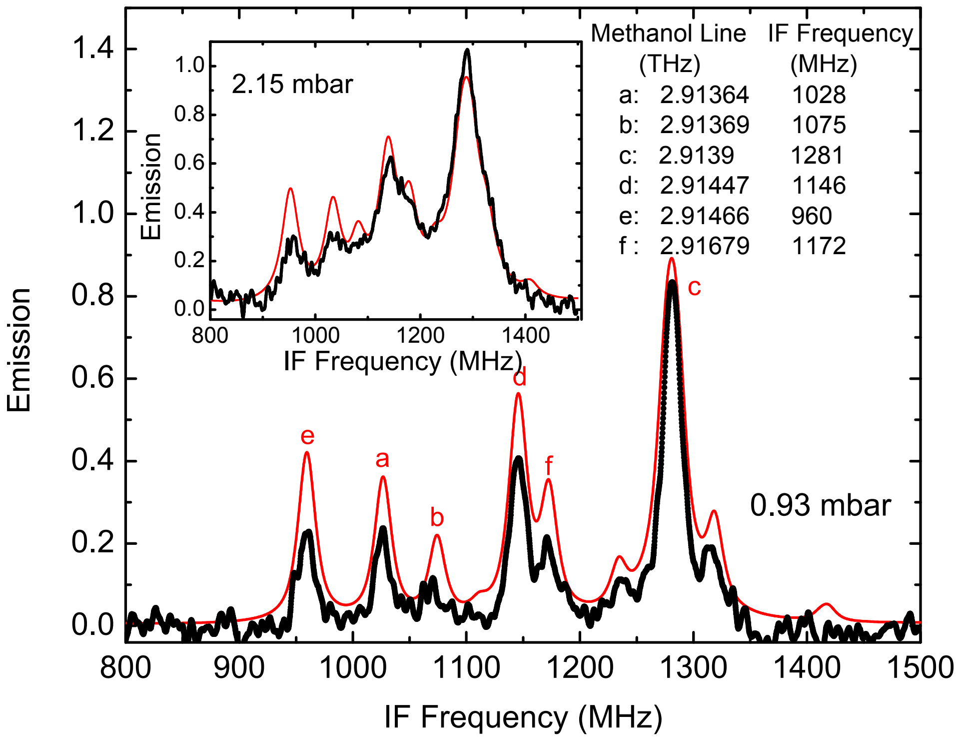

Figure 5.4. Measured methanol emission spectra (black curve) and the simulated spectra (red curve) at a gas pressure of 0.93 mbar. The spectral lines are labeled according to what is given in Fig. 5.1. The correspondence between IF frequency and THz frequency for each line is also listed. The inset shows the measured (black curve) and the simulated spectrum (red curve) at a higher pressure of 2.15 mbar.

To simulate the spectra, a theoretical model was generated based on the expected line frequencies and intensities for methanol from the JPL line catalog [14] and also the effects of line broadening, the parameters of the gas cell, and the FFTS spectrometer were included. The profile of each line shown in Fig. 5.3 is a convolution of several different broadening mechanisms: thermal Doppler broadening, pressure broadening, and opacity broadening. The Doppler broadening can be described by a Gaussian profile where the linewidth is a function of gas temperature, line frequency, and molecular mass of the gas. The pressure broadening effect is characterized by a Lorentzian profile that is determined by the gas pressure and a pressure broadening parameter. The opacity broadening (Beer-Lambert law) is an exponential function of the path length of the gas cell and describes the transmission of radiation through the gas column. Fig. 5.4 shows the calculated and measured methanol emission spectra at two different pressures. The calculated spectra show a reasonable agreement with measurements with regard to both the line frequencies and intensities. Since no pressure broadening data were available in the literature for methanol at the frequencies of our experiment, this parameter was left as a free parameter in a fitting routine. The optimum value for the pressure broadening, as defined in the HITRAN database [15], was found to be 7.4 MHz/mbar (0.25 cm^{-1}/atm) for our case.

The following effects can influence the measured amplitudes of the spectral lines and may explain the differences between data and model: a) the side band ratio of the receiver is assumed to be unity, but in practice it can deviate from unity; b) while we assume the receiver gain at the different IF frequencies between the baseband and second Nyquist band to be equal, this is not necessary true. Furthermore, the use of a broadband IF amplifier in our case can cause possible standing waves. These effects, together with the uncertainty of the measurement governed by stability of the receiver, can cause the apparent relative emission to be greater than unity (inset of Fig. 5.4) so that the brightness of the c line exceeds 300 K at higher pressure (Fig. 5.3).

5.4 Conclusions

In conclusion we have succeeded in demonstrating high-resolution spectroscopic measurement using a heterodyne receiver based on a 2.9 THz quantum cascade laser as a local oscillator and a NbN HEB as a mixer. We measured the molecular spectra of methanol gas with good agreement to simulated model spectra. Our gas cell measurement is a crucial demonstration of the QCL as an LO for practical instruments. These high-resolution spectra of the different molecular lines at such a high frequency indicate that the heterodyne spectrometer based on a QCL and a HEB mixer has unique advantages for its high resolution and excellent sensitivity, and can be applied at any THz frequency.

Bibliography

[1] B. S. Willams, *Terahertz quantum-cascade lasers*, Nature Photonics **23**, 51 (2007).

[2] J. R. Gao, J. N. Hovenier, Z. Q. Yang, J. J. A. Baselmans, A. Baryshev, M. Hajenius, T. M. Klapwijk, A. J. L. Adam, T. O. Klaassen, B. S. Williams, S. Kumar, Q. Hu, and J. L. Reno, *Terahertz heterodyne receiver based on a quantum cascade laser and a superconducting bolometer*, Applied Physics Letters, **86**, 244104 (2005).

[3] H.-W. Hübers, S. G. Pavlov, A. D. Semenov, R. Kohler, L. Mahler, A. Tredicucci, H. E. Beere, D. A. Ritchie and E. H. Linfield, *Terahertz quantum cascade laser as local oscillator in a heterodyne receiver*, Optics Express, **13**, 5890 (2005).

[4] P. Khosropanah, A. Baryshev, W. Zhang, W. Jellema, J. N. Hovenier, J. R. Gao, T. M. Klapwijk, D. G. Paveliev, B. S. Williams, S. Kumar, Q. Hu, J. L. Reno, B. Klein, and J. L. Hesler, *Phase locking of a 2.7 THz quantum cascade laser to a microwave reference*, Optics Letters, **34**, 2958 (2009).

[5] A. Barkan, F. K. Tittel, D. M. Mittleman, R. Dengler, P. H. Siegel, G. Scalari, L. Ajili, J. Faist, H. E. Beere, E. H. Linfield, A. G. Davies, and D. A. Ritchie, *Linewidth and tuning characteristics of terahertz quantum cascade lasers*, Optics Letters **29**, 575 (2004).

[6] H.-W. Hübers, S. G. Pavlov, H. Richter, A.D. Semenov, L. Mahler, A. Tredicucci, H. E. Beere, and D. A. Ritchie, *High-resolution gas phase spectroscopy with a distributed feedback terahertz quantum cascade laser*, Applied Physics Letters, **89**, 061115 (2006).

[7] B. S. Williams, S. Kumar, Q. Hu, and J. L. Reno, *Operation of terahertz quantum-cascade lasers at 164 K in pulsed mode and at 117 K in continuous-wave mode*, Optics Express, **13**, 3331 (2005).

[8] W. Zhang, P. Khosropanah, J. R. Gao, E. L. Kollberg, K. S. Yngvesson, T. Bansal, R. Barends, and T. M. Klapwijk, *Quantum noise in a terahertz hot electron bolometer mixer*, Applied Physics Letters, **96**, 111113 (2010).

[9] R. D. Higgins, D. Teyssier, J. C. Pearson, C. Risacher, and N. A. Trappe, *Calibration of the Herschel HIFI Instrument using Gas Cell Measurements*, Proceedings of the 21st International Symposium on Space Terahertz Technology ISSTT, Oxford (2010).

[10] B. Klein, I. Kramer, S. Hochgurtel, R. Gusten, A. Bell, K. Meyer, and V. Chetik, *Fast Fourier Transform Spectrometer*, Proceedings of the 20th International Symposium on Space Terahertz Technology ISSTT, Charlottesville (2009).

[11] J. Kauppinen and J. Partanen, *Fourier Transforms in Spectroscopy*, Wiley, Berlin (2001).

[12] S. Ryabchun, C.-Y. Tong, S. Paine, Y. lobanov, R. Blundell, and G. Goltsman, *Temperature Resolution of an HEB Receiver at 810 GHz*, IEEE Transactions on Applied Superconductivity, **19**, 293 (2009).

[13] H. B. Callen and T. A. Welton, *Irreversibility and Generalized Noise*, Physical Review, **83**, 34 (1951).

[14] H. M. Pickett, R. L. Poynter, E. A. Cohen, M. L. Delitsky, J. C. Pearson, and H. S. P. Muller, *Submillimeter Millimeter and Microwave Spectral Line Catalog*, Journal of Quantitative Spectroscopy and Radiative Transfer, **60**, 883 (1998).

[15] High-resolution transmission molecular absorption database, http://www.cfa.harvard.edu/HITRAN/

Chapter 6

High-resolution heterodyne spectroscopy using a QCL around 3.5 THz

A frequency tunable terahertz heterodyne spectrometer, based on a third-order distributed feedback quantum cascade laser as a local oscillator, has been demonstrated by measuring molecular spectral lines of methanol (CH_3OH) gas at 3.5 THz. By varying the bias voltage of the laser, we achieved a tuning range of $\sim$1 GHz of the lasing frequency, within which the molecular spectral lines were recorded. The measured spectra show excellent agreement with modeled ones. By fitting we derived the lasing frequency for each bias voltage accurately.

The Chapter was published as Y. Ren, J. N. Hovenier, R. Higgins, J. R. Gao, T. M. Klapwijk, S. C. Shi, B. Klein, T.-Y. Kao, Q. Hu, and J. L. Reno, Appl. Phys. Lett. **98**, 231109 (2011).

6.1 Introduction

Driven by the demands of astronomical observations and atmospheric remote sensing in the terahertz (THz) frequency range, we have recently developed a high resolution heterodyne spectrometer using a quantum cascade laser (QCL) at 2.9 THz as a local oscillator (LO) and a NbN hot electron bolometer (HEB) as a mixer [1]. However, such a spectrometer is not yet adequate for operation in a telescope because of a number of drawbacks noted during the previous experiment. Firstly, the QCL used previously was based on a metal-metal waveguide Fabry-Perot cavity design, which has no mode control of the lasing frequency and has virtually zero tuning range by the bias voltage because of a resulting strong reduction of the output power. The tuning capability is, in general, highly desirable for application in spectroscopy as it is crucial for targeting more molecular lines, and also a means to identify unknown spectral lines when a heterodyne receiver is operated in the double sideband (DSB) mode1. Secondly, a ^{4}He flow cryostat was used to operate the QCL. For any balloon-borne and space mission, the use of a liquid-He based cryostat can impose a serious obstacle due to the relatively high DC power dissipation of the laser. Therefore, a dry, liquid cryogen-free cooler such as a pulse tube cryocooler or a Stirling cooler [2] is preferred. One of the challenges in using a dry cooler is the mechanical stability. As demonstrated in Ref. [3], the vibration in the cooler can introduce deviations in the operating point of the detector, leading to instability of the receiver.

In this chapter we report on a high-resolution heterodyne molecular spectroscopic experiment applying a 3.5 THz quantum cascade laser as a LO. In comparison with the previous work [1], there are three key differences; a) a single mode, third-order distributed feedback (DFB), tunable QCL [4, 5] is used as a LO; b) a pulse tube cryocooler is applied to operate the QCL, and c) a theoretical model for methanol molecular lines has been verified at 3.5 THz, which was not possible until now because of the lack of a heterodyne technique at such a frequency.

6.2 Experiment setup

By using the third-order periodic structure with strong refractive index contrast gratings, not only is the single mode emission achieved in the DFB laser, but also the radiation power out-coupling from the laser to the free space is considerably improved. Moreover, the grating structure behaves like a linear phased array antenna, resulting in a low-divergent far field beam. As a result,

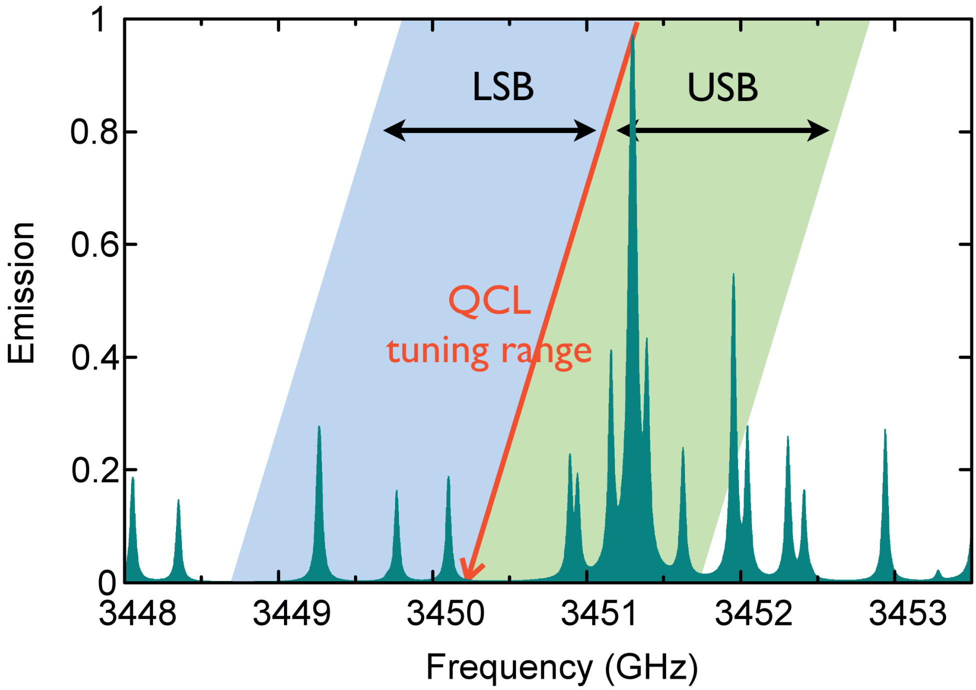

Figure 6.1. Calculated emission spectra of methanol at a pressure of 1 mbar at 300K for a 41 cm optical path length. The red arrow indicates the tuning range of the LO frequency. The blue and green shadow regions of the LSB and USB correspond to the detection band of the FFTS for the IF signal by using a 0∼1.5 GHz low pass filter.

a higher power coupling efficiency from the QCL to a HEB mixer is expected in comparison with the use of a metal-metal waveguide, Fabry-Perot cavity QCL. Our laser, based on a 10-μm thick active region, consists of 27 periods of gratings with a total length of 1070 μm. Characterized by a Fourier Transform Spectrometer with a resolution of 0.6 GHz, the laser shows a single mode emission line from 3452.0 to 3450.8 GHz by increasing the bias voltage from 13.9 V to 14.9 V. It provides a maximum output power of 0.8 mW when operated with 3 W DC input power at a bath temperature of ∼12 K. The divergence of the far-field beam is about 12 degree in both vertical and horizontal directions. We choose such a lasing frequency to demonstrate the LO technology for detecting the hydroxyl (OH) radical emission line at 3.5 THz [6]. For the detector, we use the same spiral antenna coupled NbN HEB mixer as used in Ref. [7], which has shown superior sensitivities from 1.6 to 5.3 THz.

Fig. 6.1 shows the calculated methanol emission spectrum in the vicinity of the LO frequency. To study the methanol spectrum, we apply a measurement setup similar to the one described in Ref. [1]. However, two major changes have been made. Firstly, the QCL is mounted on the second stage of a pulse tube cryocooler, where the temperature rises up to 12 K during the laser operation. It has been found [3] that the fluctuation of the coupled power from the QCL to the HEB mixer due to the piston movement of the cooler will introduce instability in the HEB. Thus an additional damper is introduced to minimize the mechanical vibration from both the refrigerator and the flexlines so that the stability of the HEB becomes comparable with the level achieved by a liquid-He-cryostat operated QCL. Secondly, although the same Fast Fourier Transform Spectrometer (FFTS) is used as the back-end spectrometer, we now only make use of the baseband (0∼1.5 GHz) for sampling the IF signals, preventing an aliasing effect [1].

The QCL is operated without any stabilization on the phase and the amplitude. The beam from the QCL passes through a high-density polyethylene (HDPE) window of the cooler and is focused to the mixer with a HDPE lens (f=26.5 mm). The signal source is a combination of a gas cell and hot/cold blackbody loads. The blackbody load is defined as a hot load at 295 K and as a cold load at 77 K. The gas cell is a 41-cm long cylinder at room temperature and has two 2-mm thick HDPE windows. The methanol emission lines around 3.5 THz from the gas cell are combined with the QCL s radiation by a 13-μm thick Mylar beam splitter and fed into the HEB mixer. The mixer downconverts the THz spectral lines at f_S to an intermediate frequency (IF) f_{IF} in the DSB mode where both the signal at upper side band (USB) $f_{USB}=f_{LO}+f_{IF}$ and lower side band (LSB) $f_{LSB}=f_{LO}-f_{IF}$ will be converted to the same IF frequency range. The IF signal is amplified first using a wide band (0.5∼12 GHz) low noise amplifier at 4.2 K that is followed by a two-stage room-temperature amplifiers with a 1.5 GHz low pass filter used in between to define the detection band width.

6.3 Tunable high-resolution heterodyne spectroscopy experiment

The same method is applied to measure the spectral lines as in Ref. [8], where three IF power spectra were measured: the spectrum $P_{emp,cold(f)}$, $P_{gas,cold(f)}$ and $P_{gas,hot(f)}$, taking 3 seconds of integration time for each single spectrum. With these three spectra, the term $2[P_{gas,cold(f)}-P_{emp,cold(f)}]/[P_{gas,hot(f)}-P_{emp,cold(f)}]$ is obtained, which reflects the relative emission of the gas with re-

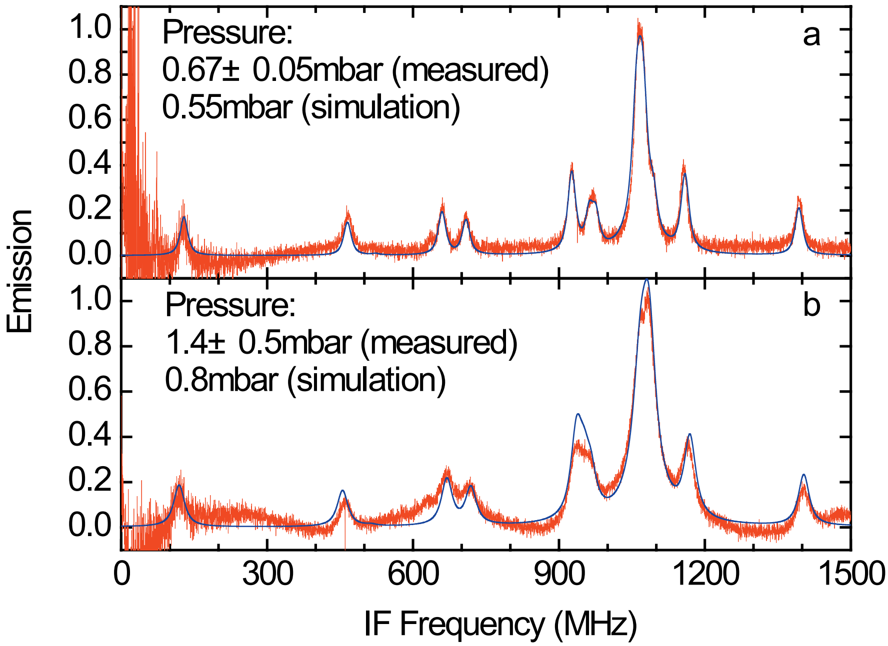

Figure 6.2. Experimental and simulated methanol spectral lines as a function of frequency at different gas pressure with a LO frequency of 3450.232GHz. (a) the low pressure spectrum; (b) the high pressure data.

spect to the 300 K blackbody radiation, and the factor of 2 reflects the DSB mode of operation of the HEB mixer.

Several methanol spectral lines around 3.5 THz were observed simultaneously within the IF frequency range. To check the consistency with the theoretical model, the spectra were taken at different pressure because of the broadening effect. We apply the model developed in our previous work [1], which is based on the expected methanol line frequencies with intensities from the JPL line catalog [9] and includes three different broadening mechanisms: thermal Doppler broadening, pressure broadening and opacity broadening. Comparisons were made between the measured and simulated methanol spectral lines at 3.5 THz. As shown in Fig. 6.2, for a low-pressure case of 0.67 mbar, an excellent agreement is obtained with respect to both the line frequencies and the relative intensities. While for the high-pressure case of 1.4 mbar, the experimental result shows deviation of the line intensities from the theoretical simulation. This deviation might be attributed to the shifting of HEB mixer s working point due to emission from the gas cell, or the so-called direct detection effect. At high gas pressure, since the emission power from the methanol molecule becomes relatively high, this effect is more prominent. The difference between the measured gas pressure and the value used for the simulation indicated in Fig. 6.2 is due to the inaccuracy of the gas pressure calibration. Furthermore, the pressure broadening coefficient, as defined in HITRAN database [9] , was found to be 14.8 MHz/mbar (0.5 cm^{-1}/atm), which is a factor of two higher than the value found at 2.9 THz, suggesting that this coefficient can vary noticeably with the frequency.

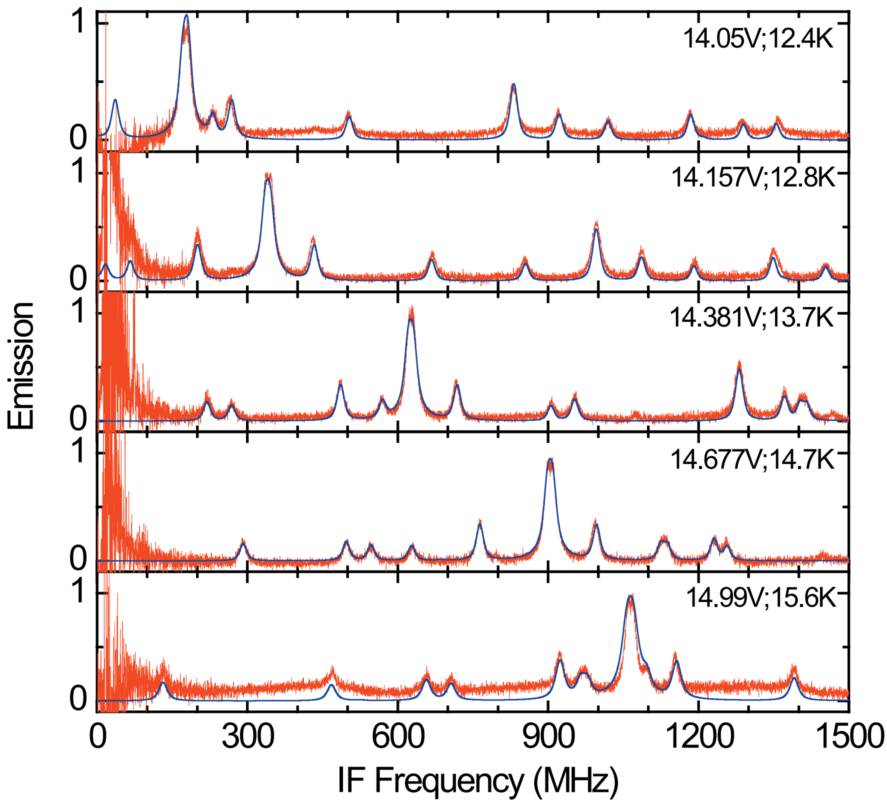

Figure 6.3. Measured methanol spectra with different LO frequency, which is tuned with the bias voltage of the QCL from 14.05 V to 14.99 V. The gas pressures for all spectra are at 0.65±0.05 mbar.

To enable a frequency tunable spectroscopic measurement, not only is a relatively large frequency tuning range of the laser crucial, but also the emission power should be sufficient to operate the mixer at all frequencies. As we demonstrate in this work, the third-order DFB lasers can meet both of these requirements. Fig. 6.3 illustrates several methanol spectra recorded at different LO frequencies, tuned by the QCL bias voltage. As the QCL frequency decreases with increasing bias voltage, a strong methanol emission line located at 3451.2988 GHz shifts from 13 MHz in LSB to 1064 MHz in USB. Fig. 6.3 shows only the spectra starting from 170 MHz in USB. Within the entire frequency tuning range of about ∼1 GHz, we made comparisons between the measured spectra and theoretical ones. As shown partly in Fig. 6.3, excellent agreements were achieved for the entire frequency region. By fitting with the model, we derived the lasing frequency as a function of the bias, which is shown in Fig. 6.4. Moreover, in contrast to a previously reported first-order DFB laser that shows single-mode operation within only a limited bias range [10], we confirmed single-mode emission behavior of a third-order DFB QCL for the entire operation range [4] since all the measured molecular spectra could be well described.

QCL frequency tuning is dominated by the change of the refractive index with the temperature change of the active region. To distinguish electrical tuning from thermal tuning we also measured the frequency tuning by varying only the bath temperature. The results are summarized in the inset of Fig. 6.4. A 150 MHz tuning range is shown for a temperature range from 13.2 to 17.6 K, where a thermal tuning coefficient of -33 MHz/K was obtained. After subtraction of the thermal effect, an electrical tuning coefficient of -859 MHz/V is derived for our case. This tuning coefficient is smaller than those reported from Fabry-Perot cavity lasers [11, 12] This can be explained by the fact that the gain medium used for this laser has dual gain peaks at 3.3 and 3.8 THz. At 3.5 THz, the effects of the frequency pulling from these two peaks partially cancel out each other and thus reduce the tuning coefficient.

6.4 Temperature and frequency resolution

To evaluate the temperature resolution of such a heterodyne spectrometer, a calibrated spectrum within the IF frequency range between 0∼1.5 GHz is obtained, as shown in Fig. 6.5. Several methanol spectral lines with different intensity around 3.5 THz were simultaneously observed. For a Dicke-type

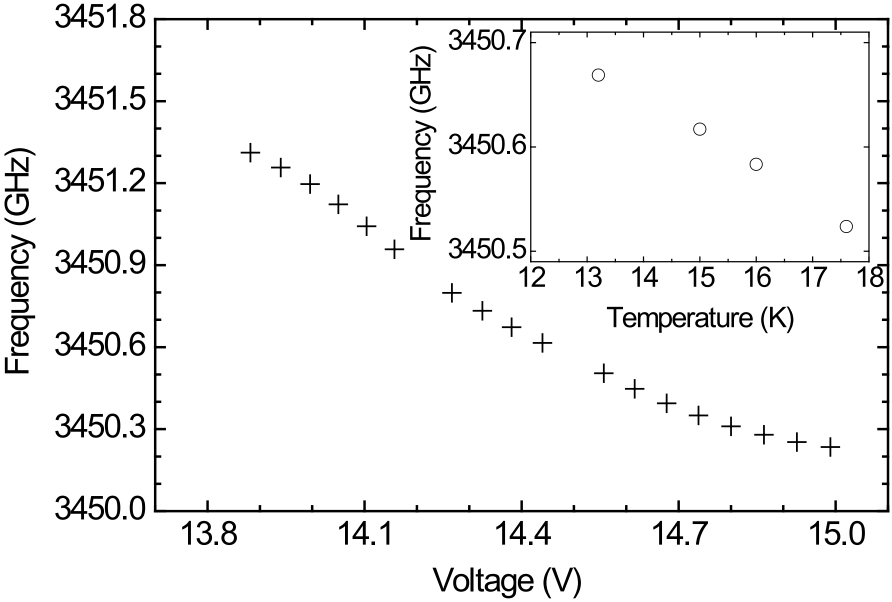

Figure 6.4. QCL emission frequency as a function of bias voltage. The inset shows the measured QCL frequency at different bath temperature.

radiometer, the temperature resolution is given by [8],

$$\Delta T = \sqrt{\frac{(T_A + T_R)^2}{B\tau_A}\frac{1}{d_A} + \frac{(T_{ref} + T_R)^2}{B\tau_{ref}}\frac{1}{d_{ref}}}, \tag{6.1}$$

where T_A is the effective antenna temperature; T_R the receiver noise temperature; T_{ref} the reference signal temperature; B the detection bandwidth; τ_A the integration time for the spectral line signal; τ_{ref} the integration time for the reference signal; d_A and d_{ref} are the duty cycles of the observation time for the spectral line signal and reference signal, respectively. In our case, T_A=300 K, T_R=3800 K, T_{ref}=77 K, and B=183 kHz. For each single spectrum, it takes 3 seconds of integration time. So for a single spectrum, τ_A=τ_{ref}=3 sec, and d_A=d_{ref} =1/3, from which we expect a ΔT of 13.2 K. As shown in Fig. 6.5, the standard deviation of measured noise level was 13.8 K. We also performed 18 series of the $P_{gas,cold}$(f) spectrum measurement and 21 series of the $P_{emp,cold}$(f) spectrum measurement. The calibrated spectrum was subsequently averaged as plotted inFig. 6.5. In the time averaged case, τ_A=3 sec×18

(18 times average), τ_{ref}=3 sec×21 (21 times average), d_A =18/(18+21+1), d_{ref} =21/(18+21+1), from which we expect a ΔT of 2.5 K. Our experimental data indicate a temperature resolution of 3.5 K. Then the time averaged spectrum was smoothed to the 1.83-MHz resolution, as plotted in Fig. 6.5. Since B=1.83 MHz, we expect a ΔT of 0.79 K, where our experiment data is 1.44 K. Based on those data, we conclude that the temperature resolution in the single measurement follows the value expected from the radiometer equation. However, a factor of 2 difference was observed for the multiple, time averaged case. For the latter case, as the QCL was operated in the free-running mode, the 1/f noise in the amplitude of the QCL could attribute to the discrepancy between the measured results and the value from the radiometer equation. This effect may relate to the issue of the Allan variance time of the whole receiver system [13]. Since we are doing spectroscopic measurements, so the relevant Allan variance time is a spectroscopic Allan time, which should be much longer than, e.g. 3 sec. However, we do not know the upper limit of the Allan time in our case. To get such information this merits in-depth studies in the future work. The worse temperature resolution for the spectrum below 500 MHz is mainly due to higher noise contribution from the cryogenic amplifier, which is beyond its operating frequency range.

Also the frequency resolution is crucial for a heterodyne spectrometer. In the current experiment, with the free-running QCL as a LO the narrowest linewidth for the measured methanol spectral line is 11 MHz at a pressure of 0.43 mbar. We inferred that the linewidth of the QCL should be in order of 1 MHz. The linewidth of this laser has been studied separately and is reported in Ref. [14]. In the free-running mode it was found to be around 900 KHz. Together with a 183 KHz resolution FFTS, the frequency resolution of the heterodyne spectrometer increases to 1.1 MHz. This value agrees with that inferred from our experiment. We note that for astronomical observations at THz frequencies, atomic and molecular gases are at lower pressure and lower temperature, resulting in narrow spectral linewidths of 1 MHz. Obviously, to reduce the linewidth, phase or frequency locking of the QCL will be required. As shown in Ref. [14], the linewidth of the QCL is reduced to 18 KHz by locking to a molecular absorption line. This locked linewidth together with the FFTS we used enable a THz heterodyne spectrometer with a frequency resolution of 200 KHz ($\upsilon/\Delta\upsilon>10^7$). And the rich molecular absorption lines in combination with the frequency tunability facilitate the frequency locking scheme and hold the advantage for higher frequencies.

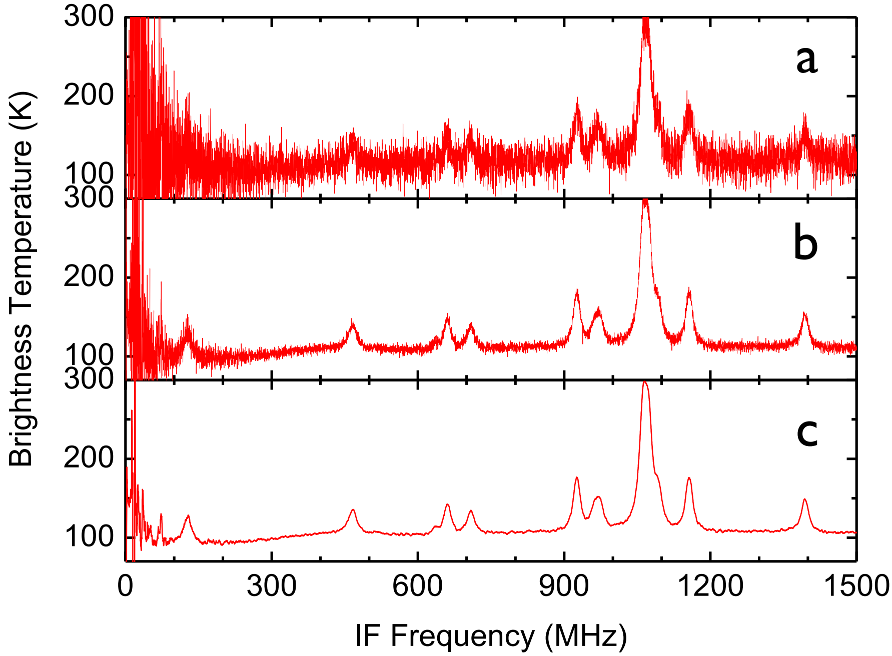

Figure 6.5. High resolution methanol (CH_3OH) emission spectrum measured within the IF frequency range between 0∼1.5 GHz. (a) the original spectrum, with 3 seconds integration time for 3 spectrum traces; (b) the time averaged spectrum, where 18 series of the $P_{gas,cold}$(f) spectrum and 21 series of the $P_{emp,cold}$(f) spectrum were averaged; (c) the time and frequency averaged spectrum, the time averaged spectrum was smoothed to the 1.83-MHz resolution.

6.5 Conclusions

In conclusion we succeeded in demonstrating a tunable high-resolution heterodyne spectrometer using a 3.5 THz third-order DFB QCL operated in a pulse tube cryocooler as a local oscillator. By adjustment of the bias voltage, a frequency tuning range of ∼1 GHz has been achieved in heterodyne spectroscopic measurements. Within the entire frequency tuning range, the measured spectra show excellent agreement with the theoretical simulations. By fitting with the model we derived the lasing frequency versus bias voltage accurately. Even though the observed tuning range is still small, this result demonstrates the benefits to be expected from a further increase of the tuning range of THz QCLs, such as the development reported recently in Ref. [15].

Bibliography

[1] Y. Ren, J. N. Hovenier, R. Higgins, J. R. Gao, T. M. Klapwijk, S. C. Shi, A. Bell, B. Klein, B. S. Williams, S. Kumar, Q. Hu, and J. L. Reno, *Terahertz heterodyne spectrometer using a quantum cascade laser*, Applied physics letters, **97**, 161105 (2010).

[2] H. Richter, M. Greiner-Bar, S. G. Pavlov, A. D. Semenov, M. Wienold, L. Schrottke, M. Giehler, R. Hey, H. T. Grahn, and H.-W. Hübers, *A compact, continuous-wave terahertz source based on a quantum-cascade laser and a miniature cryocooler*, Optics Express, **18**, 10177 (2010).

[3] H. Richter, A. D. Semenov, S. Pavlov, L. Mahler, A. Tredicucci, K. Il'in, M. Siegel, and H.-W. Hübers, *Terahertz heterodyne receiver with quantum cascade laser and hot electron bolometer mixer in a pulse tube cooler*, Applied physics letters, **93**, 141108 (2008)

[4] M. I. Amanti, M. Fischer, G. Scalari, M. Beck, and J. Faist, *Low-divergence single-mode terahertz quantum cascade laser*, Nature Photonics, **3**, 586 (2009).

[5] M. I. Amanti, G. Scalari, F. Castellano, M. Beck, and J. Faist, *Low divergence Terahertz photonic-wire laser*, Optics Express, **18**, 6390 (2010).

[6] P. Khosropanah, W. Zhang, J. N. Hovenier, J. R. Gao, T. M. Klapwijk, M. I. Amanti, G. Scalari, and J. Faist, *3.4 THz heterodyne receiver using a hot electron bolometer and a distributed feedback quantum cascade laser*, Journal of Applied Physics, **104**, 113106 (2008).

[7] W. Zhang, P. Khosropanah, J. R. Gao, E. L. Kollberg, K. S. Yngvesson, T. Bansal, R. Barends, and T. M. Klapwijk, *Quantum noise in a terahertz hot electron bolometer mixer*, Applied physics letters, **96**, 111113 (2010).

[8] S. Ryabchun, C.-Y. Tong, S. Paine, Y. lobanov, R. Blundell, and G. Goltsman, *Temperature Resolution of an HEB Receiver at 810 GHz*, IEEE Transactions on Applied Superconductivity, **19**, 293 (2009).

[9] High-resolution transmission molecular absorption database, http://www.cfa.harvard.edu/HITRAN/

[10] B. S. Williams, S. Kumar, Q. Hu, and J. L. Reno, *Distributed-feedback terahertz quantum-cascade lasers with laterally corrugated metal waveguides*, Optics Letters, **30**, 2909 (2005).

[11] A.L. Betz, R.T. Boreiko, B.S. Williams, S. Kumar, Q. Hu and J.L. Reno, *Frequency and phase-lock control of a 3 THz quantum cascade laser*, Optics Letters, **30**, 1837 (2005).

[12] P. Khosropanah, A. Baryshev, W. Zhang, W. Jellema, J. N. Hovenier, J. R. Gao, T. M. Klapwijk, D. G. Paveliev, B. S. Williams, S. Kumar, Q. Hu, J. L. Reno, B. Klein, and J. L. Hesler, *Phase locking of a 2.7 THz*

quantum cascade laser to a microwave reference, Optics Letters, **34**, 2958 (2009).

[13] J. W. Kooi , J. J. A. Baselmans, A. Baryshev, R. Schieder , M. Hajenius, J. R. Gao, T. M. Klapwijk, B. Voronov, and G. Gol'tsman, *Stability of heterodyne terahertz receivers*, Journal of Applied Physics, **100**, 064904 (2006).

[14] Y. Ren, J. N. Hovenier, M. Cui, D. J. Hayton, J. R. Gao, T. M. Klapwijk, S. C. Shi, T-Y. Kao, Q. Hu, and J. L. Reno, *Frequency locking of signle-mode 3.5-THz quantum cascade lasers using a gas cell*, Applied physics letters, **100**, 041111 (2012).

[15] Q. Qin, B. S. Williams, S. Kumar, J. L. Reno, and Q. Hu, *Tuning a terahertz wire laser*, Nature Photonics, **3**, 732 (2009).

Chapter 7

Frequency locking of single-mode 3.5-THz quantum cascade lasers using a gas cell

We report frequency locking of two 3.5-THz third-order distributed feedback (DFB) quantum cascade lasers (QCLs) by using methanol molecular absorption lines, a proportional-integral-derivative controller, and a NbN bolometer. We show that the free-running linewidths of the QCLs are dependent on the electrical and temperature tuning coefficients. For both lasers, the frequency locking induces a similar linewidth reduction factor whereby the narrowest locked linewidth is below 18 kHz with a Gaussian-like shape. The linewidth reduction factor and the ultimate linewidth correspond to the measured frequency noise power spectral density.

The Chapter was published as Y. Ren, J.N. Hovenier, M. Cui, D.J. Hayton, J.R. Gao, T.M. Klapwijk, S.C. Shi, T-Y. Kao, Q. Hu, and J. L. Reno, Appl. Phys. Lett. **100**, 041111 (2012).

7.1 Introduction

A phase- or frequency-stabilized solid-state source is of crucial importance for its application as local oscillator (LO) for high-resolution heterodyne spectroscopy in the terahertz (THz) frequency range for astronomical and atmospheric research, particularly from space. As solid-state sources above 2 THz, quantum cascade lasers (QCLs) have shown great advantages, based on their broad frequency coverage, single-mode emission and high output power [1]. It has been shown theoretically [2, 3] and experimentally [4, 5]* that THz QCLs can have narrow intrinsic linewidths of below tens of kHz. However, caused by the fluctuations in the electrical bias and in the operating temperature, the practical linewidth of a free-running THz QCL measured over a long period (>1 s) is usually much broader, typically greater than 1 MHz [4, 6].

Phase locking of a THz QCL to an external up-converted reference source has been demonstrated [6, 7], where both the phase and frequency of the laser radiation are stabilized. However, in this phase locking approach, an additional THz reference source is required, that can be difficult to implement at frequencies above 3 THz due to the lack of suitable sources. Alternatively, phase locking of a 2.5 THz QCL to a frequency comb using a GaAs photomixer was developed recently [8]. The advantage of this approach is the possibility of using a room temperature detector. Additionally, the technique can be applied, in principle, to any frequency. In some applications such as a heterodyne interferometer [9], phase locking of multiple LOs to a common reference is essential. However, for an observation based on a single telescope, frequency locking, where the LOs average frequency is stabilized, but where its linewidth remains intrinsic, is often sufficient. A frequency stabilization scheme based on a molecular line as reference frequency was demonstrated for a 2.5 THz QCL [10]. In this case the QCLs frequency was stabilized, resulting in a full width at half maximum (FWHM) linewidth of 300 kHz. It is worth noting that the locked linewidth is at least an order of magnitude greater than the intrinsic linewidth [2–5] suggesting that the full potential of this technique was not achieved yet. However, this approach is simple and robust because it requires in essence only a gas cell unit and a direct power detector which does not have to be operated at very low temperature.

Here we perform the frequency stabilization measurements using a methanol (CH_3OH) absorption line, but with two advanced, frequency controllable distributed feedback (DFB) QCLs [11] at much higher frequencies. Furthermore,

* The intrinsic linewidth of 90 Hz was inferred from the measured frequency noise spectral density of a THz QCL.

we apply a superconducting NbN bolometer as a power detector to monitor the radiation signal after a gas cell. We report not only a much narrower locked linewidth, but also address the device dependence on the free running linewidth and line shape.

7.2 Experiment setup

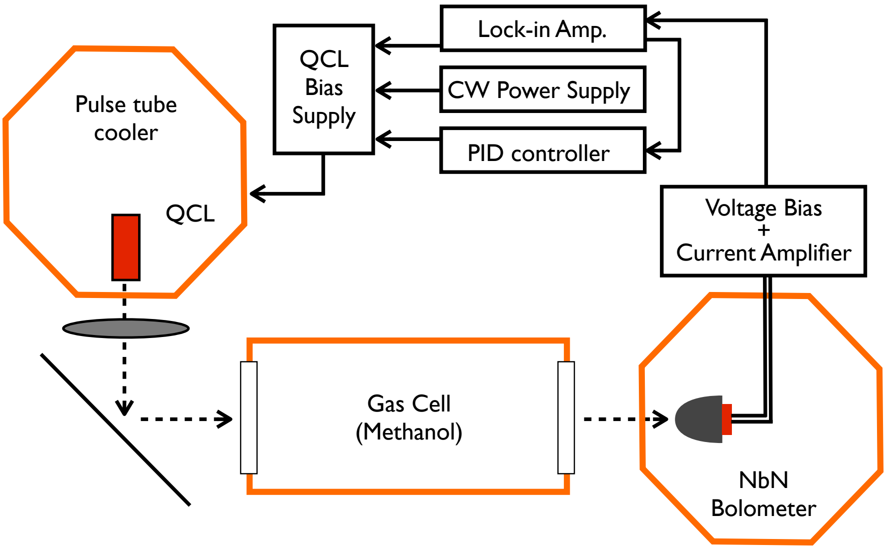

Figure 7.1. Schematic of the frequency locking measurement setup.

The QCLs used are two third-order DFB QCLs. The QCL lasing at 3.45 THz is labeled as "laser A" and the other at 3.35 THz as "laser B ". The two lasers, based on a 10-μm thick active region, consist of 27 periods of gratings, but with slightly different periodicity. The lasers are designed and fabricated by the MIT group. As demonstrated previously [12], by using the third-order periodic structure with strong refractive index contrast gratings, not only can single mode emission be achieved, but also a less divergent, single spot far-field beam. Each QCL is mounted on the second stage of a pulse tube cryocooler ($\sim$12 K under load) without further temperature stabilization.

The measurement setup is schematically described in Fig. 7.1. The QCL beam is first focused with a high-density polyethylene (HDPE) lens (f=26.5 mm), and then guided through a gas cell by a 13-μm thick Mylar beam splitter. The gas cell, containing methanol gas at room temperature, is a 41-cm long cylinder with two 2-mm thick HDPE windows. Methanol gas is chosen since it contains abundant absorption lines around the QCL frequencies. The transmitted signal through the gas cell is monitored by a superconducting NbN bolometer operated at liquid helium temperature as a direct detector whereby we benefit from a NEP of $10^{-12} \sim 10^{-13}$ [13] and a fast response (∼40 psec).

7.3 Frequency locking of a THz QCL to a molecular absorption line

To perform frequency locking, we apply a summing bias circuit that allows combining three input signals to independently control the bias voltage of a laser [10]. The first input is a standard DC bias voltage, which sets the operating point of the laser. The second input is an AC sinusoidal modulation signal at around 1 kHz with relatively small amplitude ($< 0.01\%$ of the DC bias). By feeding the detector output current to a lock-in amplifier with the AC modulation signal as reference frequency, the derivative signal of the absorption profile is obtained. The third one is the control signal from a feedback loop. A proportional-integral-derivative (PID) controller is used to actively lock this derivative signal to be maintained at zero value, and a compensatory signal is fed back to the bias circuit of the QCL. In this way, the QCL frequency can be stabilized to a particular molecular absorption line.

We measured the methanol absorption spectrum (versus frequency) by sweeping the QCL bias voltage since the voltage regulates its emission frequency. Fig. 7.2 shows an obtained strong absorption line at around 3.45 THz. Also shown in the figure is the first derivative of the absorption profile, which is obtained by using a lock-in technique. The lock-in derivative signal is in turn utilized for the PID control loop, whereby a feedback signal is generated and fed to the bias circuit of the QCL in order to yield a stabilized lock-in signal. Around the frequency of the absorption peak, the linear region of the lock-in signal indicates the frequency locking range. We apply the exact same locking scheme for both QCLs. To illustrate the locking process, the inset of Fig. 7.2 plots the lock-in signal for laser A. When the laser is unlocked, the observed fluctuations reflect the frequency fluctuations of the QCL. The observed 1 Hz frequency feature in the lock-in signal is the result of the typical temperature oscillation of the pulse tube cooler. After the PID feedback loop is enabled, the lock-in signal becomes well stabilized and maintained at the 0 mV setpoint. Thus, the laser frequency is stabilized.

The laser linewidth can be estimated by transforming the variation in volt-

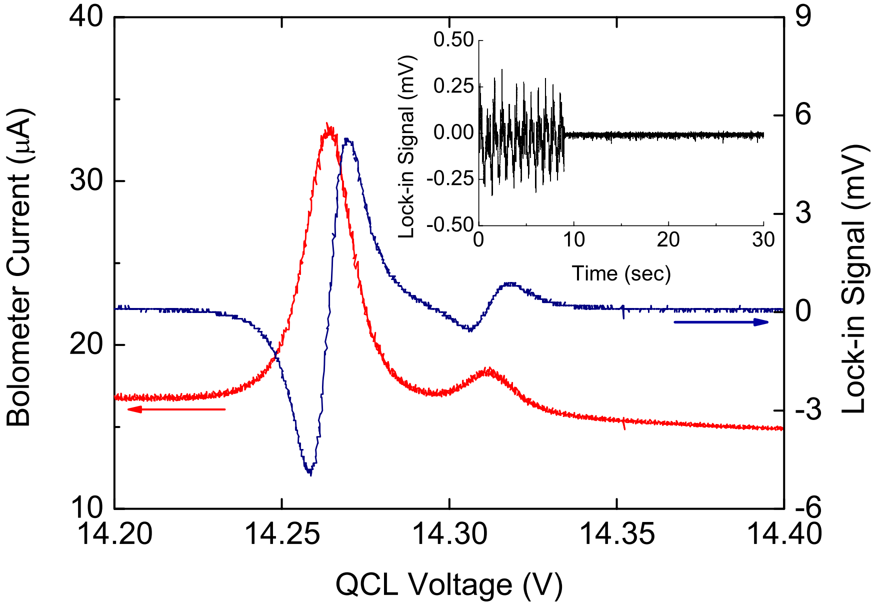

Figure 7.2. Absorption profile of methanol lines at 1.1 mbar as measured for "laser A". By using a NbN bolometer detector and a lock-in amplifier, the error signal was measured, labeled as lock-in signal. The voltage window (linear region for the lock-in signal) used for lock-in feedback loop is 8 mV. The inset shows the lock-in signal in the unlocked and locked state after about 8 s for "laser A".

age of the lock-in signal, which represents the error signal, into the frequency domain. The lock-in signal is first converted to the equivalent variation in the QCL bias voltage using the measured linear profile in the main figure of Fig. 7.2. Subsequently, two different methods are applied to calibrate the numerical correspondence between frequency and voltage. Method one is based on spectroscopic measurements [12], where the frequency tuning coefficients of the QCL due to the bias voltage are obtained. Then the frequency can be obtained by multiplying the voltage (the lock-in signal) with the tuning coefficient. The second method is to make use of the methanol gas pressure broadening coefficient at 3.5 THz [12], which is established from a set of methanol absorption lines at different gas pressures. In this way a lock-in signal can also be transformed into frequency. We find that the two different approaches give similar results to within 10%. Fig. 7.3 plots a histogram of the

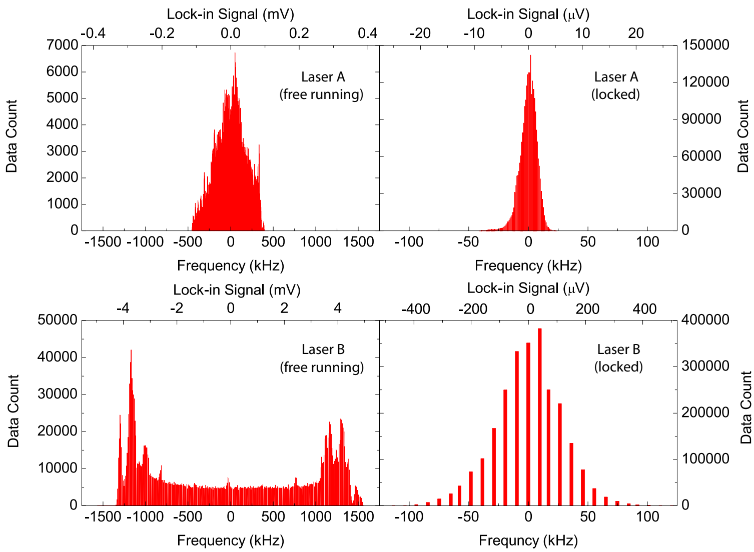

Figure 7.3. Histogram of the relative frequency deviation to the center frequency for two lasers in the free running and locked states, calculated based on the lock-in signal fluctuations of a 10 s observation time.

relative frequency fluctuations of a 10 sec observation time in order to present the standard deviation of the center freuqency. We find that the free running laser linewidth for laser A is roughly 1 MHz, while the locked linewidth is less than 18 kHz (both estimated using the FWHM of the profile). For laser B we obtain the free running linewidth of around 3 MHz and the locked linewidth of 51 kHz, both of which are about 3 times larger than that found for laser A. We also notice that in Fig. 7.3 the free running line shape of laser B is double-peaked, while it is single-peaked for laser A. When locked, both QCLs show a Gaussian-like shape.

Now we discuss the line shape and linewidth. It is known that the frequency noise of the QCL governs the free running line shape [10]. In our experiment the frequency noise is mainly due to temperature and electric (DC and AC voltage signal) fluctuations. The temperature fluctuations are directly caused by the intrinsic fluctuations of the pulse tube cryocooler with a frequency around 1

Hz, while the electric fluctuations are due to the current noise in the DC bias and due to the AC modulation signal. The latter is typically at a relatively high frequency (~kHz).

We have simulated the line shape in this case by assuming that the temperature fluctuations, $A_T sin(2\pi f_T t)$, and AC voltage modulation, $A_E sin(2\pi f_E t)$, are the dominant fluctuations and that they give linear response to the frequency fluctuations, where $A_{T,E}$ and $f_{T,E}$ are the amplitude and frequency, respectively. We find that when the amplitude A_T and A_E are comparable, the line shape appears to be single peaked. In contrast, when $A_T \gg A_E$, the line shape becomes double-peaked. To verify this, we now examine what are the dominant fluctuations. For this, we measured the temperature and voltage tuning coefficients for each laser. We find that both lasers have a similar electric tuning coefficient, but a different temperature tuning coefficient. The latter for laser B is more than 2 times higher than laser A. Therefore, we conclude that the higher temperature tuning coefficient in laser B are predominant, which attributes to the observed double-peaked line shape. For the same reason we also understand its larger free-running linewidth. As for why there is such a difference in the temperature tuning coefficient between two similar lasers, however, is unclear.

With regard to the locked linewidth, we notice that the obtained minimal linewidth is consistent with the published results in [4], where a linewidth of 30 kHz was measured within a short period of 3 ms, and in [14] where a a linewidth of 6.3 kHz was obtained with a different frequency locking technique.

Fig. 7.4 shows the measured noise power spectral densities of the lock-in signals for both lasers with and without the frequency locking. In this measurement, the 30-millisecond time constant set in the lock-in amplifier has induced a small noise bandwidth of ~5 Hz in the figure. The frequency locking results in suppression of the noise level over 30 dB at frequencies below about 5 Hz for both QCLs, illustrating the effective laser linewidth reduction. Furthermore, the higher frequency noise levels for laser B correspond to the measured larger linewidths. Although the noise data beyond 5 Hz may also be useful to understand the physical process, they are less straightforward because of the interplay between the lock-in bandwidth (~5 Hz) and the PID bandwidth (~1 kHz). This interplay determines the bandwidth of the entire feedback loop, which in turn governs the linewidth reduction factor.

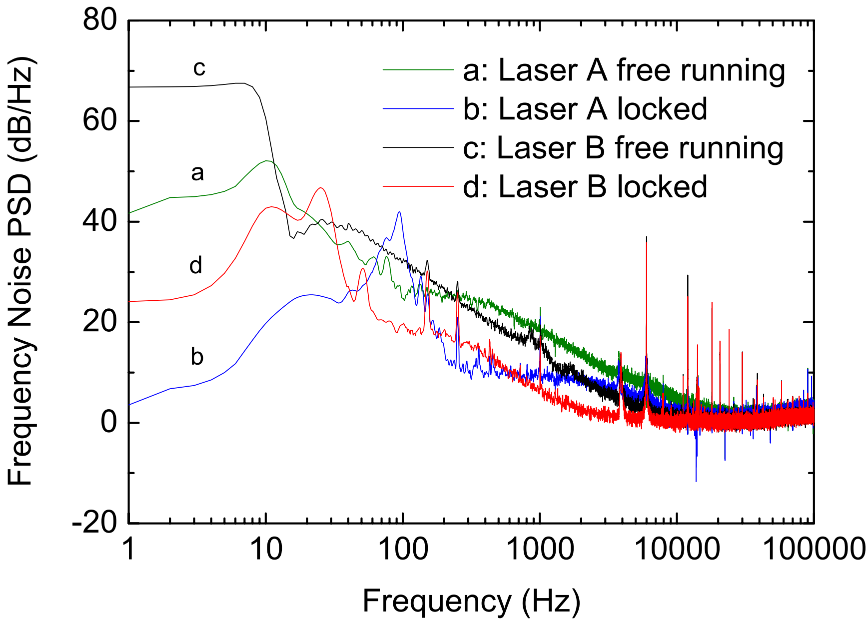

Figure 7.4. Frequency noise power spectral density of the lock-in signal for two lasers in the free running and locked states.

7.4 Conclusions

In conclusion, we succeeded in frequency locking of two 3.5-THz DFB quantum cascade lasers by using methanol molecular absorption lines. Two different methods were applied to converting the lock-in signal in voltage to the linewdith of the lasers and both result in similar linewidths. The electrical and temperature tuning coefficients play a crucial role in determining the free-running line widths and shapes. The minimal linewidth is found to be below 18 kHz, which is sufficiently small for local oscillator applications. For the future practical applications like SOFIA, we plan to use a high-Tc (77K and above) superconducting bolometric detector in place of the low temperature NbN bolometer shown here to simplify the instrument.

Bibliography

[1] B. S. Willams, *Terahertz quantum-cascade lasers*, Nature Photonics, **23**, 51 (2007).

[2] M. Yamanishi, T. Edamura, K. Fujita, N. Akikusa, and H. Kan, *Theory of the Intrinsic Linewidth of Quantum-Cascade Lasers: Hidden Reason for the Narrow Linewidth and Line-Broadening by Thermal Photons*, IEEE Journal of Quantum Electronics, **44**, 12 (2008).

[3] C. Jirauschek, *Monte Carlo study of intrinsic linewidths in terahertz quantum cascade lasers*, Optics Express, **18**, 25922 (2010).

[4] A. Barkan, F. K. Tittel, D. M. Mittleman, R. Dengler, P. H. Siegel, G. Scalari, L. Ajili, J. Faist, H. E. Beere, E. H. Linfield, A. G. Davies, and D. A. Ritchie, *Linewidth and tuning characteristics of terahertz quantum cascade lasers*, Optics Letters, **29**, 575 (2004).

[5] M. S. Vitiello, L. Consolino, S. Bartalini, A. Taschin, A. Tredicucci, M. Inguscio, P. De Natale, *Quantum-limited frequency fluctuations in a Terahertz laser*, Nature Photonics, **6**, 525 (2012).

[6] P. Khosropanah, A. Baryshev, W. Zhang, W. Jellema, J. N. Hovenier, J. R. Gao, T. M. Klapwijk, D. G. Paveliev, B. S. Williams, S. Kumar, Q. Hu, J. L. Reno, B. Klein, and J. L. Hesler, *Phase locking of a 2.7 THz quantum cascade laser to a microwave reference*, Optics Letters, **34**, 2958 (2009).

[7] D. Rabanus, U. U. Graf, M. Philipp, O. Ricken, J. Stutzki, B. Vowinkel, M. C. Wiedner, C. Walther, M. Fischer, and J. Faist, *Phase locking of a 1.5 Terahertz quantum cascade laser and use as a local oscillator in a heterodyne HEB receiver*, Optics Express, **17**, 1159 (2009).

[8] M. Ravaro, C. Manquest, C. Sirtori, S. Barbieri, G. Santarelli, K. Blary, J.-F. Lampin, S. P. Khanna, and E. H. Linfield, *Phase-locking of a 2.5 THz quantum cascade laser to a frequency comb using a GaAs photomixer*, Optics Letters, **36**, 3969 (2011).

[9] A. Wootten and A. R. Thompson, *The Atacama Large Millimeter/Submillimeter Array*, Proceedings of the IEEE, **97**, 1463 (2009).

[10] H. Richter, S. G. Pavlov, A. D. Semenov, L. Mahler, A. Tredicucci, H. E. Beere, D. A. Ritchie, and H.-W. Hübers, *Submegahertz frequency stabilization of a terahertz quantum cascade laser to a molecular absorption line*, Applied Physics Letters, **96**, 071112 (2010).

[11] M. I. Amanti, M. Fischer, G. Scalari, M. Beck, and J. Faist, *Low-divergence single-mode terahertz quantum cascade laser*, Nature Photonics, **3**, 586 (2009).

[12] Y. Ren, J. N. Hovenier, R. Higgins, J. R. Gao, T. M. Klapwijk, S. C. Shi, B. Klein, T.-Y. Kao, Q. Hu, and J. L. Reno, *High-resolution heterodyne spectroscopy using a tunable quantum cascade laser around 3.5 THz*, Applied Physics Letters, **98**, 231109 (2011).

[13] Y. Ren, W. Miao, Q. J. Yao, W. Zhang, and S. C. Shi, *Terahertz direct detection characteristics of a superconducting NbN bolometer*, Chinese Physics Letters, **28**, 010702 (2011).

[14] A. Baryshev, J. N. Hovenier, A. J. L. Adam, I. Kasalynas, J. R. Gao, T. O. Klaassen, B. S. Williams, S. Kumar, Q. Hu, and J. L. Reno, *Phase locking and spectral linewidth of a two-mode terahertz quantum cascade laser*, Applied Physics Letters, **89**, 031115 (2006).

Chapter 8

Frequency and amplitude stabilized terahertz quantum cascade laser as local oscillator

We demonstrate an experimental scheme to simultaneously stabilize the frequency and amplitude of a 3.5 THz third-order distributed feedback quantum cascade laser as a local oscillator. The frequency stabilization has been realized using a methanol absorption line, a power detector and a proportional-integral-derivative (PID) loop. The amplitude stabilization of the incident power has been achieved using a swing-arm voice coil actuator as a fast optical attenuator, using the direct detection output of a superconducting mixer in combination with a 2nd PID loop. Improved Allan Variance times of the entire receiver, as well as the heterodyne molecular spectra, have been demonstrated.

The Chapter was published as Y. Ren, D.J. Hayton, J.N. Hovenier, M. Cui, J.R. Gao, T.M. Klapwijk, S.C. Shi, T-Y. Kao, Q. Hu, and J. L. Reno, Appl. Phys. Lett. **101**, 101111 (2012).

8.1 Introduction

A terahertz (THz) quantum cascade laser (QCL) is the most promising solid-state source as the local oscillator (LO) for a high resolution ($\upsilon/\Delta\upsilon > 10^6$, where υ is the frequency) heterodyne receiver operating at frequencies above 2 THz and, in particular, for an multi-pixel array receiver because of its high output power (typically mW) [1, 2]. Among different types of applications, such a heterodyne receiver plays a vital role in astronomical observations, for instance mapping a large number of fine structures and molecular lines associated with the formation of stars and planets in the Milky Way and nearby galaxies [3]. Those spectral lines at high frequencies are typically narrow ($\leq$ a few MHz). Furthermore, the signals are, in general, very weak and deeply embedded within the noise [3].

The narrow spectral lines require either frequency or phase stabilization of a local oscillator. Since the intrinsic linewidth of a THz QCL is much narrower ($<$ kHz) [4] compared to typical astronomical targeting lines, frequency locking of a QCL will be sufficient. Until now, a considerable amount of progress has been made to achieve either phase locking or frequency locking to a THz QCL since the first demonstration of a THz QCL [5–7]. In essence, these experiments have established that the THz QCL, like other solid-state oscillators, is a voltage-controlled oscillator (VCO) whose frequency is determined by a control DC voltage.

The weak signal lines require a long integration time during an observation in addition to the high sensitivity of a mixer. The effective integration time is limited by the stability of the entire receiver, which is characterized by the Allan Variance time for a given measurement bandwidth [8]. The latter is a function of many factors and will be discussed in detail later. For a receiver based on a superconducting hot electron bolometer (HEB) mixer, the stability is predominated by the amplitude stability of the incident LO power [9]. It is known that the output power of a THz QCL is determined by both DC bias and operating temperature. Thus, any fluctuation or drift either on the bias or in the temperature may give rise to the output power fluctuation. The power stability becomes problematic when the QCL is operated in a pulse tube cryocooler, where temperature fluctuations are intrinsically present. Furthermore, the DC bias regulates the emission frequency of the laser at a given temperature. In order to stabilize the frequency and amplitude of the laser simultaneously, another means of tuning, besides from the DC bias, is desired, especially when the frequency and amplitude fluctuations are anti-correlated to the bias.

In this chapter we apply a swing-arm actuator placed in the optical beam path to block part of the QCL beam in order to stabilize the incident power from a 3.5 THz QCL. The amplitude stabilization loop consists of a PID controller and it takes advantage of the direct power detection of a HEB mixer. As demonstrated in Ref. [9], by stabilizing the power from a THz gas laser as a LO, this technique can improve the stability of a 2.5 THz heterodyne receiver drastically. The frequency of the QCL is locked to a methanol (CH_3OH) absorption line. By implementing these two stabilization schemes at the same time, we demonstrate a fully stabilized heterodyne receiver, which is further characterized by Allan Variance and heterodyne spectroscopy.

8.2 Experiment setup

The LO used is a third-order distributed feedback (DFB) QCL based on a metal-metal, lateral corrugated waveguide, which, until now, is the most advanced THz QCL for the purpose of local oscillators [10]. Its unique features are tunable single mode frequency operation and low-divergent main lobe in the beam. The latter, as a result of the grating structure that behaves as a linear phased array antenna, is crucial for better coupling of the radiation power between the laser and an HEB mixer. Such 3rd DFB lasers have the potential of higher operating temperatures ($>$77 K) and lower DC dissipation power ($<$1 W) because of the metal-metal waveguide structure. In detail, the laser used consists of a 10 μm thick MBE grown GaAs/AlGaAs active region with 27 periods of gratings and a total length of 1070 μm. It radiates a single mode emission line from 3452.0 to 3450.8 GHz by varying the bias voltage from 13.9 V to 14.9 V. Its maximum output power is 0.8 mW at an operating temperature of $\sim$12 K. The divergence of the main beam is about 12 degrees in both vertical and horizontal directions. The same laser has been successfully used for demonstrating heterodyne molecular spectroscopy with tuning capability [11] and frequency locking [12].

As the mixer, we employ a superconducting NbN HEB mixer with a nanobridge of 0.2×2 μm^2 in size, operated at liquid He temperature and requiring an optimal LO power of 150 nW at the detector itself [13]. The HEB mixer is the most sensitive heterodyne detector operated at frequencies between 1.5 THz and 6 THz. The mixer performance such as the mixing conversion gain and IF output power depends strongly on the LO power as well as DC bias power. Thus, any variations in the total power of the LO and DC bias can affect the operating state and thus induce instability in the mixing performance. Since the DC bias of a mixer can be very stable, the stability of the heterodyne performance is dominated by the amplitude stability of incident LO signal. THz radiation is coupled to the NbN bridge using a combination of a Si lens and a broadband planar spiral antenna.

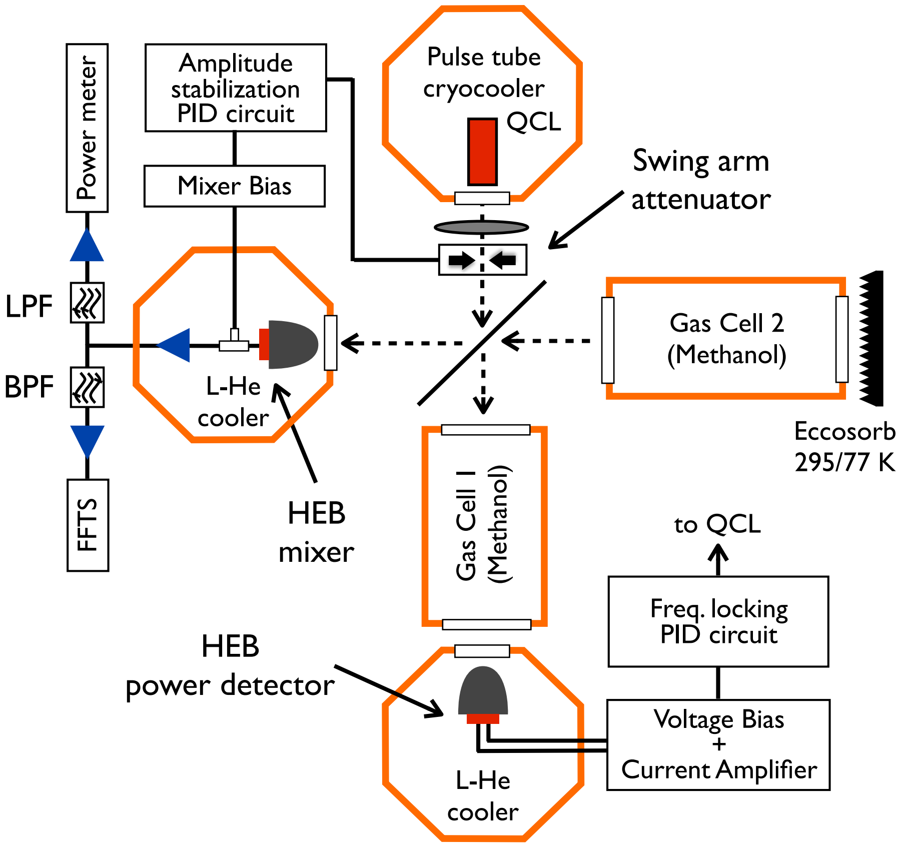

Figure 8.1. Schematic of the measurement setup for demonstrating both amplitude and frequency stabilization of a 3.5 THz QCL as local oscillator for a heterodyne receiver. It is also the setup for the Allan Variance and spectroscopic measurements.

Fig 8.1 sketches the complete setup for the amplitude and frequency stabilization experiment as well as for the heterodyne spectroscopy measurements. We start with the setup required only for the stabilization experiment. The QCL is operated in a pulse tube cryocooler at an stabilized operating temperature of 16 K. The THz radiation from the QCL is firstly focused with a high-density polyethylene (HDPE) lens, and then passes through the voice coil attenuator. Then, the QCL signal is split into two beams by a 13 μm thick Mylar beam splitter, where the reflected signal works as a LO to pump the HEB mixer, while the transmitted beam is used for the frequency locking. The frequency locking loop consists of a gas cell (Gas cell 1) at room temperature, whereby a methanol absorption line is used as the frequency reference. Furthermore, a 2nd superconducting NbN hot electron bolometer, is operated only as a direct power detector, together with a PID controller and a lock-in amplifier. The technique used for the frequency locking is very similar to that reported in [12, 14]. The voice coil actuator together with a second PID feedback loop is used to realize the amplitude stabilization, where the DC current of the voltage biased HEB mixer is used as a power reference signal. If the incident LO power fluctuates, a feedback current will be generated to drive the voice coil that acts as a variable optical attenuator by interrupting partial LO beam in order to maintain a constant DC current of the mixer. The voice coil is superior to a rotational polarizer since it responds fast (up to 1 kHz), and has the advantage of high resolution and full dynamic range. This technique can reduce not only instability of LO amplitude but also other instability factors like atmospheric turbulence in the LO path and LO mechanical instability.

To characterize the stability of the receiver and measure Allan Variance times, a hot/cold (295/77 K) blackbody load is applied as the input signal. The IF signal from the HEB mixer is amplified by a wide-band cryogenic amplifier, followed by two room temperature amplifiers, with a 100 MHz bandwidth (1.4$\sim$1.5 GHz) bandpass filter inbetween. The IF signal is further sampled by a fast power meter (Agilent E4418B).

Now we turn to the setup used for heterodyne spectroscopic measurements. It is the same as the one described for the stability experiment, except for the input signal and IF readout (the backend). In this case, the signal source is a combination of a methanol gas cell (Gas cell 2) and the hot/cold blackbody load. The resulted methanol emission spectral lines together with the QCL LO signal are coupled into the HEB mixer and are down converted to the intermediate frequencies. The same IF amplifier chain is used, but with a 0-1.5 GHz low pass filter inbetween. The spectrum is recorded by a Fast Fourier Transform Spectrometer (FFTS).

8.3 Frequency with amplitude stabilisation measurement results

We briefly introduce the working principle of the frequency locking. A bias circuit for the QCL combines three input signals, where a DC bias voltage, an

AC sinusoidal modulation signal, and a feedback control signal are employed to independently control the laser [12, 14]. By feeding the output current of HEB power detector to a lock-in amplifier with the AC modulation signal as a reference frequency, the derivative signal of the absorption profile is obtained. Then, a feedback signal from a PID controller is used to actively lock this derivative signal, maintained it at zero value. In this way, the laser frequency is stabilized to a particular methanol absorption line. The frequency locking alone has been realized previously for a QCL in [12, 14].

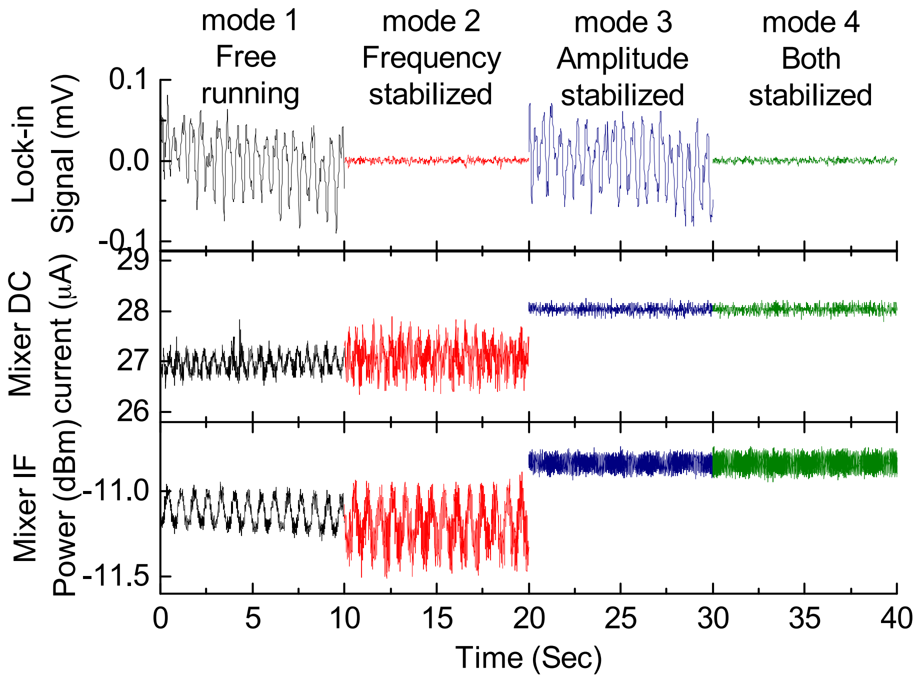

Figure 8.2. The lock-in amplifier signal, reflecting stability of the QCL frequency, the DC current of the HEB mixer, reflecting the QCL amplitude, and the output power of the IF amplifier chain, reflecting the stability the entire receiver, versus time for four different operating modes of 1) the free running; 2) only frequency stabilized; 3) only amplitude stabilized; and 4) both frequency and amplitude stabilized.

To characterize the stabilization we monitor the frequency fluctuation of the QCL by the output of the lock-in amplifier, the amplitude fluctuation of the incident power by the DC current of the HEB mixer, and the stability of the HEB receiver by the output of the IF amplifier chain in four different operation modes, covering 1) free running; 2) only frequency stabilized; 3) only amplitude stabilized; and 4) both frequency and amplitude stabilized. Fig. 2 shows the key result by plotting the lock-in amplifier output, the HEB mixer current, and the IF output power of the mixer versus time, which engages the four operation modes, respectively. In the free running mode, the observed low frequency fluctuation and drift in the lock-in signal are a result of the frequency noise of the laser due to external contributions mainly from the temperature oscillation of the cryocooler. The contribution of the cryocooler also induces amplitude instability [15], reflected by the fluctuations of the HEB mixer current and of the IF output power. In the second operating mode when the frequency stabilization loop is enabled, the lock-in signal becomes well stabilized and is maintained at the set point of zero, which implies that the QCL frequency is fully stabilized. However, in this case, the fluctuations in the amplitude of the QCL increase, reflected by those in the HEB current. Also the fluctuations in the mixer IF output are increased as a result of the fluctuations of the LO power. In the third mode when the amplitude stabilization loop becomes active, but the frequency stabilization loop is disabled, as expected, the fluctuations in the lock-in signal remain the same as in the free-running case, while the HEB mixer current is well stabilized and locked to a constant value. Consequently, the mixer IF power becomes also stabilized with no drift and with much less fluctuations. In the last operating mode when both the amplitude and frequency stabilization loops are enabled, as shown in the Fig 8.2, not only the lock-in signal but also the HEB mixer current as well as mixer IF power are stabilized. We therefore conclude that we succeed in simultaneous frequency and amplitude stabilization of the QCL.

It is interesting to discuss the physics associated to the observation in the 2nd operation mode, namely only the frequency is locked. In this case the amplitude fluctuates more. This suggests that the fluctuation or the frequency noise is anti-correlated to the fluctuation in the amplitude through the QCL bias voltage. The underlying physics is relatively straightforward. It is known that both frequency and output power of a THz QCL are a function of both DC bias and operating temperature. The emission power, in general, decreases if either the temperature increases or the DC bias decreases, which is true in the operating regime of our QCL. However, the frequency behavior can be different and is device dependent. Based on our previous measurement on the same QCL [11], we find that the frequency decreases if the temperature increases or the voltage increases, that results in a red shift in the frequency. Now we turn on only the frequency locking loop and assume that there is a small increase in temperature as a distortion. As a result, one expects a decrease in the frequency as well as in the amplitude. In response, the frequency locking loop through the PID will generate a negative voltage signal to compensate for the frequency decrease. However, in the same time, the amplitude will further decrease. In other words, the fluctuations in the amplitude will increase, having the same behaviour as shown in Fig 8.2. It becomes clear that due to the anti- correlation it is impossible by using only the QCL DC bias to realize the frequency and amplitude stabilization simultaneously. In contrast, for the 3rd operating mode, when the voice coil is applied to stabilize the amplitude, no effect has been seen to the frequency fluctuations since the amplitude adjustment is completely independent of the QCL operation.

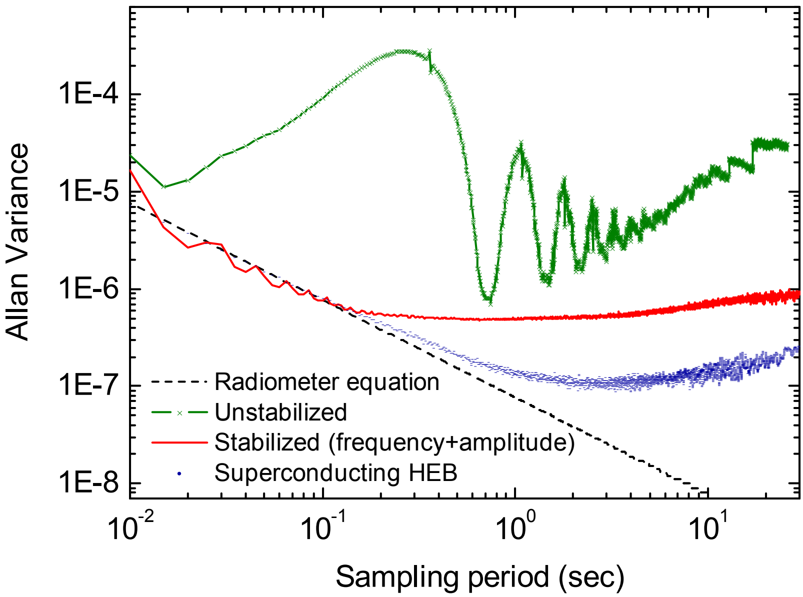

Figure 8.3. Measured total power Allan Variance of the entire receiver as a function of sampling period when the QCL LO is free running, fully stabilized, and when the HEB in a superconducting state with no electrical bias and no LO power. The radiometer equation for an effective noise fluctuation bandwidth of 13.5 MHz is also shown.

To evaluate the frequency locking quantitatively, we estimate the linewidth of the QCL. Following [12], the linewidth can be calculated by transforming the variation in voltage of the lock-in signal in the time domain into the frequency domain. We obtain a free running linewidth of about 1.5 MHz, while the locked linewidth of around 35 kHz in the fully stabilized state. This value has the same order of magnitude as that reported in [12] (18 kHz in this case) and is sufficiently narrow for practical us as a local oscillator. The difference in the absolute value can be due to the different operating point of the QCL and the detailed settings in the PID controller.

Apart from monitoring the DC current of the HEB mixer and the output of the IF amplifier chain versus time, we perform an Allan Variance measurement in the total power (continuum) mode to quantify the effect of the stability of the amplitude to the entire receiver. Allan Variance is a well-known, powerful tool for characterizing the stability of a system. It is known that random, white noise, integrates down with time as $t^{-1/2}$ according to the radiometer equation [16]. The finite stability of a real system eventually deviates from the radiometer equation at an integration time known as the Allan Variance minimum time. The quoted system Allan time thus relates to the maximum useful integration time for a given signal bandwidth. We measure the Allan Variance $\sigma_A^2(\tau)$ of the normalized IF output power, given by

$$\sigma_A^2(\tau) = \frac{1}{2}\sigma^2(\tau) \tag{8.1}$$

, where σ^2 is the average squared standard deviation of each number from its mean and τ is the sampling period. The measured $\sigma_A^2(\tau)$ for the entire receiver is plotted as a function of the sampling time in Fig 8.3 for three different measurement conditions: 1) when both frequency and amplitude are stabilized; 2) the QCL is free running; and 3) the HEB is in the superconducting state with zero bias and no LO power. For comparison, the radiometer equation for an effective noise fluctuation bandwidth of 13.5 MHz is also plotted.

The Allan time from both frequency and amplitude stabilized receiver is about 0.3 sec for a measured 13.5 MHz bandwidth. In contrast, the Allan time when the QCL in free running state is below 0.01 sec. Moreover, the measurement shows an extremely unstable behavior, suggested by the presence of strong oscillations. The latter are attributed to the low frequency temperature oscillations in the pulse tube cryocooler. An improvement of the Allan time with a factor more than 30 is achieved by introducing the amplitude stability in additional to the frequency locking. The data from the HEB superconducting state show the stability of the entire IF amplifier chain, which gives a total power Allan time at around 2 sec. The Allan times for the stabilized receiver and from the superconducting state are all shorter than what reported in [9] indicate the non-optimazied IF amplifier chain is the main limiting factor, and suggest that there is room to further increase the Allan time by carefully designing and arranging the setup.

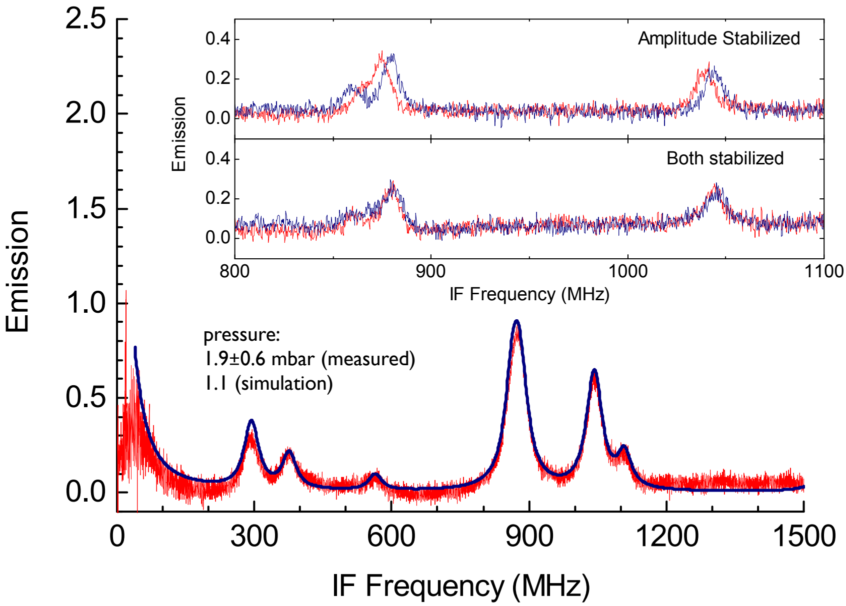

Figure 8.4. In the main figure: a measured 3.5 THz methanol spectrum in the intermediate frequencies when both frequency and amplitude of the LO is stabilized (in red). The gas pressure is 1.9±0.6 mbar. A simulated methanol spectrum with a pressure of 1.1 mbar is in blue. One inset shows a methanol spectrum when the LO is only amplitude stabilized (the upper one), measured twice with 1 hour interval time. The 2nd inset shows a methanol spectrum when both amplitude and frequency are stabilized. The gas pressure is reduced to 0.12±0.05 mbar.

To further verify the performance of the stabilized receiver, we perform two types of molecular spectroscopic measurements. One is to measure methanol emission lines using the QCL-HEB receiver with both frequency and amplitude stabilized. This is to check whether the stabilization scheme can affect the functionality of the receiver. Another one is to measure, using amplitude stabilization, methanol emission lines over an extended time interval with and without frequency locking. In this way, one can verify the effect of the frequency stabilization directly and as a simulation of an astronomic observation in a telescope. The main figure in Fig 8.4 plots methanol emission lines in the intermediate frequencies between 0∼1.5 GHz, limited by the FFTS, which are down converted from 3.5 THz methanol lines. Also, a modeled spectrum for the same frequency range is plotted in the main figure. It can be seen that an excellent agreement between the calculation and the data is obtained with respect to both the line frequencies and the relative intensities. Because of the amplitude stabilization, one measurement with only three traces [11] can lead to a reliable spectrum. No averaging among many different measurements is required.

The inset of Fig 8.4 shows two sets of measured methanol lines in the frequency range of 0.8$\sim$1.1 GHz for a gas pressure reduced to 0.12 mbar and using a 3 seconds integration time for each data trace. Each spectrum is re-measured after a 1 hour interval. We find that two spectra can overlap well when both frequency and amplitude are stabilized, while there is a frequency offset of about 5 MHz between the two spectra when only amplitude is stabilized (but no frequency stabilization). The latter implies a frequency drift of the LO. It proves that the LO frequency can be indeed locked, that is crucial for the spectroscopic measurement. It is worthwhile to note that, because of the full stabilization, we can resolve fine spectral lines as narrow as 10 MHz at the low gas pressure.

8.4 Conclusions

In conclusion, we succeed in demonstrating a fully stabilized 3.5 THz QCL, both in its amplitude and frequency, as a local oscillator operated in a pulse tube cryocooler for a heterodyne receiver. The frequency is locked to a methanol absorption line through the PID and the bias voltage, resulting in a linewidth as narrow as 35 kHz. The amplitude is stabilized by applying a swing-arm actuator blocking part of the LO beam for rapid feedback LO intensity control. The effectiveness of the amplitude stabilization and frequency locking is supported by the improved Allan time of the entire heterodyne receiver and also the high resolution heterodyne spectroscopic measurements.

Bibliography

[1] R. Köhler, A. Tredicucci, F. Beltram, H. E. Beere, E. H. Linfield, A. G. Davies, D. A. Ritchie, R. C. Iotti, and F. Rossi, *Terahertz semiconductor-heterostructure laser*, Nature, **417**, 156 (2002).

[2] B. S. Willams, *Terahertz quantum-cascade lasers*, Nature Photonics, **1**, 517 (2007).

[3] E. F. van Dishoeck, and A. G. G. M. Tielens, *Space-borne observations of the lifecycle of interstellar gas and dust*, The Century of Space Science, eds. J.A.M. Bleeker et al. 607 (2001).

[4] M. S. Vitiello, L. Consolino, S. Bartalini, A. Taschin, A. Tredicucci, M. Inguscio, P. De Natale, *Quantum-limited frequency fluctuations in a Terahertz laser*, Nature Photonics, **6**, 525 (2012).

[5] D. Rabanus, U. U. Graf, M. Philipp, O. Ricken, J. Stutzki, B. Vowinkel, M. C. Wiedner, C. Walther, M. Fischer, and J. Faist, *Phase locking of a 1.5 Terahertz quantum cascade laser and use as a local oscillator in a heterodyne HEB receiver*, Optics Express, **17**, 1159 (2009).

[6] A. A. Danylov, T. M. Goyette, J. Waldman, M. J. Coulombe, A. J. Gatesman, R. H. Giles, W. D. Goodhue, X. Qian, and W. E. Nixon, *Frequency stabilization of a single mode terahertz quantum cascade laser to the kilohertz level*, Optics Express, **17**, 7525 (2009).

[7] S. Barbieri, P. Gellie, G. Santarelli, L. Ding, W. Maineult, C. Sirtori, R. Colombelli, H. Beere and D. Ritchie, *Phase-locking of a 2.7-THz quantum cascade laser to a mode-locked erbium-doped fibre laser*, Nature Photonics, **4**, 636 (2010).

[8] D. W. Allan, *Statistics of Atomic Frequency Standards*, Proceedings of the IEEE, **54**, 221 (1996).

[9] D. J. Hayton, J. R. Gao, J. W. Kooi, Y. Ren, W. Zhang, and G. de Lange, *Stabilized hot electron bolometer heterodyne receiver at 2.5 THz*, Applied Physics Letters, **100**, 081102 (2012).

[10] M. I. Amanti, G. Scalari, F. Castellano, M. Beck, and J. Faist, *Low divergence Terahertz photonic-wire laser*, Optics Express, **18**, 6390 (2010).

[11] Y. Ren, J. N. Hovenier, R. Higgins, J. R. Gao, T. M. Klapwijk, S. C. Shi, B. Klein, T.-Y. Kao, Q. Hu, and J. L. Reno, *High-resolution heterodyne spectroscopy using a tunable quantum cascade laser around 3.5 THz*, Applied Physics Letters, **98**, 231109 (2011).

[12] Y. Ren, J. N. Hovenier, M. Cui, D. J. Hayton, J. R. Gao, T. M. Klapwijk, S. C. Shi, T-Y. Kao, Q. Hu, and J. L. Reno, *Frequency locking of signle-mode 3.5-THz quantum cascade lasers using a gas cell*, Applied physics letters, **100**, 041111 (2012).

[13] W. Zhang, P. Khosropanah, J. R. Gao, E. L. Kollberg, K. S. Yngvesson, T. Bansal, R. Barends, and T. M. Klapwijk, *Quantum noise in a terahertz hot electron bolometer mixer*, Applied Physics Letters, **96**, 111113 (2010).

[14] H. Richter, S. G. Pavlov, A. D. Semenov, L. Mahler, A. Tredicucci, H. E. Beere, D. A. Ritchie, and H.-W. Hübers, *Submegahertz frequency stabilization of a terahertz quantum cascade laser to a molecular absorption line*, Applied Physics Letters, **96**, 071112 (2010).

[15] H. Richter, A. D. Semenov, S. Pavlov, L. Mahler, A. Tredicucci, K. Il'in, M. Siegel, and H.-W. Hübers, *Terahertz heterodyne receiver with quantum cascade laser and hot electron bolometer mixer in a pulse tube cooler*, Applied Physics Letters, **93**, 141108 (2008).

[16] J. W. Kooi, G. Chattopadhyay, M. Thielman, T. G. Phillips, and R. Schieder, *Noise Stability of SIS receivers*, International Journal of Infrared and Millimeter Waves, **21**, 689 (2000).

Summary

Super-terahertz high-resolution heterodyne spectrometer using a quantum cascade laser

High-resolution spectroscopy at super-terahertz frequencies (2-6 THz) can play a vital role in astronomical observation and atmospheric remote sensing. It provides unique and important information on the history of our universe and its evolution, by getting into the insight of the physical and chemical conditions. Moreover, it can help to address questions about our own atmosphere such as ozone layer depletion and climate change problems. However, up to now this frequency region has rarely been accessible for high-resolution spectroscopy due to the lack of suitable local oscillator technology. The recently developed terahertz quantum cascade lasers become the most promising candidate as a novel solid-state terahertz source.

Terahertz quantum cascade lasers, after one decade development from the first demonstration in 2002, are now capable of delivering milliwatts or more of continuous-wave coherent radiation over the terahertz frequency range. For the local oscillator application, a heterodyne sensitivity measurement has been performed, which proved a prominent power stability with no additional inherent noise for a terahertz quantum cascade laser. However, a finial and crucial step to demonstrate a heterodyne receiver system is a direct high-resolution heterodyne spectroscopic experiment, which is also an important approach to characterize the performance of the entire system.

In this thesis, we have realized a high-resolution heterodyne spectrometer by introducing a terahertz quantum cascade laser as a local oscillator, a superconducting hot electron bolometer as a mixer and a Fast Fourier Transform

Spectrometer as a back-end spectrometer. The first molecular spectrum by using a terahertz quantum cascade laser as local oscillator was obtained at a frequency of 2.9 THz. We push further this heterodyne spectrometer up to 3.5 THz with a more advanced terahertz quantum cascade laser, where the first 3.5 THz methanol (CH_3OH) spectra were obtained with ~1 GHz tuning range from the local oscillator. Excellent agreement between the measured spectra to the theoretical calculation was achieved with respect to both line intensity and frequency.

Furthermore, we have explored the frequency locking capability of such terahertz quantum cascade lasers by using a terahertz molecular absorption line as a reference frequency. Based on a compact gas cell and a power detector, the frequency stabilization is achieved with a minimal linewidth of 18 kHz and a Gaussian-like shape. Such kHz linewidth with a compact locking scheme is favorable for any space- or ballon-borne instrument.

For actual observation applications, the effective integration time is a crucial issue that determines the efficiency of the observation. A robust experimental scheme has been demonstrated to simultaneously stabilize the frequency and amplitude of a terahertz quantum cascade laser. The frequency stabilization has been realized using a methanol absorption line, a power detector and a proportional-integral-derivative loop. The amplitude stabilization of the incident power has been achieved using a swing-arm voice coil actuator as a fast optical attenuator, and using the direct detection output of a superconducting mixer in combination with a 2nd feedback loop. As a result, a fully stabilized heterodyne spectrometer at super-terahertz freqeuencies was demonstrated, with improved Allan Variance times, and also supported by measured heterodyne molecular spectra.

Based on all this work, terahertz quantum cascade lasers become technologically much more mature and convincing to be used as local oscillator. A direct outcome is a new NASA mission: Galactic/Xgalactic Ultra long duration balloon Spectroscopic Stratospheric THz Observatory (GUSSTO), in which terahertz quantum cascade lasers have been proposed as local oscillators for the 4.7 THz receiver channel. Within the Phase-A-Concept study period, in collaboration with Q. Hu's group at MIT and C. Walker's group at University of Arizona, we demonstrated a heterodyne receiver using an advanced third-order distributed feedback quantum cascade laser as a local oscillator, whose emission frequency is only a few GHz away from the OI line at 4.7448 THz. Excellent receiver sensitivity together with a heterodyne spectrum have been demonstrated. All these efforts should lead soon to the first realization of a terahertz quantum cascade laser for astronomical application in a telescope.

Also the local oscillator technology described in this thesis, offers the technique for other instruments such as Oxygen Heterodyne Camera (OCAM) proposed on SOFIA and also creates new mission opportunities in the future.

Samenvatting

Super-terahertz hoge-resolutie heterodyne spectrometer met een kwantum cascade laser

Hoge-resolutie spectroscopie op super-terahertz frequenties (2-6 THz) kan een essentile rol spelen in astronomische waarnemingen en in remote sensing van de atmosfeer. Het kan unieke en belangrijke informatie geven over de geschiedenis van ons universum, door inzicht te verschaffen in zijn fysische en chemische condities en zijn evolutie. Bovendien kan het helpen vragen over onze eigen atmosfeer aan de orde te stellen, zoals die naar het verdwijnen van de ozonlaag en klimaatverandering. Echter, tot nu toe is deze frequentieband slecht toegankelijk geweest voor hoge-resolutie spectroscopie, door het ontbreken van een geschikte technologie voor het genereren van het lokale-oscillator signaal. Recent is de terahertz kwantum cascade laser ontwikkeld als de meest veelbelovende vaste-stof terahertz bron.

Terahertz kwantum cascade lasers zijn, na tien jaar ontwikkeling sinds de eerste demonstratie in 2002, in staat om meer dan een milliwatt aan continue, coherente straling te leveren in het terahertz frequentie gebied. Voor de toepassing als lokale-oscillator is een heterodyne gevoeligheidsmeting gedaan, die een goede stabiliteit van het vermogen bewees, zonder extra intrinsieke ruis van de terahertz kwantum cascade laser. Desondanks is een laatste en cruciale stap nodig om de heterodyne ontvanger te demonstreren, namelijk een hoge-resolutie heterodyne spectroscopie experiment. Daarnaast is dat een belangrijk experiment om de prestaties van het hele systeem te karakteriseren.

In dit proefschrift hebben we een hoge-resolutie heterodyne spectrometer gerealiseerd, door een terahertz kwantum cascade laser te gebruiken als lokale-oscillator, een supergeleidende hete-elektronen bolometer als mixer en een Fast Fourier Transform spectrometer als back-end spectrometer. Het eerste heterodyne moleculaire spectrum, verkregen met een terahertz kwantum cascade laser als lokale-oscillator, werd gemeten op een frequentie van 2.9 THz. We breiden de technologie uit naar 3.5 THz met een geavanceerdere kwantum cascade laser. De eerste 3.5 THz methanol (CH_3OH) spectra werden verkregen met een afstellingsbereik voor deze lokale-oscillator van ~1 GHz. De overeenstemming van de gemeten spectra met de theoretische verwachting die werd bereikt, was uitstekend, zowel wat betreft de intensiteit van de spectrale lijnen als de frequentie.

Verder hebben we de mogelijkheid tot frequentievergrendeling van deze kwantum cascade lasers onderzocht met behulp van een moleculaire absorptie lijn als frequentiereferentie. Frequentiestabilisatie met een minimale lijnbreedte van 18 kHz en een bijna Gaussische bundel is gerealiseerd door middel van een compacte gas cel en een vermogensdetector. Een lijnbreedte van die orde grootte met een compacte vergrendelingstechniek is wenselijk voor elk instrument dat wordt gebruikt in een satelliet of ballon.

Voor concrete toepassing in waarnemingen is de effectieve integratietijd een kritisch punt, dat de efficintie van de waarneming bepaalt. Er werd een robuust experimenteel schema gedemonstreerd om tegelijkertijd de frequentie en de amplitude van een terahertz quantum cascade laser te stabiliseren. De frequentie stabilisatie werd gerealiseerd met behulp van een absorptielijn van methanol, een vermogensdetector en een proportioneel-integrerend-en-differentirend systeem. De stabilisatie van de amplitude van het invallende vermogen werd bereikt door gebruik te maken van een voice-coil actuator, die functioneert als snel te variren optische verzwakker. Hierbij wordt gebruik gemaakt van het directe-detectie signaal van de supergeleidende mixer, gecombineerd met een tweede feedback systeem. Het resultaat is een volledig gestabiliseerde heterodyne spectrometer op super-terahertz frequenties met een verbeterde Allan-variantie tijd, wat ondersteund wordt door de gemeten moleculaire spectra.

Het resultaat van al dit werk is dat terahertz kwantum cascade lasers rijper en overtuigender worden voor de toepassing als lokale-oscillator. Een direct gevolg is een nieuwe missie van NASA: Galactic/Xgalactic Ultra long duration balloon Spectroscopic Stratospheric THz Observatory (GUSSTO), waarin terahertz kwantum cascade lasers zijn voorgesteld als lokale-oscillator in de ontvanger op 4.7 THz. Binnen de A-fase concept-studie periode hebben we, in samenwerking met Q. Hu's groep bij MIT en C. Walker's groep aan de Universiteit van Arizona, een heterodyne ontvanger gedemonstreerd, waarin een derde-orde, gedistribueerde feedback kwantum cascade laser als lokale-oscillator is gebruikt. De frequentie van deze laser ligt maar een paar GHz bij de OI lijn op 4.7448 THz vandaan. Voor deze ontvanger werd een uitstekende gevoeligheid, gecombineerd met een heterodyne spectrum gedemonstreerd. Al deze inspanningen zouden spoedig moeten leiden tot het gebruik van kwantum cascade lasers voor astronomische waarnemingen in telescopen. Ook kan de lokale-oscillator technologie, zoals beschreven in dit proefschrift, gebruikt worden voor andere instrumenten, zoals de Oxygen Heterodye Camera (OCAM) die is voorgesteld voor SOFIA, en creert het nieuwe mogelijkheden voor missies in de toekomst.

Curriculum Vitæ

Yuan Ren

26–06–1985	Born in Xi'an, China
1999-2002	High School Xi'an Senior High School, China
2002-2006	Undergraduate in Electronics Engineering Xi'an Jiaotong University, China
2006-2008	M.Sc in Astronomy Purple Mountain Observatory, Chinese Academy of Sciences, China
2009-2012	Ph.D thesis: Super-terahertz heterodyne spectrometer using a quantum cascade laser Delft University of Technology and Purple Mountain Observatory, Chinese Academy of Sciences. under supervision of Prof. dr. ir. T. M. Klapwijk, Prof. S. C. Shi and Dr. J. R. Gao

List of publications

Journal articles

- W. Miao, Y. Delorme, A. Feret, R. Lefevre, B. lecomte, F. Dauplay, J.M. Krieg, G. Beaudin, W. Zhang, **Y. Ren**, and S. C. Shi, *Comparison between hot spot modeling and measurement of a superconducting hot electron bolometer mixer at submillimeter wavelengths*, Journal of Applied Physics, **106**, 103909 (2009).

- **Y. Ren**, J. N. Hovenier, R. Higgins, J. R. Gao, T. M. Klapwijk, S. C. Shi, A. Bell, B. Klein, B. S. Williams, S. Kumar, Q. Hu, and J. L. Reno, *Terahertz heterodyne spectrometer using a quantum cascade laser*, Applied Physics Letters, **97**, 161105 (2010).

- **Y. Ren**, W. Miao, Q. J. Yao, W. Zhang, and S. C. Shi, *Terahertz direct detection characteristics of a superconducting NbN bolometer*, Chinese Physics Letters, **28**, 010702 (2011).

- **Y. Ren**, J. N. Hovenier, R. Higgins, J. R. Gao, T. M. Klapwijk, S. C. Shi, , B. Klein, T-Y. Kao, Q. Hu, and J. L. Reno, *High-resolution heterodyne spectroscopy using a tunable quantum cascade laser around 3.5 THz*, Applied Physics Letters, **98**, 231109 (2011).

- E. L. Kollberg, K. S. Yngvesson, **Y. Ren**, W. Zhang, P. Khosropanah, and J. R. Gao, *Impedance of Hot-Electron Bolometer Mixers at Terahertz Frequencies*, IEEE Terahertz Science and Technology, **1**, 383 (2011).

- **Y. Ren**, J. N. Hovenier, M. Cui, D. J. Hayton, J. R. Gao, T. M. Klapwijk, S. C. Shi, T-Y. Kao, Q. Hu, and J. L. Reno, *Frequency locking of single-mode 3.5-THz quantum cascade lasers using a gas cell*, Applied Physics Letters, **100**, 041111 (2012).

- D. J. Hayton, J. R. Gao, J. W. Kooi, **Y. Ren**, W. Zhang and G. de Lange, *Stabilized hot electron bolometer heterodyne receiver at 2.5 THz*, Applied Physics Letter, **100**, 081102 (2012).

- M. Cui, J. N. Hovenier, **Y. Ren**, A. Polo, and J. R. Gao, *Terahertz wavefronts measured using the Hartmann sensor principle*, Optics Express, **20**, 14380-14391 (2012).

- **Y. Ren**, D. J. Hayton, J. N. Hovenier, M. Cui, J. R. Gao, T. M. Klapwijk, S. C. Shi, T-Y. Kao, Q. Hu, and J. L. Reno, *Frequency and amplitude stabilized terahertz quantum cascade laser as local oscillator*, Applied Physics Letters, **101**, 101111 (2012).

- M. Cui, J. N. Hovenier, **Y. Ren**, J. R. Gao, T-Y. Kao, Q. Hu, and J. L. Reno, *Intrinsic wavefront of a 3rd distributed feedback terahertz quantum cascade laser*, in preparation.

- J. L. Kloosterman, D. J. Hayton, **Y. Ren**, T-Y. Kao, J. N. Hovenier, J. R. Gao, T. M. Klapwijk, Q. Hu, C. K. Walker, and J. L. Reno, *Hot electron bolometer heterodyne receiver with a 4.7-THz quantum cascade laser as a local oscillator*, Submitted to Applied Physics Letters.

Conference proceedings

- W. Miao, Y. Delorme, A. Feret, R. Lefevre, L. Benoit, F. Dauplay, J. M. Krieg, G. Beaudin, W. Zhang, Y. Ren, and S. C. Shi, *Performance Investigation of a Quasi-Optical NbN HEB Mixer at Submillimeter Wavelength*, Proceedings of the 20th International Symposium on Space Terahertz Technology, Charlottesville, USA (2009).

- Y. Ren, J. R. Gao, J. N. Hovenier, R. Higgins, W. Zhang, T. M. Klapwijk, S. C. Shi, A. Bell, B. Klein, B. S. Williams, S. Kumar, Q. Hu, and J. L. Reno, *Heterodyne gas cell measurements at 2.9 THz using a quantum cascade laser as local oscillator*. Proceeding of SPIE, **7741**, 774118, San Diego, USA (2010).

- Y. Ren, J. N. Hovenier, R. Higgins, J. R. Gao, T. M. Klapwijk, S. C. Shi, A. Bell, B. Klein, B. S. Williams, S. Kumar, Q. Hu, and J. L. Reno, *Terahertz heterodyne spectrometer using a quantum cascade laser*, Proceedings of the 2010 annual symposium of the IEEE Photonics Benelux Chapter, Delft, The Netherlands (2010).

- Y. Ren, J. N. Hovenier, W. Zhang, P. Khosropanah, A. Bell, B. Klein, J. R. Gao, T. M. Klapwijk, S. C. Shi, T-Y. Kao, S. Kumar, Q. Hu, and J. L. Reno, *Gas cell measurement using a 2.9 THz heterodyne receiver based on a quantum cascade laser and a superconducting hot electron bolometer*, Proceedings of the 21st International Symposium on Space Terahertz Technology, Oxford, UK (2010).

- Y. Ren, J. N. Hovenier, W. Zhang, P. Khosropanah, J. R. Gao, T. M. Klapwijk, S. C. Shi, T-Y. Kao, S. Kumar, Q. Hu, and J. L. Reno, *3.5 THz surface emitting distributed feedback QCL operated at above 60 K as local oscillator*, Proceedings of the 21st International Symposium on Space Terahertz Technology, Oxford, UK (2010).

- Y. Ren, J. N. Hovenier, M. Cui, D. J. Hayton, J. R. Gao, T. M. Klapwijk, S. C. Shi, T-Y. Kao, Q. Hu, and J. L. Reno, *Frequency locking of a 3.5-THz quantum cascade laser using a gas cell*, Proceedings of the 22nd International Symposium on Space Terahertz Technology, Tucson, USA (2011).

- Y. Ren, P. J. de Visser, J. N. Hovenier, W. Zhang, J. R. Gao, T. M. Klapwijk, S. C. Shi, T-Y. Kao, S. Kumar, Q. Hu, and J. L. Reno, *3.5 THz Quantum Cascade Laser at 70 K as local oscillator*, Proceedings of the 22nd International Symposium on Space Terahertz Technology, Tucson, USA (2011).

- Y. Ren, J. N. Hovenier, J. R. Gao, T. M. Klapwijk, S. C. Shi, T-Y. Kao, Q. Hu, and J. L. Reno, *Temperature and frequency resolution of a 3.5 THz heterodyne spectrometer using a quantum cascade laser*, Proceedings of the 22nd International Symposium on Space Terahertz Technology, Tucson, USA (2011).

- M. Cui, J. N. Hovenier, Y. Ren, J. R. Gao, and T. M. Klapwijk, *Measure the beam wavefronts of a terahertz source*, Proceedings of the 22nd International Symposium on Space Terahertz Technology, Tucson, USA (2011).

- Y. Ren, J. N. Hovenier, R. Higgins, J.R. Gao, T. M. Klapwijk, S. C. Shi, B. Klein, T-Y. Kao, Q. Hu, and J. L. Reno, *High-resolution heterodyne spectroscopy using a tunable quantum cascade laser around 3.5 THz*, 11th International Conference on Intersubband Transitions in Quantum Wells, Sardinia, Italy (2011). **Invited talk**

- Y. Ren, J. N. Hovenier, M. Cui, D. J . Hayton, J. R. Gao, T. M. Klapwijk, S. C. Shi, T-Y. Kao, Q. Hu, and J. L. Reno, *Frequency locking of a 3.5-THz quantum cascade laser using a gas cell*, 11th International Conference on Intersubband Transitions in Quantum Wells, Sardinia, Italy (2011).

- Y. Ren, J. N. Hovenier, D. J. Hayton, M. Cui, J. R. Gao, T. M. Klapwijk, S. C. Shi, T. Y. Kao, Q. Hu, and J. L. Reno, *Stabilized HEB-QCL heterodyne spectrometer at super-terahertz*, 23rd International Symposium on Space Terahertz Technology, Japan (2012).

- Y. Ren, J. N. Hovenier, D. J. Hayton, M. Cui, J. R. Gao, T. M. Klapwijk, S. C. Shi, T. Y. Kao, Q. Hu, and J. L. Reno, *Stabilized HEB-QCL heterodyne spectrometer at super-terahertz*, SPIE Astronomical Telescopes + Instrumentation, Amsterdam, the Netherlands (2012).

Acknowledgements

After four years of my life in Delft, a PhD thesis raises. For sure, the development of terahertz heterodyne spectrometer will continue. But now it comes to the time to thank very one who made a contribution to this thesis in a different way.

First of all I want to mention my promoters, Teun Klapwijk, Sheng-Cai Shi, and Jian-Rong Gao. Teun, it has been a great pleasure to work with you, from a wide range of physics topics of view and also for all the enthusiastic encouragement from you. Shi, thanks for bringing me into the research field and also offering this challenging but great opportunity. Your philosophy on both research and life inspires me deeply. Gao, thanks for all your daily supervision, kindly help and support from my first day arrival in Delft, for your sharp advices, creative testing ideas, and your company with the experiment late in the lab. It's my honour to work with you on this exciting topic and also wish you successes in "GUSSTO".

Then, it's time to thank Niels Hovenier, for all the help with building the experimental setup. It's a great pleasure to work with you, not only for the tea time everyday, but also for all the mismatch problems, sand absorber, and all the travelling experiments we had. Also for Mascha, thanks for all the bondings you made. Morris, it's a fantastic experience to work with you, for varieties of topics you are interested in, except "terahertz". Your knowledge on the optics broadens our understanding of the laser. Although your ideas of magic holes were published on QCL firstly by other groups, never mind, there are still Higgs, archaeology, and Naruto waiting for you. Nathan, thanks for your help with the clean room work on the laser and also fruitful discussions on the super-terahertz meeting every week. Darren, thanks for your help with our joint experiments, all the proof readings and especially your voice coil! Ronan Higgins, thanks for your knowledge of the molecular spectrum calculation and all the useful suggestions you made. Also I appreciated the kind help from A. Bell and B. Klein for your great FFTS and several times travel to Delft. Also for Marco, good luck to your master thesis.

Next up I like to thank to our collaborator Prof. Qing Hu for providing the state-of-art quantum cascade lasers. Also to Prof. Benjamin Williams, Sushil Kumar, and especially Wilt Kao, thanks for all your great devices and useful discussions, which at the end lead to my publications. Also I appreciated the fruitful discussion with Dr. Saverio Bartalini on the frequency stabilization issue.

Of course, also thanks to all the group members. Thanks for my roommates Akria, thanks for all the free KIDs telecom you brought. Also for Pieter-Jan and Shao-Jiang Zhu, it's my pleasure to share the office with all the interesting discussions. Also for others in our lab, for Pieter who helps me a lot on the experiments at the first half year; Eduard for your sharp points everyday, Rik for all the football discussion we had, Reinier for all his sister's cakes, David for the nice trip we had in Tucson, and Alessandro for interesting points from Taiwanese perspective. Also thanks J.J.A. Baselmans, B. Knoors, C. Sfiligoj, S. M. H. Javadzadeh and all the former group members, for your contribution to the social atmosphere of our group. And of course to Maria, Irma and Dorine, for all your kindly help and support.

At PMO, for all the HEB group members: Ling Jiang, Wen Zhang, Wei Miao, Ning Li and Kang-Min Zhou, I am appreciate all the help and support from you, which comes along with me from my master study until now, and all the good time we share together makes up my mind to keep doing research. For Jing Li, for your company for the last year in Delft, for all your encouragement and all the free home made foods, thanks so much and also wish your "kids" will happily grow up. Also for all the other people in PMO, Sheng Li, Jia-Qiang Zhong, Dong Liu, Kun Zhang, Jin-Pin Yang, Zheng Lou, Zheng Wang, Wen-Ying Duan, Zi-Rui Li, Qing-Gen Huang, Zhen-Hui Lin, Qi-Jun Yao, and Wen-Lei Shan, I look forward to working with you in the near future.

As the only hobby, I enjoy playing football with lots of friends in the DCF team: Qiang Xu, Yu-Song Pang, Xiao-Chen Liu, Yun-He Zhang, Xin-An Zhu, Chen-Xiang Ning, Bo-Ya Dai, Yue Chen, Meng Wang, Min Xu, Ya-Xun Wu, Zhan Zhang, Guo-Liang Zhu, Zhi-Ming Yang, Jia-Kun Gong, Bo Song, Hao Yin and Xi Shan. Thanks for all the pleasure time shared with you on the field, in front of the TV and for several campaign trips. Of course there are more people behind the DCF group, Nan Xiu, Mei Mei, Jing Chu, Jing Wang, Xiao-Min Yin, and Ying Cao. Thanks for all the parties, foods and drinks, and especially to Ying Cao for your prototype design of the cover for this thesis.

Also thanks to my roommates, Wei-Jie Wu, Yuan-Bo Nie, Quan Pan, Li-Hua Ma, and Yun-Long Yu. Your company drives my loneliness away.

Most importantly, I like to thank my parents for their unconditional love and support. 爸爸妈妈，谢谢你们！